THE ROLE OF HEAT SHOCK PROTEIN 20 IN THE PATHOGENESIS OF *HELICOBACTER PYLORI* INFECTIONS

GOH YUN SHAN

NATIONAL UNIVERSITY OF SINGAPORE

2007

THE ROLE OF HEAT SHOCK PROTEIN 20 IN THE PATHOGENESIS OF *HELICOBACTER PYLORI* INFECTIONS

GOH YUN SHAN
B. Sc. (Hons.), NUS

A THESIS SUBMITTED

FOR THE JOINT DEGREE OF MASTER IN INFECTIOUS DISEASES, VACCINOLOGY AND DRUG DISCOVERY

DEPARTMENT OF MICROBIOLOGY

NATIONAL UNIVERSITY OF SINGAPORE

2007

ACKNOWLEDGEMENTS

I would like to express my heartfelt gratitude to:

Associate Professor Ho Bow, my supervisor, for his patient guidance and invaluable advices to the project and beyond.

Shu Xian, for her invaluable friendship, the excellent assistance and great support when things were not smooth.

Josephine Howe, for her patient guidance in electron microscopy work.

Meiling, for her kind friendship, the many invaluable suggestions and advices to the project.

Yan Wing, for the great friendship and all the wonderful time in the laboratory.

Munfai, for the great help he has provided with me in this project.

All other laboratory mates: **Han Chong, Gong Min, Ammar, Chow Goon, Alvin** and **Samantha** for their friendship and putting up with me during the course of the project.

My family, for all the love, encouragement and support throughout this project.

TABLE OF CONTENTS: PAGE

Summary

Heat Shock Protein (HSP20) is a recently identified surface localized protein of *Helicobacter pylori*. It was shown to co-immunoprecipitate with CagA (cytotoxin-associated gene A), a well-studied pathogenic factor of *H. pylori*. Interestingly, CagA being a cytoplasmic protein has been reported to be surface exposed before being translocated across Type IV secretion system (T4SS) into the host cells during *H. pylori* infection. The interaction between the two proteins suggests the potential role of HSP20 as a chaperone to CagA in pathogenesis of *H. pylori* infections. This project aims to examine the association of HSP20 and CagA in the establishment of T4SS, translocation of CagA into host and modulation of host response to translocated CagA.

With the use of two antibodies (anti-CagA and anti-recombinant HSP20), transmission electron microscopy (TEM) findings show that upon host contact there is a redistribution of *H. pylori* HSP20 from the cell membrane to cytoplasm. This results in the co-localization of HSP20 with CagA in the cell cytoplasm. These findings suggest that HSP20 might act as a chaperone in intracellular transport of CagA.

By using scanning electron microscopy, the study indicates that the association of HSP20 and CagA as seen in the TEM studies is a necessity for T4SS establishment as the latter was also observed to be present in *hsp20* deletion mutant, *cagA* deletion mutant and *hsp20/cagA* deletion mutant of 26695 *H. pylori*. Western blotting study shows that in the absence of HSP20 the efficiency of CagA translocation was evidently reduced. This indicates that HSP20, not only play a role in intracellular transport of CagA, but also assists in CagA translocation into host cells.

Although HSP20 was not found to modulate the ability of CagA to induce cell elongation (hummingbird phenotype) and IL8 secretion, it was able to modulate CagA-mediated ectopic assembly of the tight junction protein (ZO-1) to extra-junctional bacterial attachment sites from the tight junctional sites (i.e. the cell periphery). In the presence of rHSP20, ZO-1 recruitment to extra-junctional sites was exacerbated. This indicates that HSP20 might be a chaperone that assists CagA in ZO-1 redistribution. This redistribution had been shown to have a causal relationship with the disruption of paracellular barrier function of the tight junction complexes. The ZO-1 recruitment resulted in a substantial elevated leakage of biotinylated albumin across the cell monolayer, indicating disruption of tight junction barrier function of the infected cell monolayer. The level of leakage decreased considerably in the absence of HSP20.

Taken together, the role of HSP20 as a chaperone to CagA in facilitating *H. pylori* infections cannot be undermined. Hence extensive investigation should be performed to establish the chaperonic role of HSP20 in an attempt to give us further insights in the pathogenesis of *H. pylori* infections.

List of Tables

List of Figures

INTRODUCTION

Helicobacter pylori is a gram negative, microaerophilic, S-shaped bacterium, which colonizes the gastric mucosal layer. As recorded in "Helicobacter pioneers" (Marshall, 2002), the presence of *H. pylori* in the gastric mucosa of the stomach has been observed as early as 1893 by Bizzozero and later in 1939 by Doenges. However, it was only in 1984 that Marshall and Warren reported it as Camphylobacter like organism (CLO) and later it was renamed as *Helicobacter pylori*. The role of this organism in the etiology of peptic ulcer disease (PUD) (George *et al.*, 1990), and gastric carcinoma (Parsonnet *et al.*, 1991) has since been well established.

1.1 *Helicobacter pylori* in the human stomach

H. pylori infects almost 50% of the world population (Bumann *et al.*., 2001). The organism resides at the gastric mucosa in the human stomach. *H. pylori* infections are first initiated by adhesion and colonization (Megraud *et al.*, 1991).

In order to prevent *H. pylori* from being washed away by the natural cleansing mechanisms in the human stomach, it has to be able to colonize the host quickly (Sharon and Ofek, 2000). *H. pylori* binds to the host through many bacterial proteins called adhesins, which are involved in the early stages of *H. pylori* infection by mediating the interactions between the host and the bacterium (Karlsson, 1998).

To colonize and survive in the acidic human stomach, *H. pylori* burrows through the mucous layer. This is aided by its spiral shape and the presence of its sheathed flagella. As the mucosa layer protects the epithelial cells from the acidic gastric juices secreted by gastrin cells scattered among the epithelial lining cells of the antrum pyloric glands, the presence of *H. pylori* in the mucosa layer thus aids in its survival in the acidic

stomach microenvironment. The production of urease by the bacterium converts urea into ammonia and bicarbonates, both of which are strong bases that can neutralize the gastric juices, thus creating a more alkaline environment in the stomach, benefiting the survival of *H. pylori* (Marshall and Warren, 1984; Goodwin *et al*., 1985).

When *H. pylori* binds onto cell lines such as Kato III (a gastric carcinoma cell line), there will be a thickening of cell membrane or "pedestal formation" (Vijayakumari *et al*., 1994). The intimate association of the bacteria with its host could possibly allow them to deliver toxins or other substances more efficiently.

1.2 Type IV secretion system

The *cag* pathogenicity island of *H. pylori* consists of many genes that code for the Type IV secretion system (T4SS). The best-studied model of T4SS is that of *Agrobacterium tumefaciens*. In this plant pathogen, T4SS is used to deliver DNA and proteins into plants cells introducing bacterial DNA into the plant genome to induce tumour formation. The T4SS of *H. pylori* bears strong resemblamce to that of *A. tumefaciens* (Bourzac and Gullenmin., 2005). In *H. pylori*, the only reported substance found to be translocated across the T4SS, is cytotoxin association gene A, CagA (Backert *et al*., 2000). Through the T4SS pilus, CagA is directly injected into host cells. Once in the host cells, CagA is tyrosine phosphorylated, thereby induces many cellular activities such as formation of hummingbird phenotype and cytokine production (Bourzac and Gullemin., 2005).

1.3 Heat Shock Proteins

Heat shock proteins (HSPs) belong to a group of highly conserved proteins found in all prokaryotic and eukaryotic cells (Laksanalamai *et al.*, 2004). These are diverse sets of proteins, usually classified based on their molecular weights, such as HSP60. Under normal conditions, these proteins were maintained at a basal level serving as a molecular chaperon in protein folding and degradation. However, this level is significantly upregulated to induce the heat shock response in the presence of certain factors such as growth factors, virus infection and stress (Debbie *et al.*, 1991).

HSP60 has been considered to be a virulence factor of *H. pylori* infections as it helps in stimulating adhesion, stabilizing proteins, and enhancing bacterial survival under stress (Yamaguchi *et al.*, 1998). It has also been reported to trigger autoimmune response and induce cytokine production (Yamaguchi *et al.*, 1999).

Du and Ho (2003} described a newly identified Heat Shock Protein 20 that was shown by transmission electron microscopy (TEM) studies to be a surface localized protein of *H. pylori.* As HSP20 is observed to be on the cell surface of *H. pylori* and the low antibody titer detected in human hosts (Du and Ho, 2003), we postulate that HSP20 could potentially acts as a chaperone in bacterial adhesion and colonization in *H. pylori* infections.

1.4 Interacting Protein of Heat Shock Protein 20

Du and Ho (2004) identified an interaction between HSP20 and cytotoxin associated gene A (CagA) using a co-immunoprecipitation assay as described by Voland *et al* (2003). In the assay, using antibody against rHSP20, a single protein CagA was

pulled down from the protein extract of the wild type *H. pylori*. This interaction was further confirmed by repeating another assay using antibody against rCagA.

1.5 Cytotoxin associated gene A

H. pylori has many virulence factors, which include urease (Mobley *et al.*, 1995), flagellin (Andrutis *et al.*, 1997), CagA (Hocker and Hohenberger, 2003) and VacA (Kusters *et al*, 2006). Among the virulence factors identified, cytotoxin associated gene A (*cagA*) is one of the well-studied virulence factors in *H. pylori* infections. It has been linked to enhanced pathogenicity of the bacterium (Hocker and Hohenberger, 2003). Its effects in the pathogenesis of *H. pylori* infections include induction of the hummingbird phenotype and proinflammatory responses (Bourzac and Gullemin., 2005).

Upon direct contact with the gastric epithelial layer, *H. pylori* delivers CagA into the host cells via its type IV secretion system (Backert *et al.*, 2000). It has been reported to be surface exposed before being translocated into the human cells (Covacci *et al.*, 1993). CagA has also been found to mediate an ectopic assembly of tight junction proteins at the sites of bacterial attachment (Amieva *et al.*, 2003). However, how was CagA being presented to the surface has not been established.

1.6 The gastric epithelial layer

The gastric epithelial layer consists of many apical junctional complexes (Figure 1.1), which consists of many tight junction proteins (Stevenson, 1999). These tight junctional complexes (Figure 1.2) are made up of many peptide components, including zonula occludens (ZO) 1, 2, and 3, occludin, claudins, junction adhesion molecules

(JAM), cingulin and symplekin (Harhaj *et al.*, 2002). The tight junctions are localized at cell-cell contact sites. They serve as a paracellular barrier to restrict the movement of ions and proteins across epithelium. They also serve as the primary barrier to bacterial infections in the human stomach. The disruption of tight junction function is common in malignant cancers of the epithelial tissues (Bilder *et al.*, 2000).

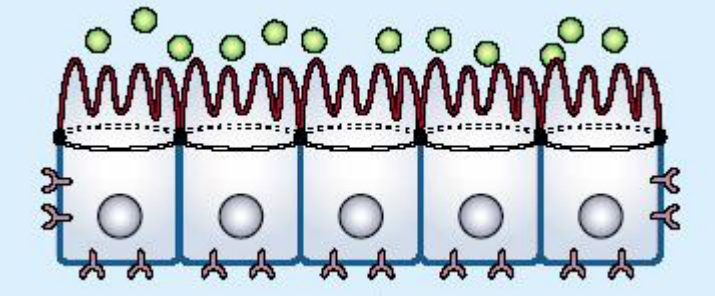

Figure 1.1. The gastric epithelial layer. Epithelial cells have an apical surface (red) that is separated from the baso-lateral surface (blue) by tight junctions (black). The epithelial layer serves as a paracellular barrier to ions and biomolecules (green balls). Figure adapted from Mostov and Zegers, 2003.

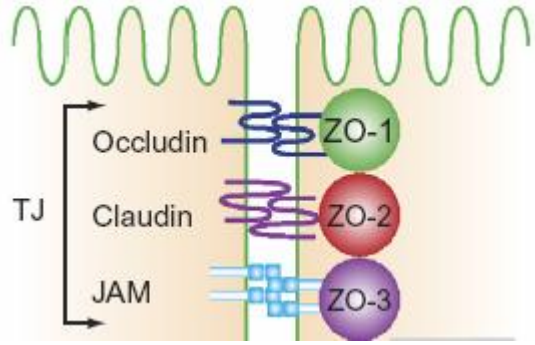

Figure 1.2. Composition of tight junction (TJ). The TJ is made up of many different proteins. Some of the proteins involved in the formation of tight junctions include ZO-1, ZO-2, ZO-3, occludin, claudin and junction adhesion molecule (JAM). Figure adapted from Miyoshi and Takai, 2005.

1.7 Aim of study

It is the aim of this project to study the association between HSP20 and CagA in relation to pathogenesis of *H. pylori* infections. The project will examine the potential role of HSP20 in the establishment of Type IV secretion system (T4SS), translocation of CagA into host and collaboration with CagA in affecting tight junction protein (ZO-1).

SURVEY OF LITERATURE

2.1 *Helicobacter pylori*

2.1.1 The organism

Helicobacter pylori has been observed to reside in the gastric mucosal layer of mammals as early as 1893 (Bizzozero). However, it was only in 1984 that Marshall and Warren successfully cultivated the bacteria from human gastric biopsy specimens. Identified first as Camphylobacter like organism (CLO), it was later renamed *Helicobacter pylori* (Goodwin *et al.*, 1985). The role of *H. pylori* in the etiology of peptic ulcer disease (PUD) (George *et al.*, 1990) and gastric carcinoma (Parsonnet *et al.*, 1991) is now well established.

2.1.2 Present epidemiology of *H. pylori* infections

H. pylori infects the stomachs of up to 50% of the world's human population (Bumann *et al*., 2001). In many developing countries, *H. pylori* infection is almost universal in adults. Covacci *et al.* (1999) reported that in third world countries, prevalence rates increase with poor sanitization, low standards of living and public health.

A local study in 1996 on a cohort of 2626 aged between 6 months and over 65 years showed that 31.4% were seropositive for *H. pylori* (Epidemiological News Bulletin, 1996). *H. pylori* infection is thus reported to be dependent upon the age, geographic location and the socioeconomic status of the subjects studied (Malaty *et al*., 2003; Taylor *et al.,* 1991).

2.1.3 Modes of transmission

Until today, the mode of transmission of *H. pylori* remains to be elucidated. The most widely accepted held hypotheses are that the organism is transmitted directly from person to person by fecal-oral spread, gastric contents (gastric-oral spread) or improperly cleaned endoscopic equipment (Vincent, 1995).

2.1.4 *H. pylori* and gastric carcinoma

Carcinoma of the stomach is the second most common cancer worldwide (Parkin *et al*., 1988) and adenocarcinoma accounts for nearly 95% of all gastric cancers. The association of *H. pylori* and cancer was first described in 1991 by Parsonnet *et al*. It was reported that *H. pylori* patients who eventually developed gastric cancer have higher *H. pylori* seropositivity rates than those who never develop the disease (Parsonnet *et al*., 1991). Also, Watanabe *et al* (1998) has shown that long term *H. pylori* infection in an animal model (Mongolian gerbils) induces formation of tumours located in the pyloric region, similar to the human topography gastric adenocarcinoma. This is the first study to prove a direct cause-effect relationship between *H. pylori* infection and gastric carcinogenesis in an animal model. However, this study has not been able to be repeated anywhere (elsewhere) in the world. Interestingly, *H. pylori* has been classified by the World Health Organization as a type I carcinogen (an agent that is carcinogenic in humans) since 1994 (IARC).

2.2 Heat shock proteins

HSPs are diverse sets of proteins. However, the majority of them share amino acid sequence similarity with the vertebrate eye lens α-crystallin proteins. Many reports

have indicated that both α-crystallin and HSPs are molecular chaperones (Laksanalamai *et al*, 2004; Nakamoto and Vigh, 2007)

HSPs are highly conserved proteins found in all prokaryotic and eukaryotic cells (Laksanalamai *et al.*, 2004). This group of proteins was maintained at a basal level for physiological functions like serving as a molecular chaperone in protein folding and degradation. However, these proteins are usually abundantly produced to induce the heat shock response in the presence of certain factors such as growth factors, virus infection, and stress (Debbie *et al.*, 1991). In addition, their expression levels are also upregulated during the course of most microbial infections and are often targeted by the mammalian immune response (Hoffman and Garduno, 1999).

Among other HSPs, *H. pylori* produces mainly two HSPs: a GroES analogue, class HSP A (HSP13) and a GroEL analogue, class HSP B (HSP60) (Dunn *et al.*, 1992; Suerbaum *et al.*, 1994). Dunn *et al* identified HSP60 in *H. pylori* and showed that this protein is immunogenic in individuals infected with *H. pylori*. Song *et al* (2005) has found that HSP60 induces production of pro-inflammatory cytokines (interleukin 8) in monocytic cells. Surface-associated HSP60 was found to mediate attachment to gastric epithelial cells (Hoffman and Garduno, 1999). The role for HSP60 in colonization, mucosal infection and in promoting inflammation is evident, illustrating its role as a virulence factor in *H. pylori* infections.

2.2.1 Heat Shock Protein 20 (HSP20)

Newly identified HSP20 (Du and Ho, 2003) has a pI of ~5.5 and a molecular weight of ~18kDa. In their study, where recombinant HSP20 antibody was used as a

probe in western blotting of various fractions of *H. pylori*, HSP20 was mainly detected in acid glycine extract that consists of mainly membrane and membrane-associated proteins, implying the surface location of the protein on *H. pylori*. The surface localization was further confirmed using the electron microscopy (Du and Ho, 2003).

HSP20 is identified as Hs1V based on open reading frame prediction of genome sequences. It is a homologue of Hs1V of *Escherichia coli*, a peptidase involved in protein degradation. Hs1V functions with Hs1U, which provides the essential ATPase activity, as a two component protease to degrade SulA, a cell division inhibitor in *E. coli* (Seong *et al*., 1999).

Using ELISA, Du and Ho (2003) showed that the optical density reading clustered within a low range of 0.21 ± 0.02 for both patients with gastroduodenal diseases and control subjects. The authors suggested that HSP20 may not play a vital role in the pathogenesis of *H. pylori* infections. However, since HSP20 is expressed on the cell surface of *H. pylori* and the antibody titer detected in human hosts is low, the potential role of HSP20 as a chaperone in bacterial adhesion and colonization in *H. pylori* infections cannot be excluded.

2.3 Type IV secretion system

The *cag* pathogenicity island (*cag* PAI) of *H. pylori* consists of many genes that code for the Type IV secretion system (T4SS). The *cag* PAI is 40 kilobases long, with a G+C content different from the overall chromosome (Figure 2.1) (Covacci and Rappuoli, 1998).

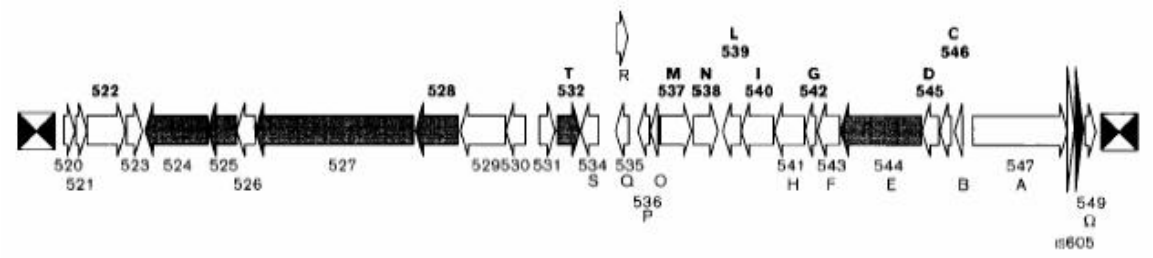

Figure 2.1. The *cag* PAI map. The *cag* PAI is 40 kilobases long and consists many genes that code for the T4SS. (Figure adapted from Covacci and Rappuoli, 1998)

The best-studied model of T4SS is that of *Agrobacterium tumefaciens*. In this plant pathogen, T4SS is used to deliver DNA and proteins into plants cells to introduce bacterial DNA into the plant genome leading to tumour formation.

The T4SS of *H. pylori* bears great resemblance to that of *A. tumefaciens* (Figure 2.2) (Bourzac and Gullenmin, 2005). HP0532 and HP0528, homologues of VirB7 and VirB9 in *A. tumefaciens*, were reported by Tanaka *et al* (2003) to be localized along the length of *H. pylori* T4SS pilus. HP0532 has also been reported by Rohde *et al* (2003) to form a ring at the base of the pilus. It is postulated that HP0532 recruits HP0528 to form a heterodimer, which has a role to play in stabilizing the other VirB homologous proteins with intermolecular disulphide bonds (Backert *et al*, 2000; Christie and Vogel, 2000). *H. pylori* VirB11 protein is also essential in the assembly of the secretion apparatus and has ATPase activity. HP0527, the *H. pylori* homologue of VirB10 of *A. tumefaciens*, forms a sheath around the inner core of the pilus which is induced upon host contact (Rohde *et al*, 2003). HP0539 has been postulated to serve as a chaperone for HP0527 and HP0532 (Rohde *et al*, 2003).

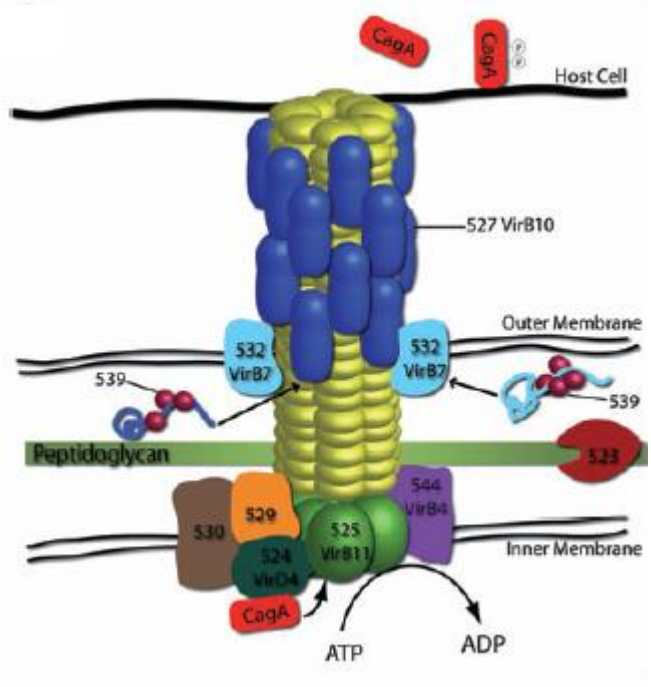

Figure 2.2. Hypothetical illustration of the *cag* PAI T4SS. The apparatus is based on *A. tumefaciens*. The substrate for the secretion system is CagA. This translocation is ATP-dependent. (Figure adapted from Bourzac and Gullemin, 2005)

HP0544 and HP0525 in *H. pylori*, homologues of VirB4 and VirB11 in *A. tumefaciens* respectively, code for inner membrane-localized ATPases that provide energy for substrate translocation. HP0524 (homologue of VirD4 in *A. tumefaciens*) codes for a coupling protein, that is believed to be essential for substrate delivery to the secretion apparatus (Fischer *et al*, 2001; Selbach *et al*, 2002). HP543 (CagF) has been recently reported by Couturier *et al* (2006) to be essential for subtrate translocation. HP0523 functions like VirB1 of *A. tumefaciens*, which is thought to be a transglycosylase that causes local lysis of the peptidoglycan layer to facilitate assembly of T4SS apparatus across the bacterial cell wall (Rohde *et al*, 2003; Terradot *et al*, 2005). It is also essential for maturation of HP0527, HP0532, and HP0539 (Rohde *et al*, 2003). In *H. pylori*, CagA is the only reported substance found to be translocated across the T4SS (Backert *et al.*,

2000). Once in the host cells, tyrosine phosphorylated CagA triggers off many cellular pathways to result in activties such as formation of hummingbird phenotype and cytokine production (Christie and Vogel, 2000; Bourzac and Gullemin, 2005).

2.4 Cytotoxin associated gene A (CagA)

The best known virulence factors of *H. pylori* include urease, flagella, superoxide dismutase and several molecules involved in a specific adhesion to the superficial epithelial cells of the stomach. Among all these virulence factors identified, CagA is one of the well-studied virulence factors in *H. pylori* infections.

CagA is a highly immunogenic protein of 116-140 kDa molecular weight (Laqinto *et al.*, 2000). CagA is encoded by *cagA*, which is found in 60–70% of *H pylori* strains in the industrialized world (Hocker and Hohenberger, 2003) but is present in 80-90% of *H. pylori* isolates in Asian countries (Zheng *et al*., 2000; Ramelah *et al*., 2005). *cagA* is found in the *cagPAI*, a gene cluster of 29 genes spanning 37 kb of genomic DNA. Some of the genes in the *cagPAI* region encode a type IV bacterial secretion apparatus, which can translocate CagA into host target cells.

Upon direct contact with the gastric epithelial cell, *H. pylori* delivers CagA into the host cells via its type IV secretion system (Backert *et al.*, 2000). Within the target cells, CagA protein is activated by phosphorylation at defined tyrosine phosphorylation motifs and SHP-2, a Src homology 2 (SH-2) domain containing tyrosine phosphatase, binds to the phosphorylated tyrosine on the CagA protein (Sugiyama and Asaka, 2004). Once activated, CagA may trigger host signaling pathways and subsequently influence host cellular functions, including proliferation, apoptosis, cytokine release, and cell

motility. Thus, it has been linked to enhanced virulence and pathogenicity of the bacterium (Crabtree *et al*, 1991; Kuipers *et al*, 1995; Covacci *et al*, 1999; Hocker and Hohenberger, 2003) and is frequently associated with severe gastric inflammation, ulceration and an increased risk of gastric cancer (Blaser *et al*, 1995; Censini *et al*, 1996)

2.5 Hummingbird phenotype

CagA translocation has been reported to be accompanied by a dramatic elongation of the infected AGS cells (Segal *et al,* 1999; Backert *et al*, 2000, 2001, 2005; Higashi *et al*, 2002; Mimuro *et al*, 2002; Stein *et al*, 2002; Selbach *et al*, 2002, 2003; Moese *et al*, 2004). This spindle-like morphology of the infected cells is termed as the hummingbird phenotype with the presence of thin, needle-like protrusions of 20 μm to 70 μm in length. Moese *et al* (2004) observed that the establishment of the hummingbird phenotype in infected AGS cells was obtained 2 hours post infection. They also reported that this elongation phenotype was mainly dependent on the presence of CagA translocation. The induction of hummingbird phenotype has since been identified as one function of translocated CagA (Segal *et al,* 1999; Backert *et al*, 2000, 2001, 2005; Higashi *et al*, 2002; Mimuro *et al*, 2002; Stein *et al*, 2002; Selbach *et al*, 2002, 2003; Moese *et al*, 2004).

2.6 IL8 secretion

In addition to hummingbird phenotype induction, one of the well established functions of translocated CagA is the induction of cytokine production such as IL8 production (Munzenmaier *et al*, 1997; Yamaoka *et al*, 1997; Covacci *et al*, 1998; Odenbreit *et al*, 2001; Fischer *et al*, 2001; Selbach *et al*, 2002; Backert *et al*, 2004;

Brandt *et al*, 2005). IL8 is a potent neutrophil and T-cell chemoattractant and activator, which is believed to play an important role in the pathogenesis of *H. pylori*-induced tissue damage (Rieder *et al*, 1997; Yamaoka *et al*, 1998; Ogura *et al*, 2000).

Yamaoka *et al* (1997) reported that *cagA* positive *H. pylori* strains induce a much elevated level of IL8 than *cagA* negative strains. Although it has been found that the *cagA* gene is important for IL8 production, it has been reported that other functional *cag* genes such as *cagC*, *cagD*, *cagE* are also important for IL8 production too (Munzenmaier *et al*, 1997).

It was also found that CagA-mediated IL8 induction requires the activation of transcription factor nuclear factor $_k$B (NF_kB) (Munzenmaier *et al*, 1997). Recently Brandt *et al* (2005) reported that this release occurs via Ras→Raf→Mek→Erk→NF_kB signaling pathway.

2.7 The gastric epithelial layer

Polarized epithelial cells of the human stomach carry out functions such as the transport of ions and nutrients, the secretion of protein products, and the protection of the interior of the organism from invading micro-organisms. Features of cell polarity are observed in the functionally distinct portions of the plasma membrane, known as the apical domain and the basolateral domain.

The apical domain contains anion channels, H+/K+-ATPase, and transporters; whereas the lateral portion of the basolateral domain contains proteins involved in the attachment to neighboring cells and in cell–cell communication. The basal portion of the basolateral domain contains the binding sites for constituents of the basal lamina, and

receptors for hormones and other signaling molecules that regulate the function of the cell (Alberts *et al.*, 2002).

Tight junctions appear as continuous networks of parallel and interconnected strands that circumscribe the apex of lateral membranes of adjacent cells (Figure 2.3). The tight junctions, localized at the apical end of the basolateral membrane, play key roles to establish epithelial polarity (Yamamoto *et al*, 1997; Anderson and van Itallie, 1999). These junctions provide paracellular barriers to prevent leakage of molecules across the epithelia through gaps between their cells, and also serve as fences between the apical and baso-lateral domains of the plasma membranes in epithelial cells, preventing diffusion of integral proteins and lipids from one to the other (Balda and Matter, 1998). They also serve as the primary barrier to bacterial infections in the human stomach.

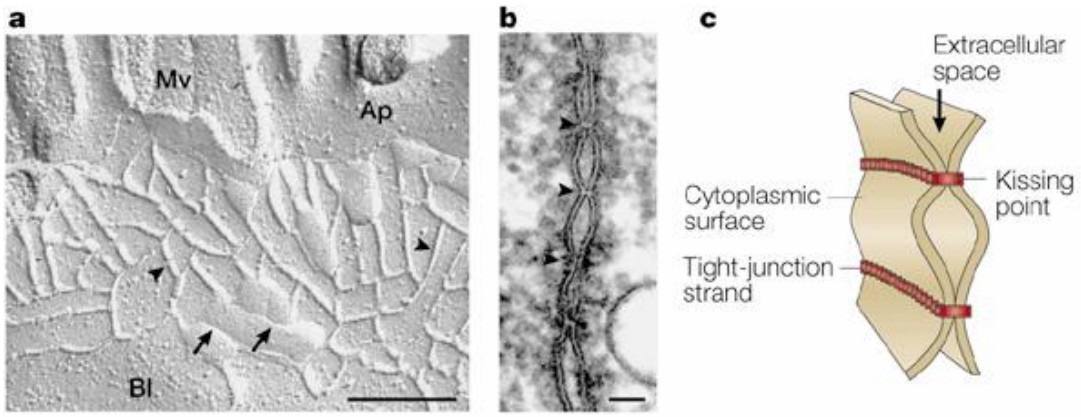

Figure 2.3. Structure of tight junction. a) Freeze-fracture replica electron microscopic image of intestinal epithelial cells. Tight junctions appear as a set of continuous, intramembranous particle strands or (Mv, microvilli; Ap, apical membrane; Bl, basolateral membrane) Scale bar, 200 nm. b) Ultrathin sectional view of tight junctions. At kissing points of tight junctions (arrowheads), the intercellular space is obliterated. Scale bar, 50 nm. c) Schematic of three-dimensional structure of tight junctions. Each tight-junction strand within a plasma membrane associates laterally with another tight-junction strand in the apposed membrane of an adjacent cell to form a paired tight-junction strand, obliterating the intercellular space (kissing point). Figure adapted from Tsukita, 2001.

2.7.1 Tight junction proteins

The tight junctions are made up of many peptide components, including zonula occludens (ZO) 1, 2, and 3, occludin, claudins, junction adhesion molecules (JAM), cingulin, and symplekin (Harhaj *et al.*, 2002). Of these tight junction proteins, ZO-1, which is the marker protein of tight junction in *H. pylori* (Yamamoto *et al*, 1997), is the tight junction protein of interest in this project.

ZO-1 is a 220 kDa phosphoprotein that contains three PDZ domains, Src-homology (SH)3 domain and an inactive guanylate kinase domain (Mitic and Anderson, 1998). Multidomain ZO-1 could bind several different protein partners to control the dynamics of tight junction assembly. For instance, ZO-1 binds the tight junction transmembrane proteins such as occludin and claudin with their N terminal (Gumbiner *et al.*, 1991; Haskins J *et al.*, 1998; Stevenson B. R. *et al.*, 1986). Tight junction disassembly is associated with increased paracellular permeability, decrement of transepithelial resistance (TER) and displacement of ZO-1 from the tight junctions.

2.7.2 Tissue culture cell lines

For *in vitro* cell studies, it is essential to choose an appropriate model such that it is able to accurately reflect the results of infection *in vivo*. For this reason, tissue culture cell lines of gastric origin are commonly chosen for *H. pylori* studies (Nilius *et al.*, 1994).

Clyne and Drumm in 1993 also discovered that *H. pylori* strains PU3, PU4, PU5, PU6 and 136292 bound better to gastric cells than to colonic or duodenal cells. Their findings also suggested that the bacteria exhibited similar tropism for gastric cells *in vivo* and *in vitro*. This is coupled by Nishihara *et al*'s findings (1999) that *H. pylori* binds well to AGS cells, which is a gastric cell line. Furthermore, many *H. pylori* studies use AGS

cells for *in vitro* studies (Heczko *et al.*, 2000; Kaji T *et al.*, 2002; Zhang ZW *et al.*, 2002). Thus, AGS cells were chosen for this project.

Although *H. pylori* binds better to gastric cells than it did to colonic cells, T84 cell line was also employed for this project. This is mainly because part of this project deals with tight junction study and T84 has been regarded as a good *in vitro* model to study tight junctions due their organized tight junctions (Amieva *et al.*, 2003; Terres *et al.*, 2003).

2.8 Tight junction function disruption

2.8.1 Other bacterial systems

In order to gain access to the deeper tissues and cause disease, bacterial pathogens must first breach the epithelial barrier. The epithelial barrier has an inherent function to serve as a first line of defense against entry of most human pathogens. Thus, it has become increasingly apparent that several bacterial pathogens are able to disrupt the tight junctions, thereby rendering the epithelial layer liable to bacterial invasion.

For *Clostridium difficile*, Hecht *et al* (1988) has revealed that infection by the bacterium for a period of 6 hours abolished trans-epithelial resistance across T84 cells. Chen *et al* (2002) reported that there was an increased translocation of ZO-1 from the tight junctions due to infection, resulting in the various paracellular permeability changes.

Cywes *et al* (2001) has recently found that *Streptococcus pyogenes* induces cytoskeletal rearrangements, which was found to be associated with the loss of both ZO-1 and E-cadherin. The resultant tight junction disruption facilitated bacterial invasion.

Enterotoxigenic strains of *Bacteroides fragilis* produce a toxin named fragilysin. This toxin results in cleavage of ZO-1 and E-cadherin (a zonula adheren protein) (Wu *et*

al., 1998), which effects in an alteration in the tight junction composition. This alteration negatively interferes with the tight junction functions.

Muza-Moons (2004) has found that enteropathogenic *Escherichia coli* infection effects in morphological changes in the tight junction proteins. ZO-1 were found to lose their apically restricted localization and uniformly distributed across the cells. As a result of this alteration of distribution, there was disruption of the tight junction function as seen by the progressive decrease of 62.7% in TER 5 post infection.

2.8.2 CagA and disruption of tight junction function

CagA, which is surface exposed before being translocated into the human cells (Covacci *et al.*, 1993), has been found to mediate an ectopic assembly of tight junction proteins (ZO-1) at the sites of bacterial attachment (Amieva *et al.*, 2003). The authors found that the CagA-mediated ZO-1 recruitment altered the composition of tight junctional complex and interfered with the normal proper functioning of the tight junctions. After infecting MDCK cells for 24 hours, the individual tight junctions were unable to function properly to exclude the apically introduced ruthenium red dye from the baso-lateral chamber.

Epithelial cells are characterized by strong cell to cell adhesion and pronounced cell polarity. However, cancers of epithelial origin lose these characteristics when they develop into malignant cancers (Bilder *et al*., 2000). Malignant cancers possess the common trait of cell invasion and metastasis. The disruption of epithelial tight junctions is one of the hallmarks of oncogenic transformation (Bilder *et al*., 2000; Dhawan *et al*., 2005; Lee *et al*., 2005).

MATERIAL & METHODS

3.1 Bacterial strains

Non-motile *H. pylori* ATCC 26695 strain was used for this study. This strain is positive for both the *hsp20* and *cagA* gene.

3.1.1 Culture of *H. pylori*

All *H. pylori* strains used in this study were cultured on chocolate blood agar (blood agar base 2, Oxoid supplemented with 5% lysed horse blood (Appendix 1). The plates were then incubated at 37°C in a 5% carbon dioxide humidified carbon dioxide incubator (Forma Scientific). Generally, 2 days old cultures comprising mainly spiral form of *H. pylori* were used for this project as cells that are older than 2 days old would convert into the viable but non-culturable coccoid form (VNBC) which is not the objective of this project.

3.1.2 Harvesting of bacterial cells

The bacterial cultures were harvested using sterile swaps (Copan) in phosphate buffer saline (PBS) (Appendix 6) and centrifuged at 6000 x g for 10 minutes at 4°C. The cell pellet was then washed in PBS. The bacterial cells were loaded onto a haemocytometer (Weber Scientific International Ltd) and enumerated under the microscope (Olympus B30) at 100 x magnification. The bacterial cells were then suspended in an appropriate volume of Brain Heart Infusion Broth (BHI) (Oxoid) (Appendix 3) for use in infecting the cell lines.

3.1.3 Maintenance of *H. pylori* cultures

H. pylori cells were harvested from culture plates with confluent growth using sterile cotton swaps (Copan) and suspended into a cryotube (Nunc) containing 1 ml of

BHI (Oxoid) (Appendix 3) supplemented with 20% glycerol. The cryotube was stored at -80°C until use.

3.1.4 Confirmating tests of *H. pylori*

The bacterial cultures were identified as *H. pylori* based on the cell morphology by Gram staining, as well as positive urease, catalase and oxidase tests.

3.1.4.1 Gram staining

The bacterial smears were air-dried and heat fixed. The smears were stained with crystal violet for 1 minute followed by 1 minute with iodine, rinsed off the stain with alcohol and washed under running water. The smear was then counterstained with carbol fuchsin for 10 minutes. The slide was blotted dry and viewed under 100 x magnification. The presence of Gram negative spiral-shaped bacteria is the key to confirming *H. pylori.*

3.1.4.2 Urease test

The bacterial culture was inoculated into urease reagent (pH 6.8) (Appendix 6). Presence of *H. pylori* was confirmed when the urea solution turned red/pink within minutes. *H. pylori* is able to survive in the acid environment as it produces abundant urease that converts urea in the medium to ammonia (NH_4^+) and carbon dioxide. NH_4 ions released increased the pH that changes the indicator from yellow to pink/red.

3.1.4.3 Catalase test

H. pylori possesses catalase, which is an enzyme that decomposes hydrogen peroxide into water and oxygen. A positive catalase test (Appendix 7) is indicated by the presence of effervescence (oxygen bubbles) upon inoculation of culture into reagent.

3.1.4.4 Oxidase test

A positive reaction was indicated by a purple colour change at the site of inoculation. The colour change was due to the presence of the enzyme oxidase which oxidises the oxidase reagent (1-% tetra-methyl-p-phenylenediamine dihydrochloride).

3.2 Identification of protein interacting with HSP20 in *H. pylori*

Interacting proteins of HSP20 was identified in earlier studies (Du and Ho, 2004). The procedure for co-immunoprecipitation analysis using antibody against rHSP20 was carried out according to that as described by Voland *et al* (2003). The protein band of interest were excised and digested according to in-gel trypsin digestion as described by Shevchenko *et al*. (1996) before sending off for mass spectrometry analysis (at Proteomics Protein Centre, NUS, Singapore)

3.3 Tissue culture cell lines

For this project, the cell lines used were AGS (ATCC CRL-1739) and T84 (ATCC CCL-248). These cell lines were obtained from the American Type Culture Collection (ATCC). AGS cells are gastric epithelial cells originally derived from gastric adenocarcinoma. This cell line was chosen as it has been proven to allow the attachment of *H. pylori* and is suitable as an *in vitro* model (Nishihara *et al*, 1999). In addition, AGS cells are commonly used for *H. pylori* studies (Kaji *et al*, 2002; Zhang *et al*, 2002; Heczko *et al*, 2000). However AGS cells form weakly organized tight junctions even though these cells have the various tight junction proteins. In view of this, a second cell line, T84 cell line, was used. T84 is an epithelial colonic cell line which forms very

organized tight junctions (Amieva *et al*, 2003), thus is an ideal model for tight junctions studies.

3.3.1 Growth conditions

AGS cells were grown in 25 cm^2 tissue culture flasks (Nunc) with Roswell Park Memorial Institute (RPMI)-1640 medium (Sigma) supplemented with 10% fetal bovine serum (GIBCO-BRL) and 2% L-glutamine (GIBCO-BRL) (Appendix 9). In contrast, T84 cells were grown with Dulbecco's Modified Eagle medium (DMEM) (Sigma) supplemented with 10% fetal bovine serum (GIBCO-BRL), 2% L-glutamine (GIBCO-BRL) and (Appendix 10). The tissue flasks were incubated at 37°C (95% humidity and 5% carbon dioxide) in a carbon dioxide water-jacketed incubator (Forma Scientific).

Both AGS and T84 cells were passaged to ensure continual division and growth every 3-4 days and 6-7 days respectively. In each case, the spent medium was first removed before washing with 5 ml of PBS to remove traces of the medium as it may contain components that may inhibit trypsin-EDTA (Sigma) (Appendix 11). After washing with PBS, the cells were incubated at 37°C for 5 minutes with 2 ml of 10% trypsin-EDTA to release the cells from the flask surface. The cells were aspirated by gentle pipetting. The cells were then harvested (by low speed centrifugation) and resuspended in the respective growth medium. The resuspended cells were transferred and seeded into new culture flasks.

3.3.2 Preservation

After decanting the spent medium, the cells were washed with PBS and incubated at 37 °C for 5 minutes with 2 ml of 10% trypsin-EDTA. A volume of 5 ml of growth

medium was added to dilute the trypsin-EDTA. The respective growth mediums were used for the different AGS (Appendix 9) and T84 cells (Appendix 10). After harvesting by low speed centrifugation, the cell pellet was resuspended in 1ml of growth medium supplemented with 10% DMSO (Appendix 12) and pipetted into a cryotube (Nunc). The cells were stored at -196°C in liquid nitrogen until use.

3.3.3 Cell count

For enumeration, AGS and T84 cells were first washed twice with 5 ml PBS (to remove floating dead cells) before the addition of 10% trypsin-EDTA and incubated at 37°C for 15 minutes to ensure that all the cells have detached from the flask surface. The cells were loaded onto the haemocytometer (Weber Scientific International Ltd) and enumerated under the microscope (Olympus B30) at 40 x magnification.

3.4 Chromosomal DNA extraction

Bacterial cells were harvested as described in section 3.1.2. Chromosomal DNA was extracted using the QIAamp DNA mini kit (Qiagen) according to manufacturer's protocol.

3.5 Polymerase Chain Reaction (PCR)

PCR was carried out to determine the presence or absence of the *hsp20* gene, *cagA* gene and *cag* empty site (Mukhopadyay *et al*, 2000; Hsu *et al*, 2002) in the chromosomal DNA of the different *H. pylori* 26695 deletion mutants used in this project. *cag* empty site was amplified using Lunil and cagR5280 (Table 3.1). These 2 primers are specific to regions in the *H. pylori* 26695 chromosome flanking the left (546882-546900

bp of the complete *H. pylori* 26695 genome) and right ends (584813-584794 bp of the complete *H. pylori* 26695 genome) of the *cag* PAI respectively. The resultant PCR product of 1908 bp consists of 282 bp of the region flanking the left ends of the *cag* PAI, 1402 bp of the kanamycin resistant gene, and 224 bp of the region flanking the right ends of the *cag* PAI.

The PCR reaction was carried out in an amplification thermal cycler (Perkin Elmer, USA). The 50 µl reaction mixture used for the detection of *hsp20*, *cagA*, and *cag* empty site included 50 ng genomic DNA, 50 pmol primers (forward and reverse) (Table 3.1), *Taq* DNA polymerase (DynaZyme), dNTPs (dATP, dGTP, dCTP and dTTP), 10x incubation buffer and sterile distilled water (Appendix 14).

The amplification reaction includes 39 cycles of denaturation at 94^0C for 1 minute, annealing at 50°C for 1 minute and elongation at 72°C for 1 minute. The reaction mixture temperature was then brought down to 4°C and stored at 4°C until use.

Aliquots of 10 µl of each of the PCR products were then electrophoresed in 1% agarose gels for 1 hour at 80 V in 1X TAE buffer (Appendix 15). The gel was placed with the wells nearer the negative ends of the gel tank. This is because DNA is negatively charged due to the exposed phosphate backbone. Hence the DNA would move towards the anode during the electrophoresis process. TAE buffer was added until the agarose gel was completely submerged. A 6X loading buffer (Appendix 16) was then mixed with 10 µl of the PCR product before loading into the well in the agarose gel. After the electrophoretic run, the ethidium bromide (Appendix 17) stained gels were then photographed with filtered ultraviolet (UV) illumination.

Table 3.1. Sequences of primers used in the PCR reaction mixture

	Primer sequence	Target DNA fragment (bp)	Reference
hsp20 detection	HSP RT-F: CGG GAT CCC TCA TTG GAG GCG ATG GGC AG HSPRT-R: GCC TGC AGC CAT TCT TTG CTG AAA TCC AC	270	-
cagA detection	FcagA: AAT ACA CCA ACG CCT CCA AG RcagA: TTG TTG CCG CTT TTG CTC TC	400	Lage *et al*, 1995
cagE detection	cagER: GTT ACA TCA AAA ATA AAA GGA AGC G cagEF: CAA TAA TTT TGA AGA GTT TCA AAG G	735	Hsu *et al*, 2002
cagG detection	cagGF: GCC ATG TTA ACA CCC CCT AG cagGR: TTA ATG CGC TAG AAT AGT GC	497	Hsu *et al*, 2002
cag PAI empty site detection	Lunil: ACA TTT TGG CTA AAT AAA CGC TG CagR5280: GGT TGC ACG CAT TTT CCC TTA ATC	1908	Mukhopadyay *et al*, 2000; Hsu *et al*, 2002

3.6 Generation of deletion mutants

The deletion mutants used in this project were constructed using the PCR-based method as described by Chalker *et al.* (2001) and Tan & Berg (2004).

3.6.1 *hsp20* deletion mutant of *H. pylori* 26695

3.6.1.1 Generation of the knockout construct

Chromosomal DNA from *H. pylori* 26695was extracted as described in section 3.3. Using the chromosomal DNA as template, 2 different PCR products were obtained with 2 different sets of primers (Table 3.2). The kanamycin resistance cassette was obtained by performing a PCR reaction with pILL600 plasmid as template (Ferrero *et al*, 1992). pILL600 plasmid was kindly provided by Dr. Labinge A of Pasteur Institute, Paris, France.

Table 3.2. Primers used for construction of *hsp20* (HP0515) deletion mutant

Target DNA fragment	Primer sequence	Length of target DNA fragment (bp)	Reference
Upstream region flanking the *hsp20* gene	hsp20F2: 5' GGA AGT AGA GCT AGA AAC AAA A 3' hsp20kanR2: 5' ATG GTT CGC TGG GTT TAT C CCA AGC TTG ACT TCA ATC TCA T 3'	564	-
Downstream region flanking the *hsp20* gene	hsp20kanF: 5' GGA TGA ATT GTT TTA GTA CC CGC TTA TTT AGA TGA ATA CAT CAT T 3' hsp20R: 5' GGC TGT TAG CGT ATT CTT GTT T 3'	556	-
Kanamycin resistant cassette	kanF: 5' GAT AAA CCC AGC GAA CCA T 3' aphAR: 5' GGT ACT AAA ACA ATT CAT CCA GTA 3'	1402	Ferrero *et al*, 1992

Sequences of primers used for each of the 3 fragments needed for the generation of knockout constructs for *hsp20* deletion mutant of *H. pylori* 26695. Sequence highlighted in yellow indicates the kanF complement while sequence highlighted in blue indicates the aphAR complement.

Table 3.3. Sequences of primers used for generation of knockout constructs for *hsp20* deletion mutant of *H. pylori* 26695.

Target DNA fragment	Primer sequence	Length of target DNA fragment (bp)
Final knockout construct	hsp20F2: 5' GGA AGT AGA GCT AGA AAC AAA A 3' hsp20R: 5' GGC TGT TAG CGT ATT CTT GTT T 3'	2522

The PCR reaction included 39 cycles of denaturation at 94 ^{0}C for 1 minute, annealing at 52°C for 1 minute and elongation at 72°C for 1-3 minute. The reaction mixture temperature was then lowered and maintained at 4°C until use. Each of the PCR products was purified using QIA quick PCR purification kit (Qiagen). Primers hsp20kanR2 and hsp20kanF consist of 5' leaders, that are complementary to kanF and aphAR with a gene specific sequence of 22 bp and 25 bp respectively. Thus, the resulting PCR products 2 and 3 (Figure 3.1) have sequences complementary to that in the

kanamycin resistant gene. In this way, the 3 purified PCR products were ligated to obtain the resultant knockout construct of 2522 bp by performing another PCR reaction (Table 3.3). The final knockout construct was then purified using QIA quick PCR purification kit (Qiagen) and stored at 4°C until use.

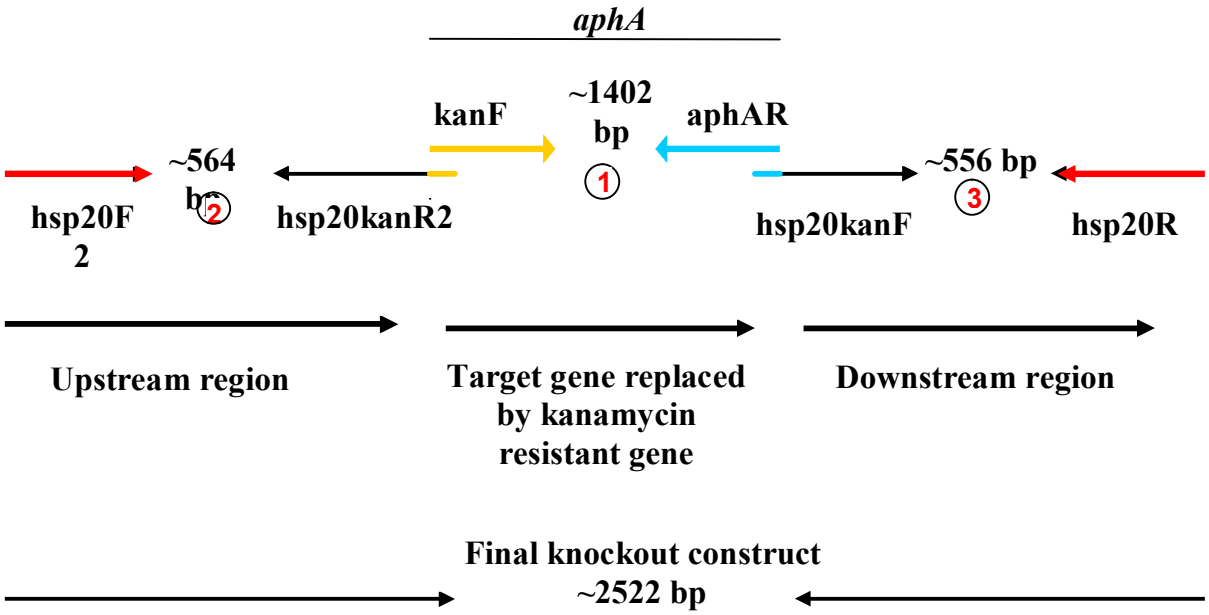

Figure 3.1. Illustration of the final knockout construct for *hsp20* deletion mutant of *H. pylori* 26695

3.6.1.2 Tranformation into *H. pylori* 26695

H. pylori 26695 strain was transferred from a 2 day old culture to a fresh chocolate blood agar plate and was left in the CO_2 incubator at 37ºC for 4-6 hours. The purified DNA knockout construct was then added onto the plate and returned to the incubator. The plate was incubated for 2-3 days till confluency was observed. To select for the kanamycin resistant *hsp20* deletion mutant, the bacteria was transferred to a selective chocolate agar supplemented with kanamycin (Appendix 2) and a further 7-10

days. Single colonies were then picked and subcultured to obtain confluent plates cultures. DNA was extracted as described in section 3.3 and PCR was carried out to confirm the absence of the *hsp20* gene, using primers stated in Table 3.1.

3.6.2 *cagA* deletion mutant and *hsp20/cagA* deletion mutant

The *cagA* (HP0547) and *hsp20/cagA* knockout constructs were generated using the method as described in section 3.6.1.1 and transformed into *H. pylori* 26695 as described in section 3.5.1.2. The 2 deletion mutants of *H. pylori* 26695 were kindly provided by Dr. SY Lui of Dept Microbiology, NUS, Singapore.

3.6.3 *cag* PAI deletion mutant

The knockout construct (Figure 3.2) was kindly provided by Prof. R Haas (Odenbreit *et al*, 2000, 2001; Rohde *et al*, 2003). The construct was first transformed into competent *Escherichia coli* Top10. Competent *E. coli* cells were incubated with the construct on ice for 30 minutes. The mixture was then given a heat shock by incubating at 42°C for 90 seconds without shaking. After cooling the mixture on ice for a minute, fresh Luria-Bertani media (Appendix 3) was added. The mixture was then incubated at 37°C with shaking (180 rpm) for 90 minutes. After the incubation, the mixture was plated out onto Luria-Bertani agar supplemented with kanamycin (Appendix 4) and incubated overnight at 37°C. Single colonies were picked and inoculated into Luria-Bertani broth. The DNA construct was extracted from the culture using the QIAprep Spin Miniprep Kit (Qiagen). The construct was checked by restriction enzyme digestion as described in section 3.5.4 and confirmed by PCR reaction as described in section 3.4.

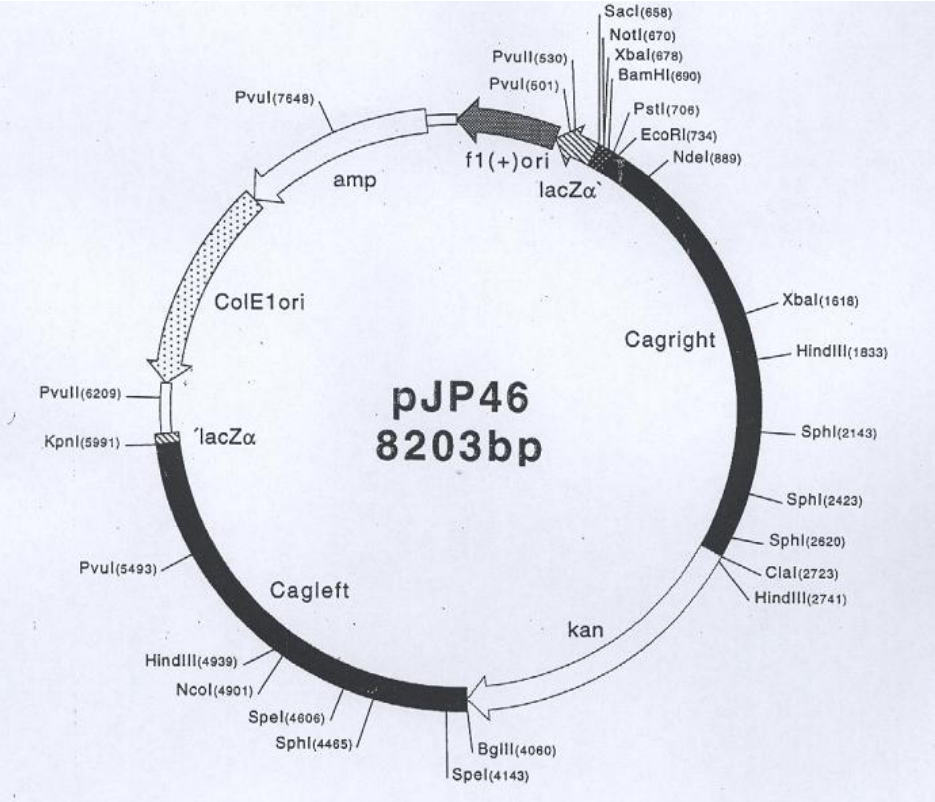

Figure 3.2. Map of *cag* PAI knockout construct. (Odenbreit *et al*, 2000, 2001)

The harvested construct was then transformed into *H. pylori* 26695 as described in section 3.5.1.2. The confirmation of the *cag* PAI deletion in *H. pylori* 26695 was carried out by checking the presence of the *cag* PAI empty site (Table 3.1) using PCR and sequencing the 1908 bp *cag* PAI empty site fragment as described in section 3.6.5.

3.6.4 Restriction Enzyme Digestion

An aliquot of 0.2 µg DNA was mixed with distilled water to a volume of 18 µl. Restriction enzymes, EcoRI and SpeI, were added after the addition of 2 µl of 10X restriction enzyme buffer. The mixture was mixed well and incubated at 37°C for 2 hours. The reaction was stopped by boiling the mixture for 10 minutes. After cooling, the mixture was verified by gel electrophoresis as described in section 3.4.

3.6.5 Sequencing

Using the genomic DNA extracted from the *cag* PAI deletion mutant of *H. pylori* 26695 as template, PCR was performed to obtain the 1908 *cag* PAI empty site fragment. Cycle sequencing was then performed on this fragment using ABI PRISM BigDye Terminator v3.1 cycle sequencing kit (Applied Biosystems). The 20 µl sequencing reaction consists of ready reaction premix, BigDye sequencing buffer, 3.2 pmol primer, 40 ng of DNA template and water. Four separate reactions were carried out using each of the 4 primers, that is Lunil and CagR5280 (Table 3.1) and kanF and aphAF (Table 3.2), in each reaction mixture. The sequencing reaction include an initial denaturation of 96°C for 1 minute, followed by 25 cycles of 96°C for 10 seconds, 50°C for 5 seconds, and 60°C for 4 minutes. At the end of the sequencing reaction, the reaction temperature was reduced and stored at 4°C.

For each of the sequencing reactions, the content was mixed with 3M sodium acetate and cold 95% ethanol and incubated on ice for 30 minutes. The mixtures were centrifuged for 30 minutes at 20000 x g at 10°C. The supernatants were then discarded and the pellets were rinsed with 70% ethanol. They were dried in vacuum centrifuge (Heto) before sending off for sequencing by ABI PRISM® 3100 Genetic Analyzer.

3.7 Infecting *in vitro* culture cell lines with *H. pylori*

AGS/T84 cell numbers were determined as described in section 3.1.2. The monolayer was washed twice with PBS. After washing, growth medium (Appendix 9 and 10) were supplied to the AGS and T84 monolayers respectively. *H. pylori* were harvested (Section 3.1.2) and diluted or concentrated accordingly in BHI to obtain the desired cells

(AGS/T84): bacteria (*H. pylori*) cell ratio of 1:50 (Rohde *et al*, 2003; Tanaka *et al*, 2003). The ratio of BHI: RPMI medium was 1:10 (Amieva *et al*, 2003). The mixture was incubated at 37°C.

3.8 Protein extraction

The spent medium of the infected monolayer cells was decanted and washed thrice with PBS. For protein extracts used for examination of CagA translocation, the monolayer was treated with 2 ml of 1X trypsin-EDTA (Sigma) for 5 minutes at room temperature to remove the adherent *H. pylori* (Backert S *et al*, 2000). The monolayer was then washed thrice with PBS. The monolayer was then harvested by scraping it and centrifuging the cell suspension at 1000 x g for 10 minutes at 4°C. The cell pellet was then washed 5 times in fresh PBS at 1000 x g for 10 minutes at 4°C each. The cells were then suspended in lysis buffer (Appendix 18) and incubated on ice for 1 hour. After which, the mixture was centrifuged at 20000 x g for 15 minutes at 4°C to obtain the supernatant which contains the proteins. The proteins were stored at -20°C until use.

3.8.1 Lowry's assay

The total protein concentration was quantified by the method as described by Lowry (1951) using bovine serum albumin (BSA) as the standard. Known quantities of BSA (0, 25, 50, 75, 100 µg) in 500 µl of deionised water were mixed with equal volume of copper solution (Appendix 19) and incubated for 10 minutes at room temperature. After which, 2 ml of Folin-Ciocalteu reagent (Merck) was added and the reaction mixture was incubated for 5 minutes at 55°C. The mixture was cooled to room temperature and

the absorbance for the samples including protein standards were read at 650 nm using DU 640B Spectrophotometer (Beckman Coulter). The BSA standard curve was plotted and used to quantify the total amount of protein in the samples.

3.9 SDS-PAGE

SDS-PAGE (Sodium dodecyl sulphate – polyacrylamide gel electrophoresis) was used to separate proteins according to their molecular weight. SDS binds to hydrophobic portions of a protein, disrupting its folded structure and allowing it to exist stably in solution in an extended conformation. As a result, the length of the SDS-protein complex is proportional to its molecular weight.

The two-gel system (stacking and separating gel) improves the resolution of separation. This is due to the effect of the protein forming a compact stack in the stacking gel before entering the separating gel.

Vertical mini-slab gels comprising 12% separating gel and 8% stacking gel (Appendix 20) were routinely casted using the Mini-protean II system (BioRad). Electrophoresis was performed at a constant voltage of 100V (Power Pac 200, Biorad) for 90 minutes.

3.10 Western blotting

All protein samples were resolved on 12% SDS-PAGE gels and transferred to PVDF membranes (ImmobilonP, Millipore) by semi-dry blotting using Trans-Blot® SD Semi-Dry Transfer Cell (Biorad). The non-specific binding sites of the membrane were

blocked overnight (Appendix 24). The membrane was then incubated with primary antibody (polyclonal rabbit anti-recombinant HSP20 (rHSP20) or monoclonal mouse anti-CagA, Santa Cruz Biotechnology) (Appendix 24) at 1:1000 dilution for 2 hours at room temperature on a belly dancer (Stovall Life Sciences, Inc). Following which, the membranes were washed with PBS-T (Appendix 23) 3 times for 10 minutes each and incubated with horseradish peroxidase-conjugated goat anti-rabbit or goat anti-mouse secondary antibody (1:2000) (DAKO) (Appendix 25) for 2 hours with slight agitation. The membranes were washed again in PBS-T and the immunoreactive protein bands were visualized using enhanced chemiluminescence (ECL™) detection system (Amersham Biosciences). Protein bands were visualized on Hyperfilm™ ECL™ (Amerham Pharmacia Biotech).

3.11 Immuno-gold labeled transmission electron microscopy (TEM)

After decanting the media, the AGS cells were washed twice with PBS. The cells were then fixed in 4% paraformaldehyde (Appendix 26) and 0.2% glutaraldehyde (Appendix 27) for ten minutes. The cells were harvested by scraping and centrifuging the cell suspension at 2200 x g for 5 minutes at 4°C. The cell pellet was re-suspended in fresh fixative for 30 minutes at 4 °C before washing thrice in PBS for 5 minutes each. The cells were then dehydrated in ascending grades series of ethanol (25%, 50%, 75%, 95%, 100%) at room temperature. The cells then underwent London Resin (LR) white infiltration at room temperature by passing the cells once through 1 part ethanol and 1 part LR white for 30 minutes followed by once through 1 part ethanol and 3 parts LR white for 30 minutes, and twice through pure LR white for 1 hour each. The cells were

then incubated with fresh pure LR white overnight. The infiltration continued the next day with 3 incubation of fresh pure LR white for 1 hour each at room temperature before an overnight incubation with fresh pure LR white. The cells were embedded in gelatin capsule and left in 50°C for 48 hours to polymerize.

After polymerization, sectioning was carried out using UltraCut E Microtome (Leica) to obtain ulta-thin sections of 70-100 nm. These sections were neutralized with 0.05M glycine (Appendix 28). After washing with PBS, the sections were blocked with 0.5% BSA-PBS and then conjugated with primary antibodies (monoclonal mouse anti-CagA antibodies and polyclonal rabbit anti-HSP20 antibodies) each at a time for 1 hour. This is followed by incubation with secondary antibodies (anti-mouse IgG conjugated with 20 nm gold and anti-rabbit IgG conjugated with 10 nm gold) each at a time for 1 hour. The immuno-gold labeled cells were then further fixed in 2% glutaraldehyde (Appendix 29) for 5 minutes and washed with deionised water. After drying, the sections were viewed under JEM-1010 transmission electron microscope (JEOL).

3.12 Scanning electron microscopy (SEM)

Samples were washed twice with PBS before fixing in 2% glutaraldehyde (Appendix 29) for 30 minutes each. The samples were then washed twice with PBS for 10 minutes each before post-fixed in 2% osmium oxide for 30 minutes. The post-fixed samples were washed twice with PBS for 10 minutes each. Following which, these samples underwent dehydration in ascending graded series of ethanol (25%, 50%, 75%, 95%, 100%) at room temperature. The samples were then transferred to a critical point dryer (Bal-Tec CPD 030) for infiltration with 3 changes of liquid carbon dioxide. After

infiltration, the dried samples were mounted onto stub to be transferred to sputter-coater (Bal-Tec SCD 005) to coat the samples with a thin layer of gold. The samples were then viewed using JSM-5660LV scanning electron microscope (JEOL).

3.13 Analysis of hummingbird phenotype

The AGS monolayer was infected as described in section 3.6. The infected cells were viewed under phase contrast microscope (Olympus CKX41) for the presence of hummingbird phenotype.

3.14 IL8 ELISA

IL8 levels were measured using the BD OptEIA^{TM} Human IL8 ELISA kit (BD Biosciences) according to the manufacturer's instructions. In brief, wells were coated with capture antibody (anti-human IL8 monoclonal antibodies) diluted with coating buffer (1:250) (Appendix 30) and left overnight in 4 °C. After aspirating the capture antibody, the wells were washed thrice with wash buffer (Appendix 23). The wells were then blocked with assay diluent (Appendix 31) by incubating at room temperature for 2 hours. The wells were washed thrice with wash buffer before incubating with samples at room temperature for 2 hours. The samples were the supernatants obtained from the spent medium of cell-bacteria. The wells were then washed 5 times with wash buffer and incubated with working detector (Appendix 32) for 1 hour at room temperature. After washing seven times with wash buffer, substrate solution (Appendix 33) was added and incubated for 30 minutes in the dark. Stop solution (Appendix 34) was added to the wells and absorbance was read at 450 nm with 30 minutes.

3.15 Confocal immunofluorescence

T84 cells were infected with 9 different inocula (*H. pylori* 26695; *hsp20* deletion mutant; *cagA* deletion mutant; *hsp20/cagA* double deletion mutant; *hsp20* deletion mutant supplemented with rHSP20; *cagA* deletion mutant supplemented with rCagA; rHSP20 alone; rCagA alone; *cagA* PAI deletion mutant). Recombinant HSP20 used in this study was kindly provided by Dr. BL Ng of Dept Microbiology, NUS, Singapore. After decanting the spent medium, the T84 monolayer was washed twice with prechilled PBS. The cells were then fixed in 4% paraformaldehyde (Appendix 26) (Merck) for 15 minutes at room temperature before permeabilized with 0.2% triton X (Appendix 35) for 10 minutes at room temperature. The cells were washed thrice for 3 minutes each with prechilled PBS. One at a time, the monolayer was then incubated with each of the two primary antibodies (polyclonal rabbit anti-*H. pylori* and monoclonal mouse anti-ZO-1 antibodies) at 1:250 dilution in 0.2% PBS-BSA for 30 minutes on ice. After washing with PBS thrice for 3 minutes each, the monolayer was incubated with each of the two secondary antibodies (goat anti-rabbit FITC and goat anti-mouse Cy3) (1:250 dilution in 0.2% PBS-BSA), one at a time, for 30 minutes on ice in the dark. The cells were washed 3 times for 3 minutes each with PBS. Proteins of interest were viewed using confocal laser microscope (Olympus FV 500).

3.16 Functional test for efficacy of tight junction

3.16.1 Determination of length of infection

To determine the appropriate period of infection for the functional test for T84 cells, 9 time points (0, 2, 4, 8, 12, 24, 36, 48, and 72 hours) were tested. The cells were infected as described in section 3.6. At each time point, the cells were first washed twice with PBS after decanting the medium before 100 µl diluted MTT solution (100 µl MTT stock solution per 1ml medium) (Appendix 36) was added to each well for a 2-hr at 37^{o}C. After the formation of formazan crystals, the culture medium supernatant was removed from the wells without disrupting of the formazan precipitate. The formazan crystals were then dissolved in 100 µl lysis solution/well (Appendix 37). The absorbance was measured at 570 nm using a microplate spectrophotometer. Cell viability was taken as a percentage using the following formulae.

$$\text{Cell viability} = \frac{\text{Absorbance}_{\text{Uninfected T84 cells}}}{\text{Absorbance}_{\text{infected T84 cells}}} \times 100$$

3.16.2 Biotinylation of albumin

Albumin was biotinylated using a method adapted from Hansen and Holm (1989). A volume of 5 ml of albumin solution (30 µM) was mixed well with 0.5 ml of biotin solution (5 mM) and incubated for 4 hours at room temperature. The final solution was then dialyzed at 4°C for 4 hours to remove the free biotin. This final solution was stored at -20 °C and used as a working stock. For the functional test, 21.6 µl of the working stock of biotinylated albumin (1.855 mg/ml) was added to 2 ml of infection medium to get a final infecting concentration of 20 µg/ml (Appendix 38).

3.16.3 Detection of solute leakage across cell monolayer

Disruption of the function of the tight junction complex was examined by detection of presence of solute (biotinylated albumin) leakage across the cell monolayer. T84 cells were infected with the 9 different inocula (*H. pylori* 26695; *hsp20* deletion mutant; *cagA* deletion mutant; *hsp20/cagA* double deletion mutant; *hsp20* deletion mutant supplemented with rHSP20; *cagA* deletion mutant supplemented with rCagA; rHSP20 alone; rCagA alone; *cagA* PAI deletion mutant) for 8 hours at 37°C. The samples extracted from the apical chamber were subjected to western blotting analysis.

AGS and T84 cells were seeded onto 6 wells inserts (Becton Dickinson) and maintained till 100% confluency before being used for infection. The cells were infected as described in section 3.6. The bacterial cells were added to the apical surface of the monolayer (Figure 3.3). After incubation for 8 hours at 37°C, the monolayer was washed twice with PBS. Biotinylated albumin (Amresco) (20 µg/ml) (Appendix 38) was added to the basolateral chamber (Figure 3.3). Samples were collected 24 hours from the apical chamber (Figure 3.3). These samples were then subjected to SDS-PAGE gel run and western blotting. The biotinylated albumin was visualized using streptavidin probe.

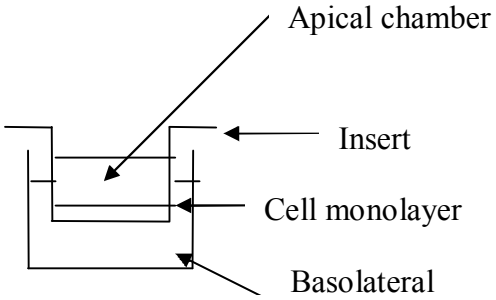

Figure 3.3. Assembly of apparatus for functional test study.

RESULTS

4.1 Confirmatory tests

4.1.1 Gram staining

In Gram staining, counter staining with carbol fuschin was carried out for 10 minutes instead of the usual 1 minute as *H. pylori* does not take up carbol fuschin as easily as other Gram negative bacteria. *H. pylori* was stained pink and the organisms were mostly spirals in the 2 day-old culture (Figure 4.1).

4.1.2 Biochemical tests

In urease test, the urea solution turned pink within minutes in the presence of *H. pylori* culture (Figure 4.2). This is because *H. pylori* produces abundant urease that converted urea in the reagent to ammonia (NH_4^+) and carbon dioxide. The presence of NH_4 ions increases the alkalinity of the medium, resulting in the colour change from yellow to pink in the presence of the pH indicator, phenol red.

For catalase test, effervescences (oxygen bubbles) were observed when *H. pylori* culture was inoculated into hydrogen peroxide reagent (Figure 4.3). This is because *H. pylori* possesses catalase which decomposed hydrogen peroxide into water and oxygen.

Oxidase test was used as confirmatory test for the presence of *H. pylori*. At the site of bacterial inoculation, purple colouration was observed (Figure 4.4). This positive reaction confirmed the presence of *H. pylori* as it produces oxidase that oxidizes 1-% tetra-methyl-p-phenylenediamine dihydrochloride to form a coloured compound, indophenol blue.

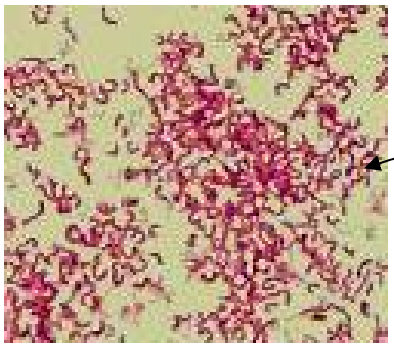

Figure 4.1. Gram stain of a 3 day old *H. pylori* culture.

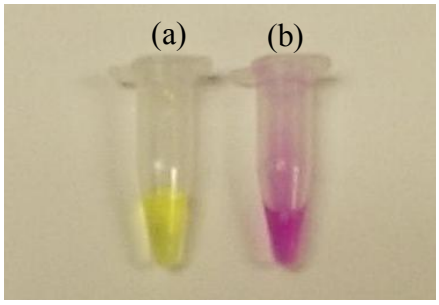

Figure 4.2. Urease test. (a) yellow colour indicates a negative test. (b) pink colour indicates a positive test

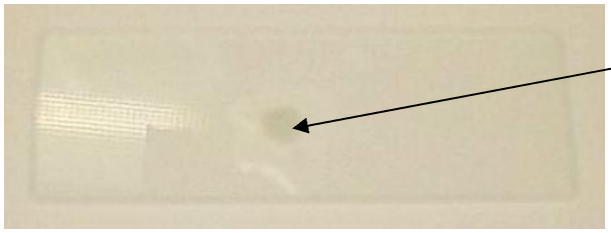

Figure 4.3. Catalase test. Presence of effervescence indicates presence of *H. pylori*.

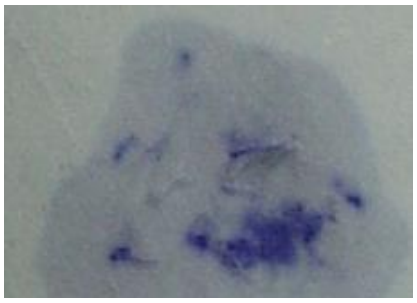

Figure 4.4. Oxidase test. Purple colouration indicates presence of *H. pylori*.

4.2 Generation of deletion mutants of *H. pylori* 26695

4.2.1 *hsp20* deletion mutant

The generation of *hsp20* deletion mutant of *H. pylori* 26695 involved the generation of the DNA knockout construct and then the transformation of *H. pylori* 26695 with the knockout construct.

The knockout construct was created as described in section 3.5.1, by which the *hsp20* gene was replaced by the kanamycin resistance gene. This was done by inserting the kanamycin resistance gene in between region upstream and downstream of *hsp20* gene (Figure 3.1). Using the chromosomal DNA from *H. pylori* 26695 as template, 2 different PCR products were obtained with 2 different sets of primers (Table 3.2). The kanamycin resistant cassette was obtained by performing a PCR reaction with pILL600 plasmid as template (Ferrero *et al*, 1992). The presence of the 3 PCR products was confirmed by agarose gel electrophoresis (Figure 4.5).

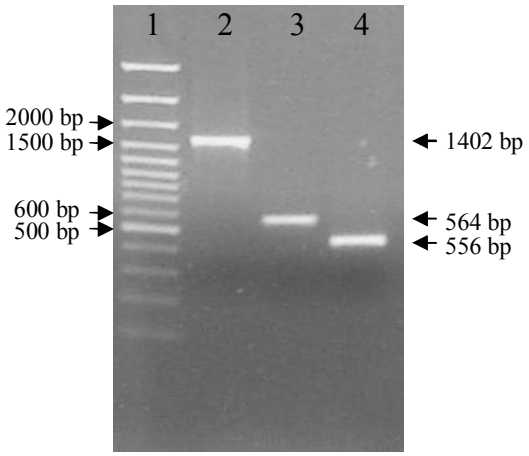

Figure 4.5. Confirmation of PCR products for generation of *hsp20* knockout construct. Lane 1: 100 bp DNA ladder. Band in Lane 2 showed the correct fragment of the kanamycin resistance gene (PCR product 1) of 1402 bp. Band in Lane 3 showed the correct *hsp20* upstream region (PCR product 2) of 564 bp. Band in Lane 4 showed the correct *hsp20* downstream region (PCR product 3) of 556 bp.

The two primers, hsp20kanR2 and hsp20kanF, consist of a 5' leader that are complementary to kanF and aphAR and a gene specific sequence of 22 bp and 25 bp respectively. Thus, the resulting PCR products 2 and 3 (Figure 4.5) have sequences complementary to that in the kanamycin resistant gene. In this way, the 3 purified PCR products obtained were ligated to obtain the final knockout construct of 2522 bp by performing another PCR reaction (Table 3.3). The final knockout construct was confirmed by agarose gel electrophoresis as shown in Figure 4.6.

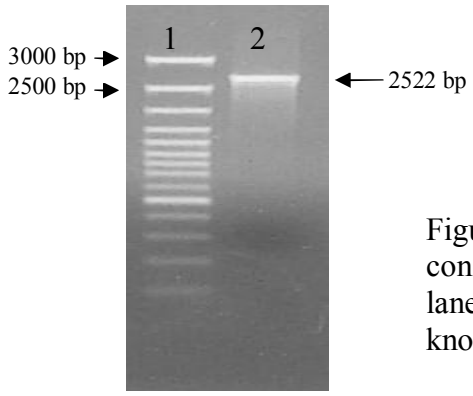

Figure 4.6. Confirmation of *hsp20* knockout construct. Lane 1: 100 bp DNA ladder. Band in lane 2 indicated the correct fragment of *hsp20* knockout construct of 2522 bp.

The *hsp20* knockout construct was transformed into *H. pylori* 26695 to obtain the *H. pylori* 26695 *hsp20* deletion mutant. To confirm that this mutant did not have the *hsp20* gene, chromosomal DNA of the deletion mutant was extracted from the mutant, analysed by PCR using the *hsp20* gene primers (Table 3.1). The resulting PCR product was run on agarose gel that showed the absence of the 270 bp *hsp20* gene fragment (Figure 4.7, Lane 4) with the presence of the 400 bp *cagA* gene fragment (Figure 4.7, Lane 7) respectively, indicating that the *hsp*20 deletion mutant does not have the *hsp20* gene but harbours the *cagA* gene.

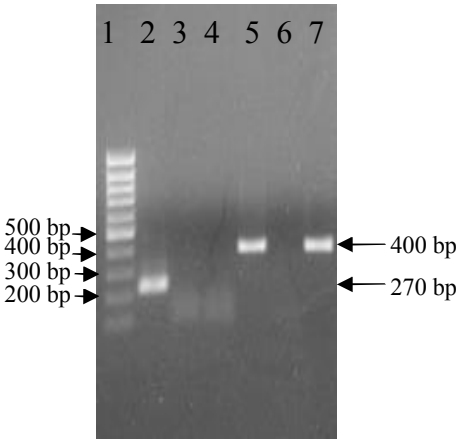

Figure 4.7. Confirmation of *hsp20* deletion mutant of *H. pylori* 26695. Lane 1: 100 bp DNA ladder. Lanes 2-4: detection of the 270 bp *hsp20* gene fragment. Lanes 5-7: detection of the 400 bp *cagA* gene fragment. Lanes 2 and 5 served as positive control, using chromosomal DNA from *H. pylori* 26695 as template. Lanes 3 and 6 served as negative control, whereby no template DNA was added into the PCR reaction. Lanes 4 and 7 shows PCR products using *hsp20* deletion mutant DNA as template.

4.2.2 *cag* PAI deletion mutant

The knockout construct (Figure 3.2) was kindly provided by Prof. Haas R (Odenbreit *et al*, 2000, 2001; Rohde *et al*, 2003). To delete the complete *cag*

pathogenicity island (*cag*-PAI) from the *H. pylori* chromosome, the regions upstream (hp518±hp519; 545254±547164 bp) and downstream (hp549±hp550; 584570±586563 bp) of the *cag*-PAI from *H. pylori* 26695 chromosome were amplified using the primer pairs JP22 (GGGGTACCTT ACCGGCTTTA TTAATG)/JP23 (GAAGATCTAA GGATCTGACA TGTTTA) and JP24 (GAAGATCTAT CGATTATTTT ATTAGCGTTA C)/ JP25 (ACCGCTCGAG CTGCAGCCCA AGAATTCAAA CG AC) respectively. These fragments were separated by a kanamycin resistance cassette (aphA-3), and both were cloned into the pBluescript vector.

The *cag* PAI knockout construct was first transformed into competent *E. coli*. The construct was harvested from the culture using the QIAprep Spin Miniprep Kit (Qiagen). It was then confirmed by double restriction enzyme digestion (Section 3.5.4) as shown in Figure 4.8A where a total of 3 bands of 463 bp, 3409 bp and 4331 bp after the construct was digested by restriction enzymes *Eco*RI and *Spe*I. The identity of the construct was checked again by performing a PCR reaction, using primers Lunil and CagR5280 (Mukhopadhyay *et al*, 2000; Hsu *et al*, 2002) as described in section 3.4. These 2 primers are specific to the regions in the *H. pylori* 26695 chromosome flanking the left (546882-546900) and right ends (584813-584794) of the *cag* PAI respectively. The resultant PCR product of 1908 bp consists of 282 bp of the region flanking the left ends of the *cag* PAI, 1402 bp of the kanamycin resistance gene and 224 bp of the region flanking the right ends of the *cag* PAI giving a total of 1908 bp. Figure 4.8B shows the presence of this *cag* PAI empty site PCR fragment of 1908 bp, confirming the identity of the construct.

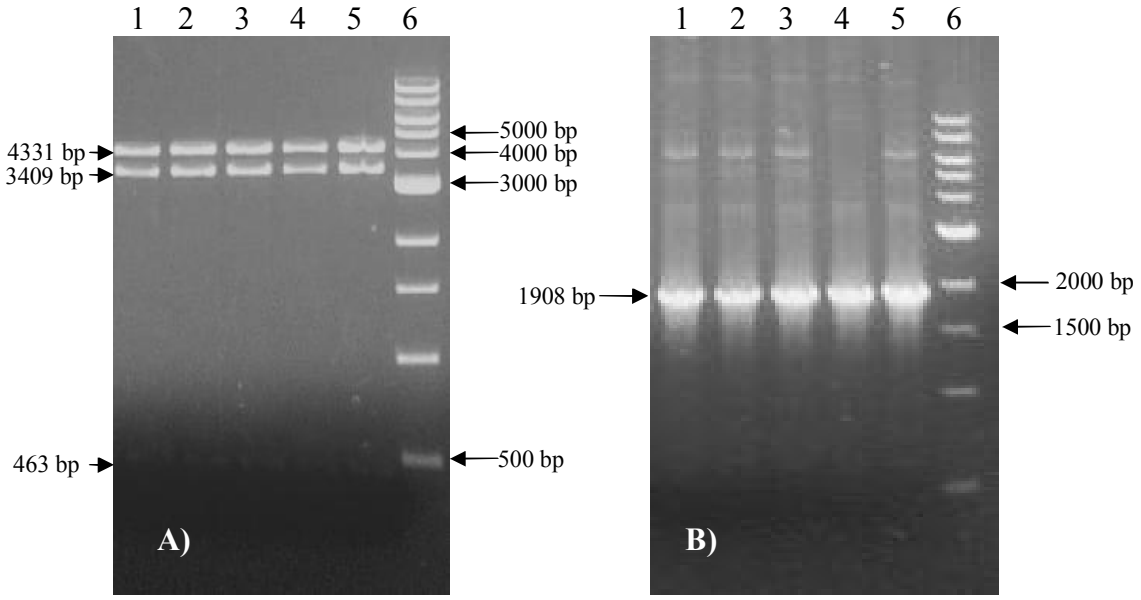

Figure 4.8. Confirmation of the *cag* PAI deletion construct. A total of 5 clones were picked randomly and plasmids DNA extracted from these 5 clones were digested with *Eco*RI and *Spe*I (A) and confirmed with PCR (B). A) Lanes 1-5: presence of 463 bp, 3409 bp and 4331 bp fragment for all 5 clones; Lane 6: 1kb DNA ladder. B) Lanes 1-5: presence of 1908 bp fragment for all 5 clones; Lane 6: 1kb DNA ladder.

The harvested construct was then transformed into *H. pylori* 26695 strain as described in section 3.5.1.2. To confirm that the *cag* PAI deletion mutant of *H. pylori* 26695 does not have the *cag* PAI, PCR was carried out on chromosomal DNA extracted from this mutant using primers, Lunil and CagR5280 (Mukhopadhyay *et al*, 2000; Hsu *et al*, 2002). The PCR product shows the presence of a PCR product of 1908 bp (Figure 4.9A) indicating that the mutant truly lacked the *cag* PAI while *hsp20* was present in all 5 clones analysed (Figure 4.9B). Analysis of PCR reaction using primers for individual genes detection in the *cag* PAI, such as *cagA*, *cagE*, and *cagG* genes (Table 3.1) indicated the absence of these genes in the genomic DNA of the mutant (Figure 4.9 C-E). This further confirmed that complete absence of the whole *cag* PAI in this deletion mutant.

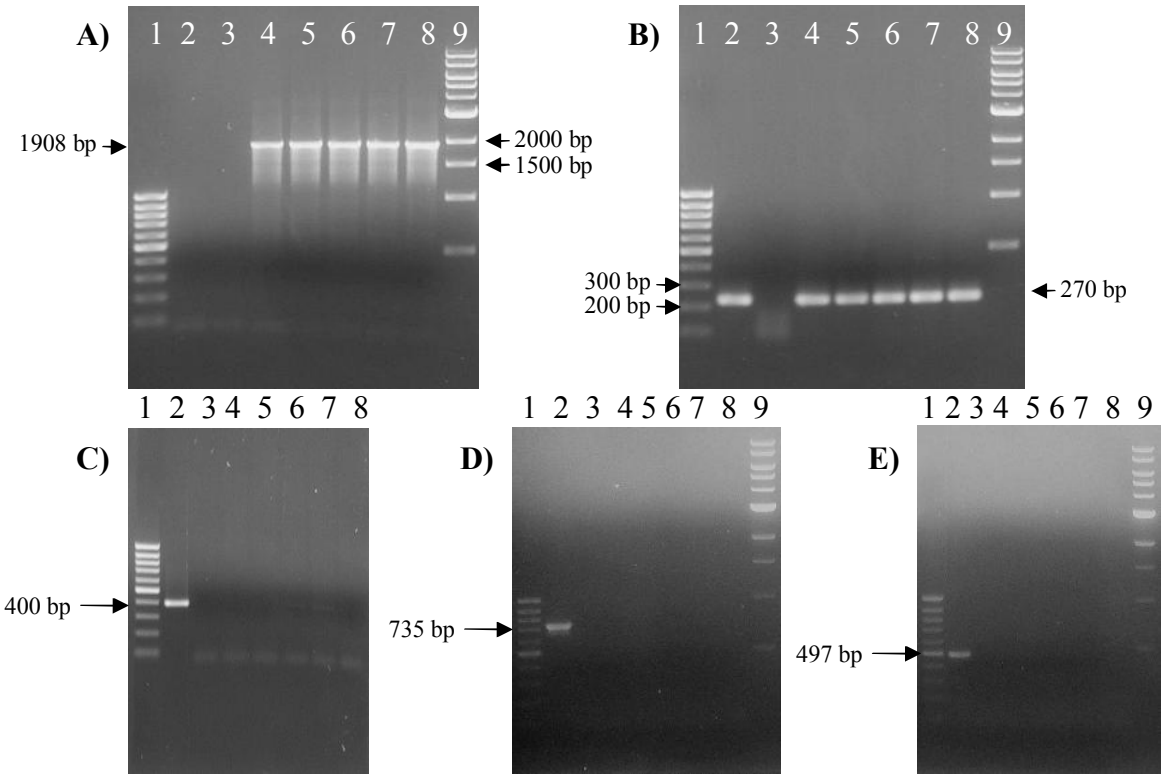

Figure 4.9. Confirmation of *cag* PAI deletion mutant of *H. pylori* 26695. Lane 1: 100 bp DNA ladder. Lane 2: using chromosomal DNA from *H. pylori* 26695 serving as positive control template shows:- absence of *cag* PAI empty site PCR fragment of 1908 bp (A); presence of 270 bp *hsp20* gene fragment (B); presence of 400 bp *cagA* gene fragment (C); presence of 735 bp cagE gene fragment (D); presence of 497 bp cagG gene fragment (E); Lane 3 served as negative control no template DNA in the PCR reaction. Lanes 4-8 (chromosomal DNA extracted from 5 individual clones of *cag* PAI deletion mutants as template): presence of *cag* PAI empty site PCR fragment of 1908 bp (A); presence of 270 bp *hsp20* gene fragment (B); absence of 400 bp *cagA* gene fragment (C); absence of 735 bp cagE gene fragment (D); absence of 497 bp cagG gene fragment (E). Lane 9: 1kb DNA ladder.

4.2.3 *cagA* deletion mutant and *hsp20/cagA* deletion mutant

These 2 deletion mutants were earlier constructed by Dr. Lui SY of our research laboratory. PCR was carried out on chromosomal DNAs extracted from both deletion mutants, *cagA* and *hsp20/cag* using the appropriate primers (Table 3.1). The PCR products show that these mutants do not harbour the *hsp20* nor *cagA* genes (Figure 4.10).

Lanes 4 and 8 in Figure 4.10 show the presence of the 270 bp *hsp20* gene fragment but not the 400 bp *cagA* gene fragment indicating that the *cagA* deletion mutant still harbours the *hsp20* gene but does not have the *cagA* gene. Lanes 5 and 9 show the absence of both the 270 bp *hsp20* gene fragment and the 400 bp *cagA* gene fragment indicating that the *hsp20/cagA* deletion mutant neither has *hsp20* nor *cagA* genes.

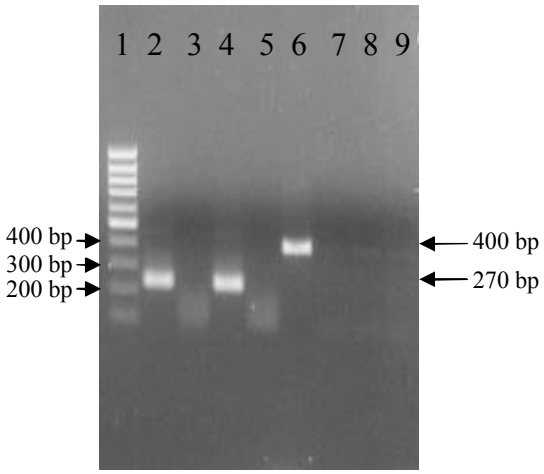

Figure 4.10. Confirmation of *hsp20* deletion mutant and *hsp20/cagA* deletion mutant. Lane 1: 100 bp DNA ladder. Lanes 2-5: the 270 bp *hsp20* gene fragment. Lanes 6-9: the 400 bp *cagA* gene fragment. Lanes 2 and 6: positive control, using *H. pylori* 26695 chromosomal DNA as template. Lanes 3 and 7: negative control with no template DNA in the PCR reaction. Lanes 4 and 8: PCR products with chromosomal DNA of *cagA* deletion mutant as template. Lanes 5 and 9: PCR products with chromosomal DNA of *hsp20/cagA* deletion mutant as template.

4.3 Localization of HSP20 and CagA

We proceeded to examine the localization of HSP20 and CagA within the bacterial cell in the absence of host contact by performing a double labeling on the ultrathin sections obtained. The localization of HSP20 was indicated by the presence of small gold particles of 10 nm in diameter while the localization of CagA was indicated by the presence of large gold particles of 20 nm in diameter.

Figure 4.11A shows that HSP20 is found to be mainly localized at the cell membrane of wild type *H. pylori* 26695 while CagA is found to be mainly localized in the cell cytoplasm of wild type *H. pylori* 26695. Similarly, CagA was also found to be mainly localized in the cell cytoplasm in *hsp20* deletion mutant (Figure 4.11B) while

HSP20 was found to be mainly localized at the cell membrane of *cagA* deletion mutant (Figure 4.11C). As *hsp20/cagA* deletion mutant does not have both the *hsp20* and *cagA* genes, both proteins were absent in the ultrathin sections obtained (Figure 4.11D).

From the TEM studies, it was found that the localization of HSP20 and CagA within the *H. pylori* 26695 changes upon host contact. HSP20 was observed to localize in the cell cytoplasm too (Figure 4.12A). More interestingly, HSP20 was found to be co-localized with CagA (Figure 4.12A). While there is an increase of HSP20 associating with CagA in the cytoplasm (Figure 4.12A), CagA was also observed to be in the cell periphery. This is also observed with *hsp20* deletion mutant (Figure 4.12B). It is interesting to note that, in *cagA* deletion mutant, HSP20 was found to remain localized at the cell membrane despite host contact (Figure 4.12C). As *hsp20/cagA* deletion mutant is devoid of both the *hsp20* and *cagA* genes, (it is therefore not surprised that) neither of these proteins was not found in the ultrathin sections (Figure 4.12D).

We went on to examine if HSP20 or CagA is translocated into AGS cells. Figure 4.13A shows a section of uninfected AGS cell serving as a negative control. HSP20 was not observed in any of the AGS cells infected with any of the *H. pylori* strains, which is indicated by the absence of small gold particles of 10 nm in diameter in all sections obtained (Figure 4.13B-E). However, CagA was found to be translocated into AGS cells infected with either wild type *H. pylori* 26695 (Figure 4.13B) or *hsp*20 deletion mutant (Figure 4.13C). But, CagA was not found in sections obtained from AGS cells infected with *cagA* deletion mutant (Figure 4.13D) and *hsp20/cagA* deletion mutant (Figure 4.13E). This finding confirms that *cagA* deletion mutant does not have the *cagA* gene while both the *hsp*20 and *cag*A genes are absent in *hsp20/cagA* deletion mutant. It is

worth noting that more large gold particles (20 nm in diameter), indicating the presence of CagA, was observed in AGS cells infected with wild type *H. pylori* 26695 than those AGS cells infected with *hsp20* deletion mutant.

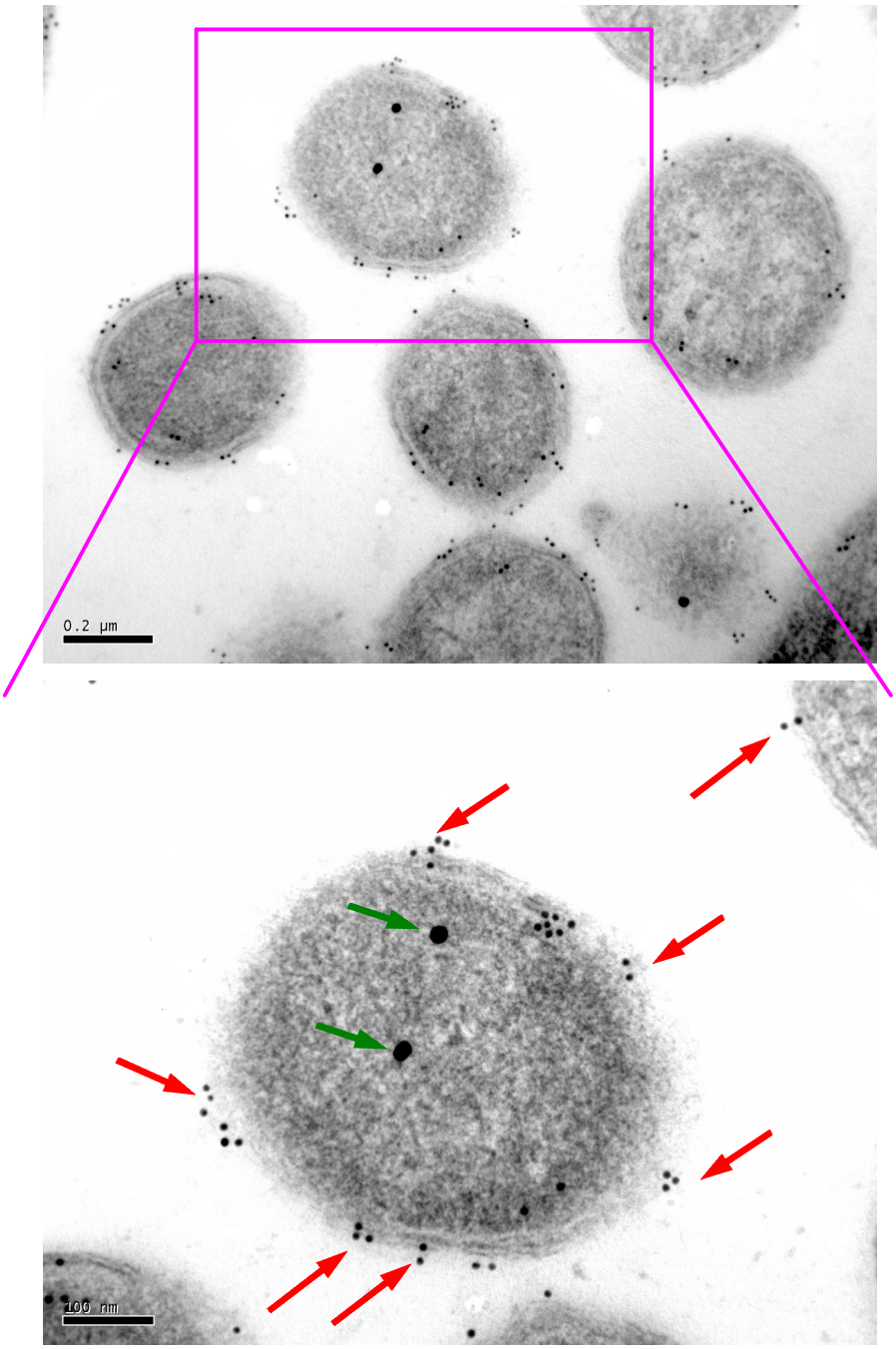

Figure 4.11. Localization of HSP20 and CagA within bacterial cells in the absence of host contact. A) wild type *H. pylori* 26695. Red arrow indicates presence of HSP20 (small gold particles, 10 nm) at the cell membrane. Green arrow indicates presence of CagA (large gold particles, 20 nm) in the cell cytoplasm.

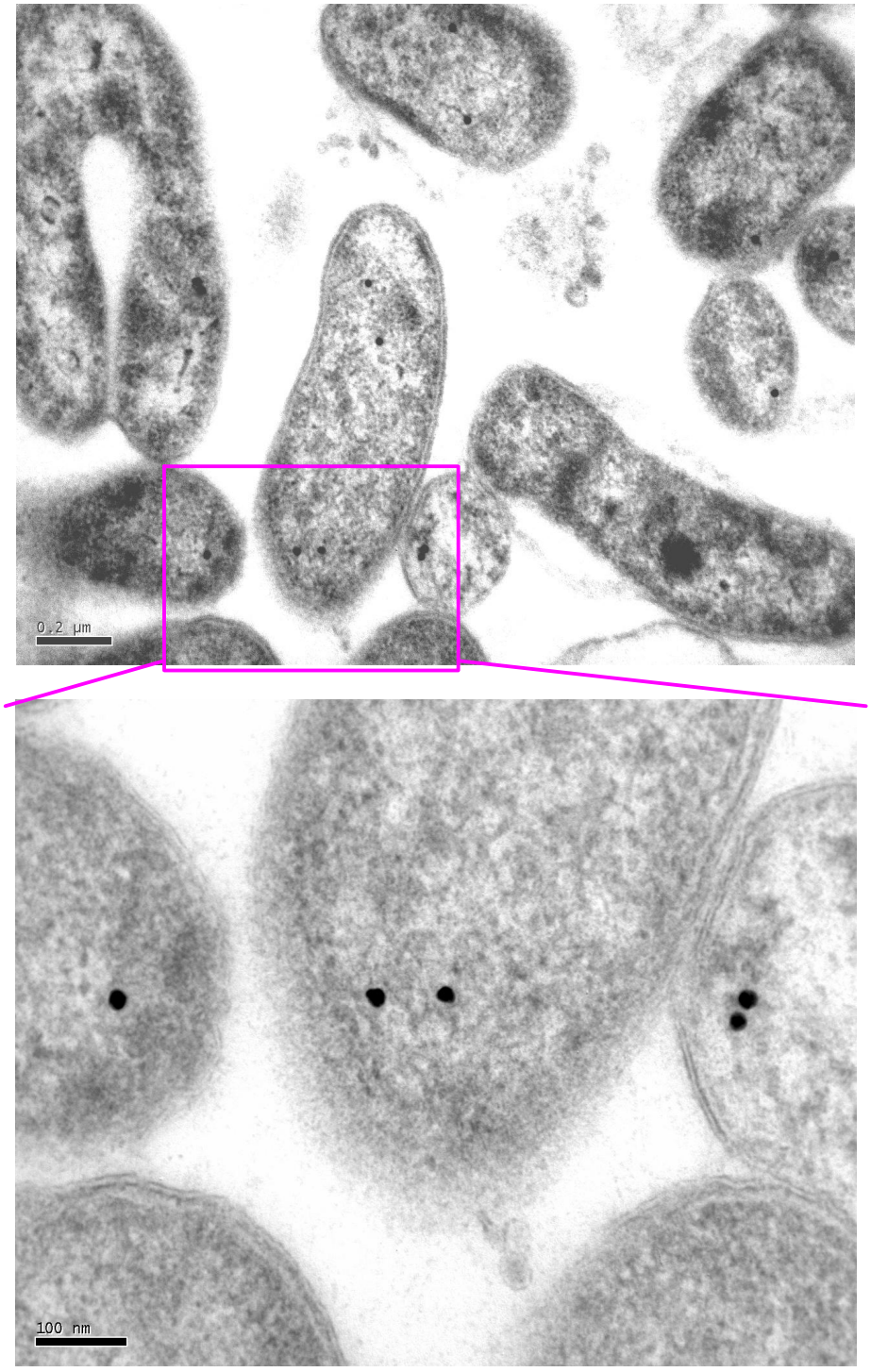

Figure 4.11. Localization of HSP20 and CagA within bacterial cells in the absence of host contact. B) *hsp20* deletion mutant. CagA (large gold particles, 20 nm) was found to be mainly localized in the cell cytoplasm. HSP20 (small gold particles, 10 nm) was not found in these ultrathin sections.

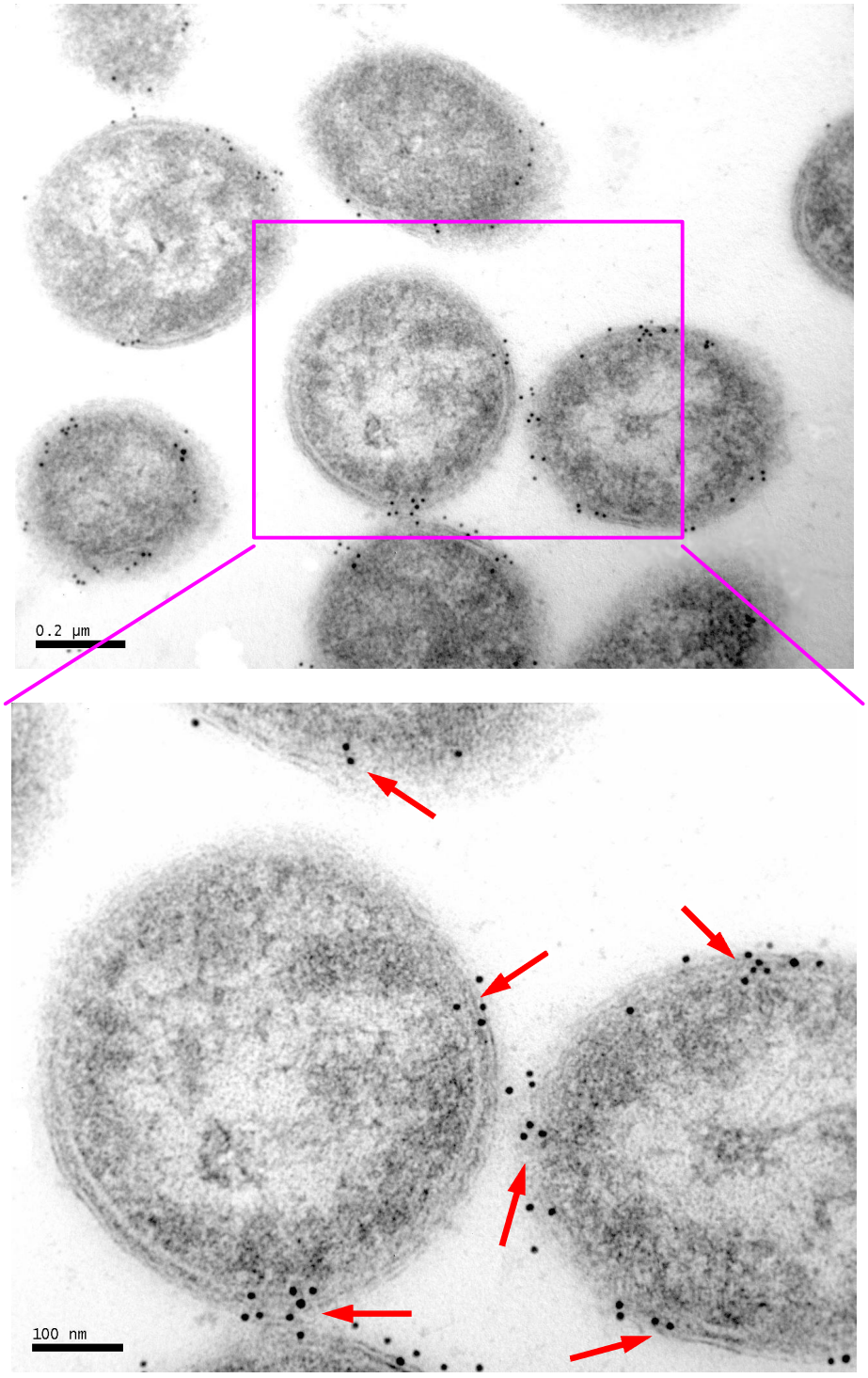

Figure 4.11. Localization of HSP20 and CagA within bacterial cells in the absence of host contact. C) *cagA* deletion mutant. Red arrow indicates presence of HSP20 (small gold particles, 10 nm) at the cell membrane. CagA (large gold particles, 20 nm) was not found in these ultrathin sections.

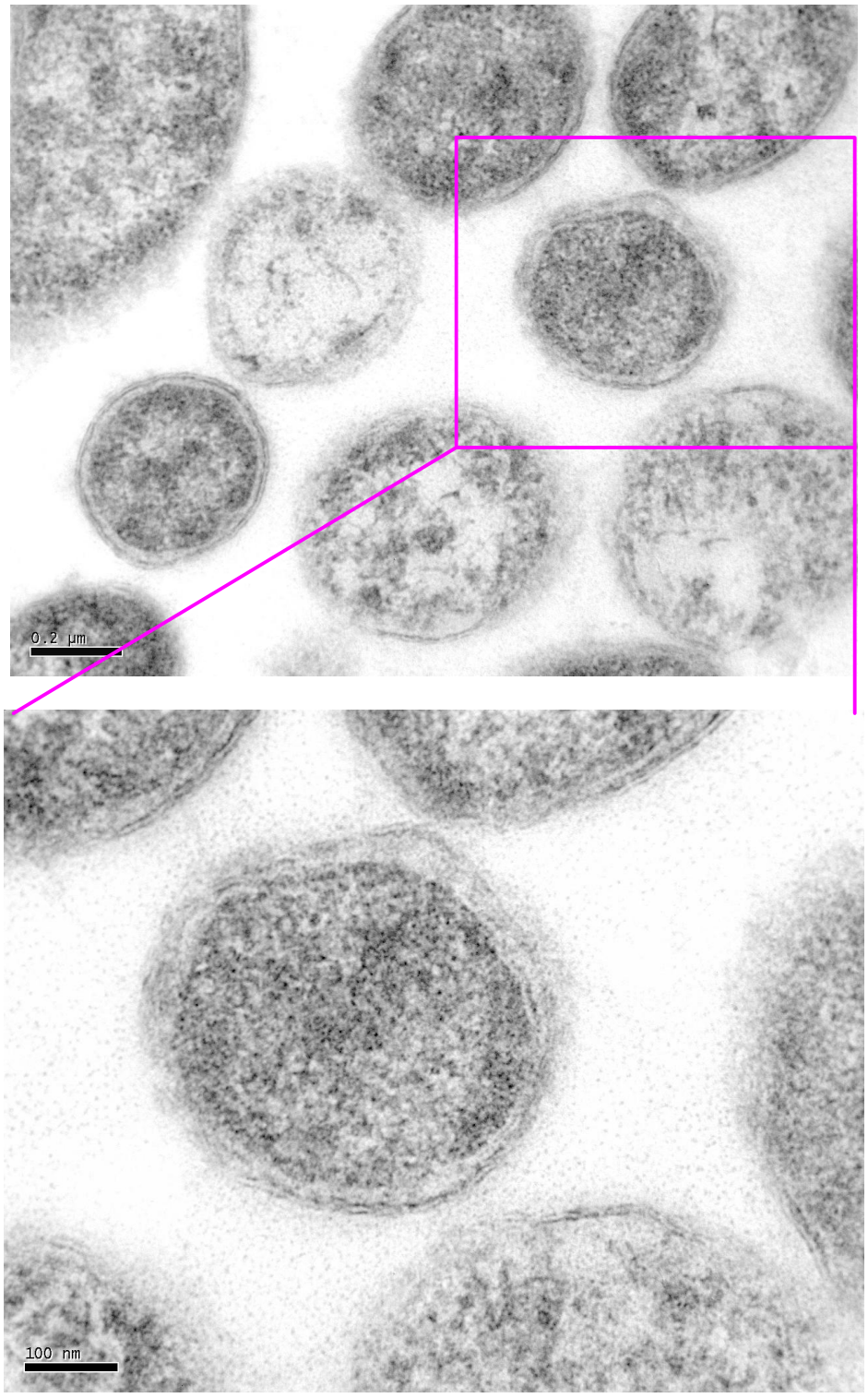

Figure 4.11. Localization of HSP20 and CagA within bacterial cells in the absence of host contact. D) *hsp20/cagA* deletion mutant. HSP20 (small gold particles, 10 nm) and CagA (large gold particles, 20 nm) were both not found in the ultathin sections obtained from this sample.

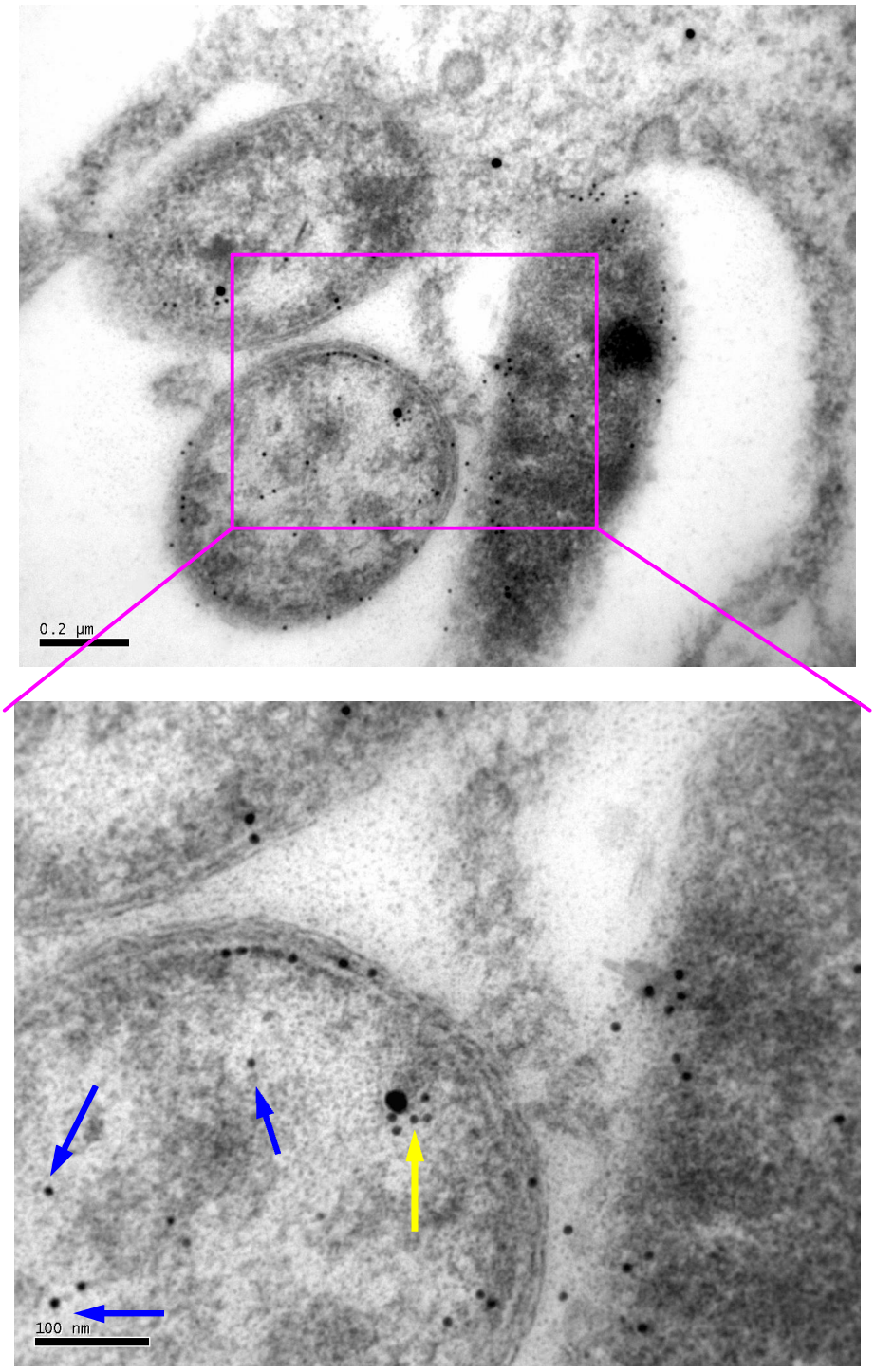

Figure 4.12. Co-localization of HSP20 and CagA within bacterial cells in the presence of host contact. A) AGS cells infected with wild type *H. pylori* 26695. Yellow arrow indicates presence of HSP20 (small gold particles, 10 nm) and CagA (large gold particles, 20 nm) co-localizing. Blue arrow indicates presence of HSP20 in the cytoplasm.

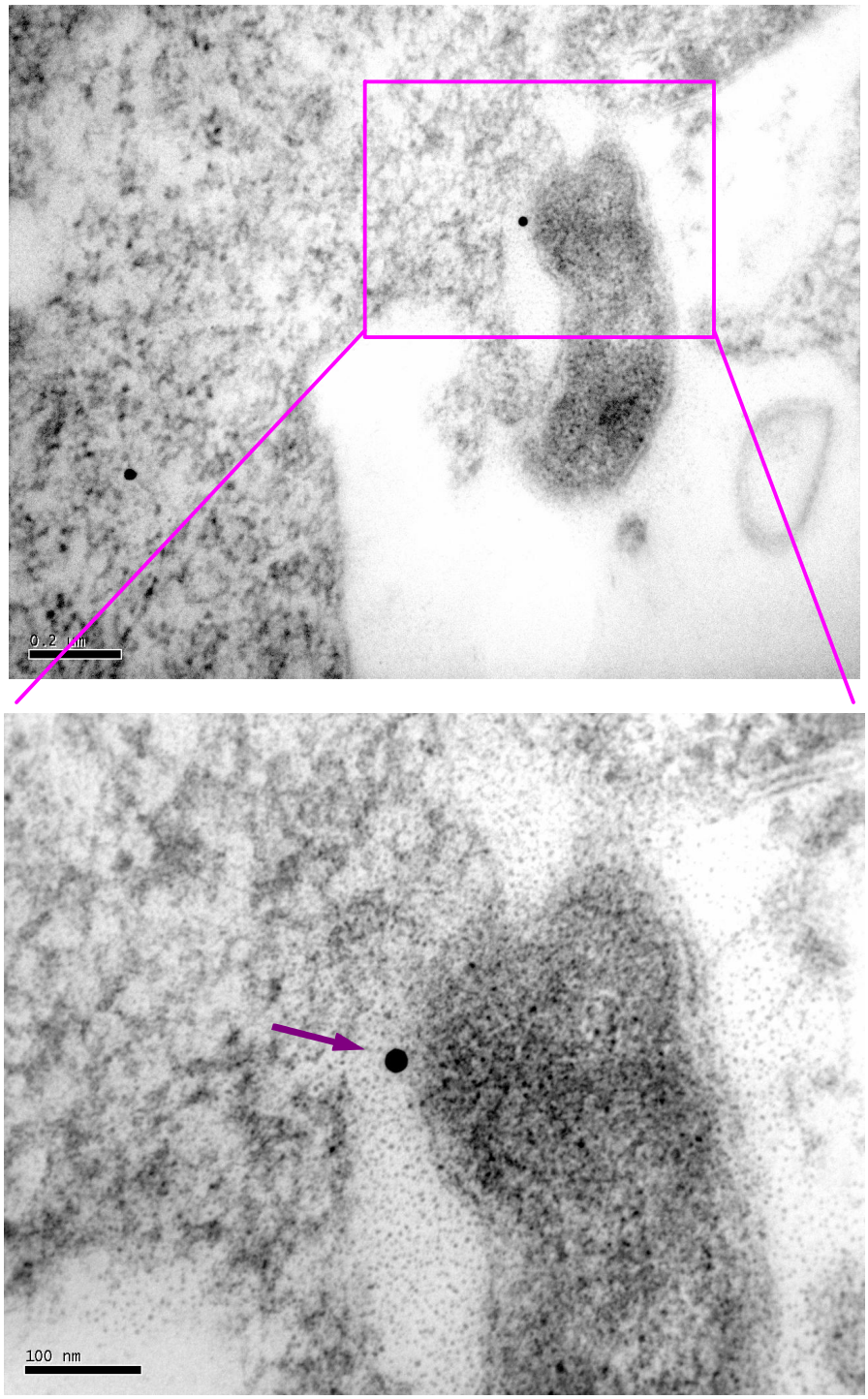

Figure 4.12. Co-localization of HSP20 and CagA within bacterial cells in the presence of host contact. B) AGS cells infected with *hsp20* deletion mutant. CagA (large gold particles, 20 nm) was found to be associated with the cell membrane. HSP20 was not found in these ultrathin sections. Purple arrow indicates presence of CagA at the cell periphery.

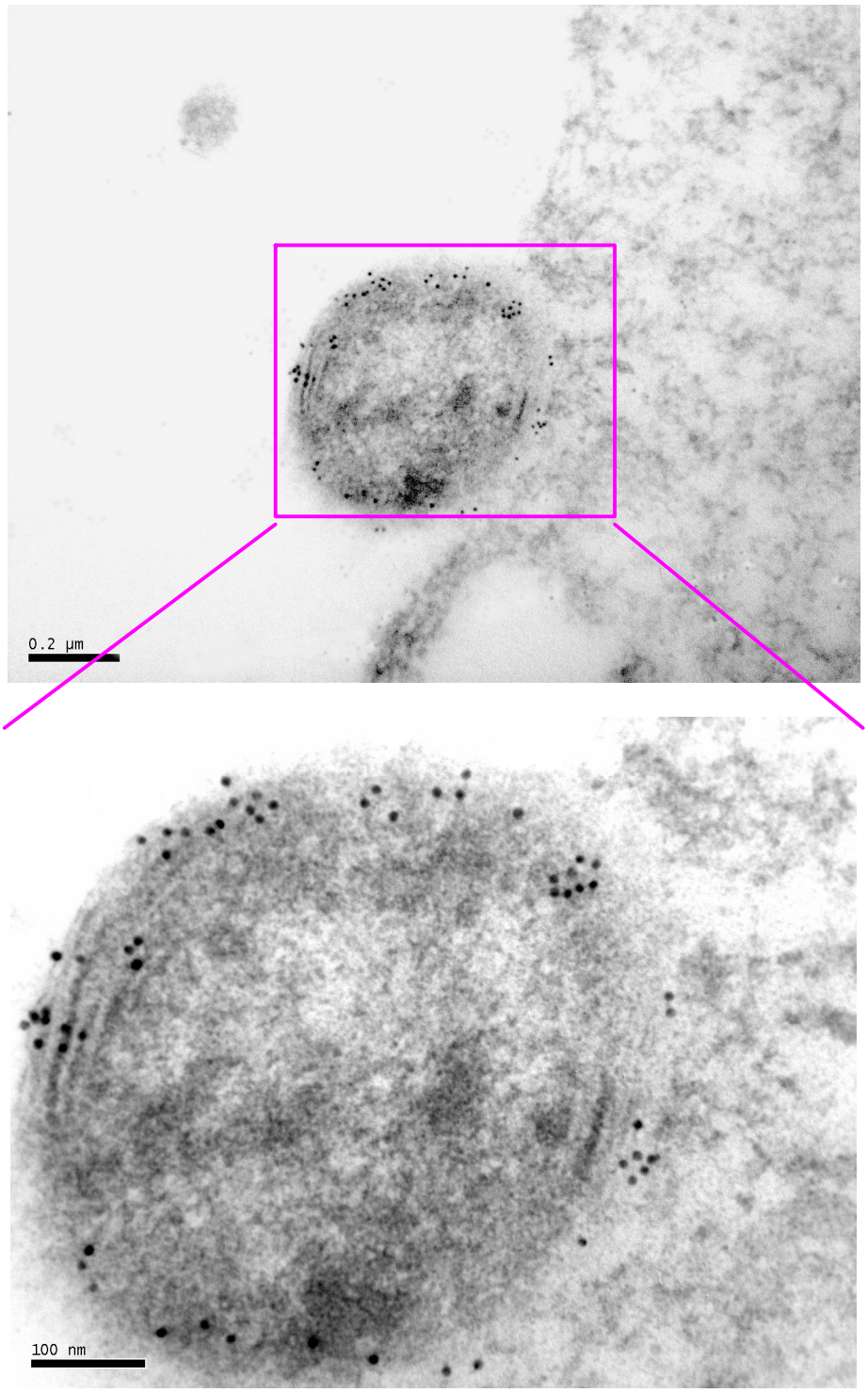

Figure 4.12. Co-localization of HSP20 and CagA within bacterial cells in the presence of host contact. C) AGS cells infected with *cagA* deletion mutant. HSP20 (small gold particles, 10 nm) was found to be associated with the cell membrane. CagA was not found in these ultrathin sections.

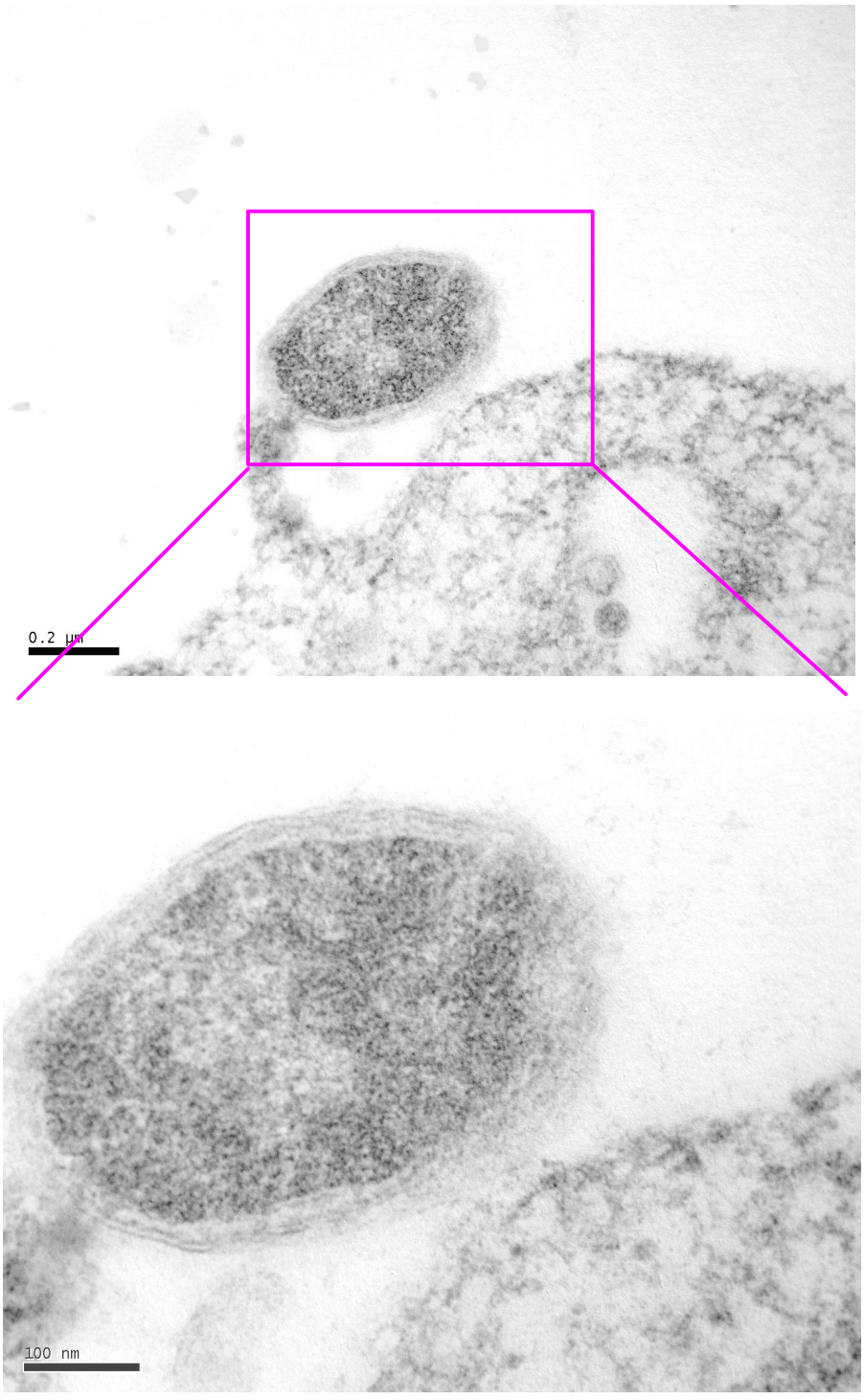

Figure 4.12. Co-localization of HSP20 and CagA within bacterial cells in the presence of host contact. D) AGS cells infected with *hsp20/cagA* deletion mutant. Neither HSP20 (small gold particles, 10 nm) nor CagA (large gold particles, 20 nm) was not found in these ultrathin sections.

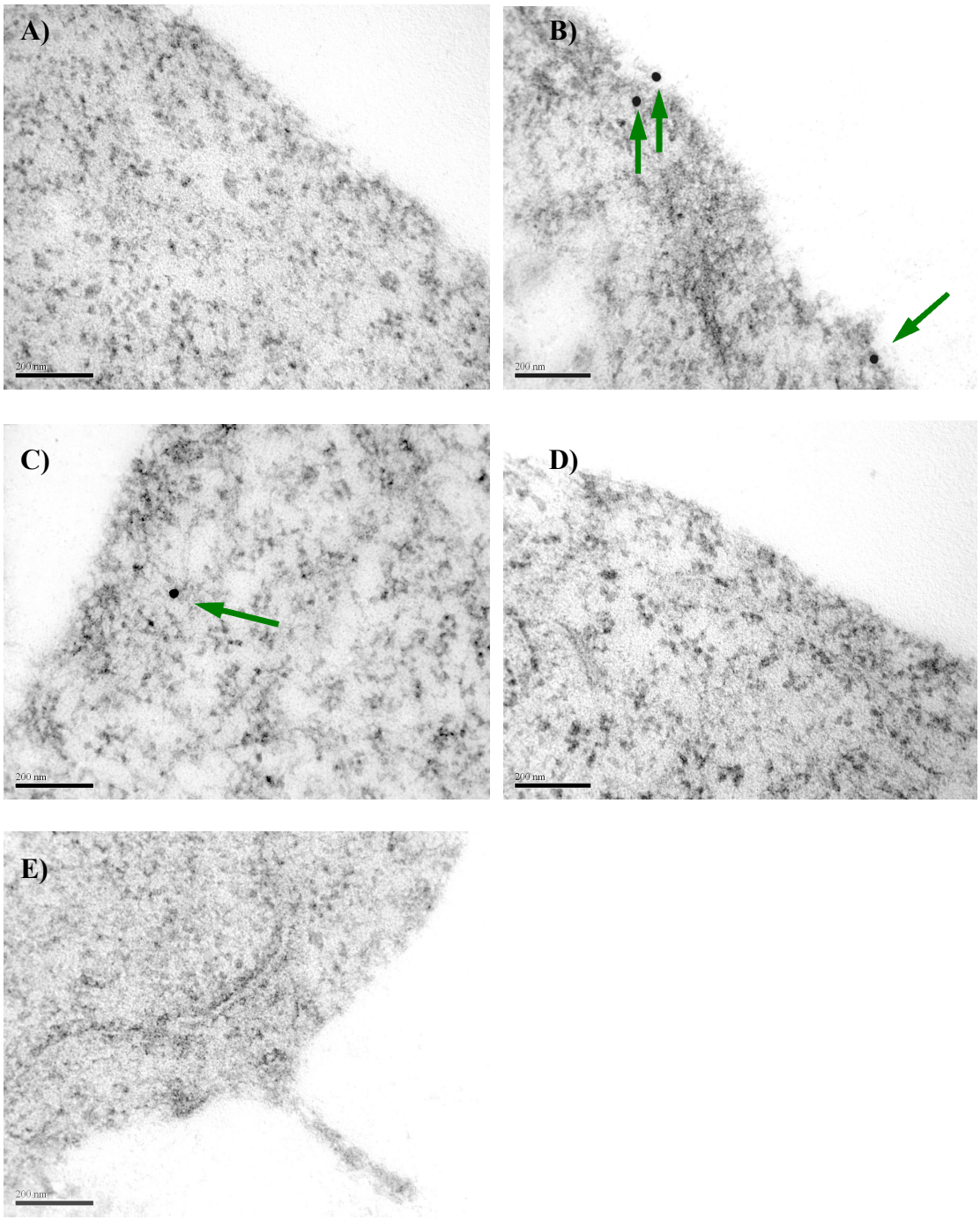

Figure 4.13. Presence of translocated CagA into host (AGS) cell. (A) Uninfected AGS cell served as a negative control. (B) Presence of CagA (large gold particles, 20 nm, arrow) translocated into AGS cells infected with wild type *H. pylori* 26695. No HSP20 (small gold particles, 10 nm) was observed. (C) CagA (arrow) was observed to be translocated into AGS cells infected with *hsp20* deletion mutant. (D) CagA was not observed in AGS cells infected with *cagA* deletion mutant. (E) No CagA was observed in AGS cells infected with *hsp20/cagA* deletion mutant. Presence of CagA was indicated by the green arrows.

4.4 T4SS formation

T4SS is the apparatus by which CagA is translocated into host cells. It has been reported that CagA translocation was only possible upon host contact (Backert *et al*, 2000). This study examined if the inability to translocate CagA could be due to the ability of *H. pylori* to form T4SS apparatus. Scanning electron microscopy was carried out for both wild type *H. pylori* 26695 in the presence or absence of host cells (AGS cells).

The formation of T4SS of approximately 60 nm was observed in *H. pylori* 26695 exposed to host cells (Figure 4.14A). Interestingly, T4SS formation of approximately 60 nm was also observed in *H. pylori* 26695 without exposure to host (Figure 4.14B).

T4SS was often observed with *H. pylori* strains with intact *cag* PAI. However, no T4SS was observed in *cag* PAI deletion mutant, with or without host contact (Figure 4.14C-D). As the surface appendages that extend from the *H. pylori* were observed to be strictly dependent on the presence of the *cag* PAI, it was assumed that these surface appendages are the T4SS of *H. pylori*.

The trigger signal for T4SS formation has not yet been elucidated. This study investigated if HSP20 or CagA plays a role in effecting T4SS formation.

Scanning electron microscopy was carried out on *hsp20* deletion mutant, *cagA* deletion mutant and *hsp20/cagA* deletion mutant. The wild type *H. pylori* 26695 served as a positive control. Figure 4.15 shows that T4SS formation (indicated by the red arrows), was still observed for each of the 3 deletion mutants. Similarly T4SS formation was observed both in the presence (Figure 4.15A-C) and absence (Figure 4.15D-F) of host contact.

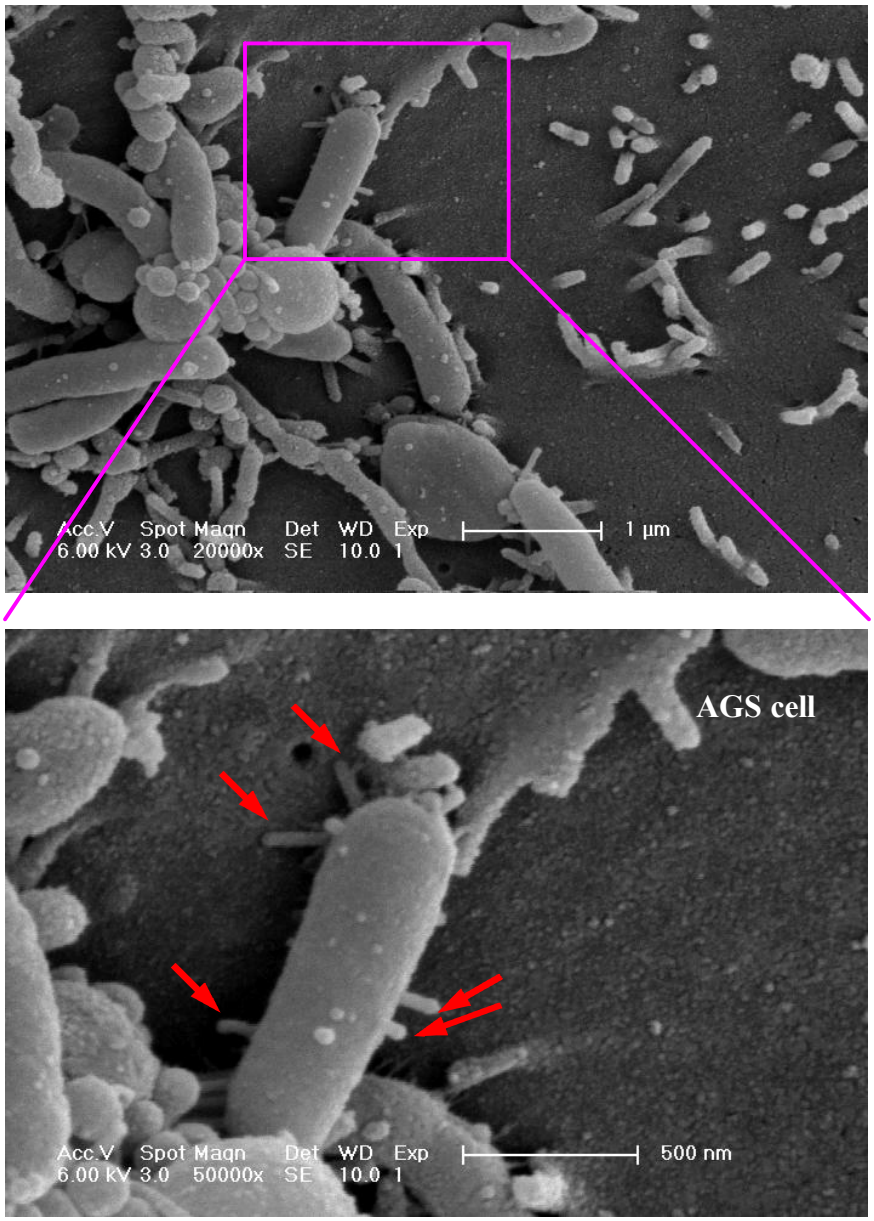

Figure 4.14. T4SS formation does not require host contact. A) wild type *H. pylori* 26695 infected AGS cells. Red arrow indicates location of T4SS of bacteria.

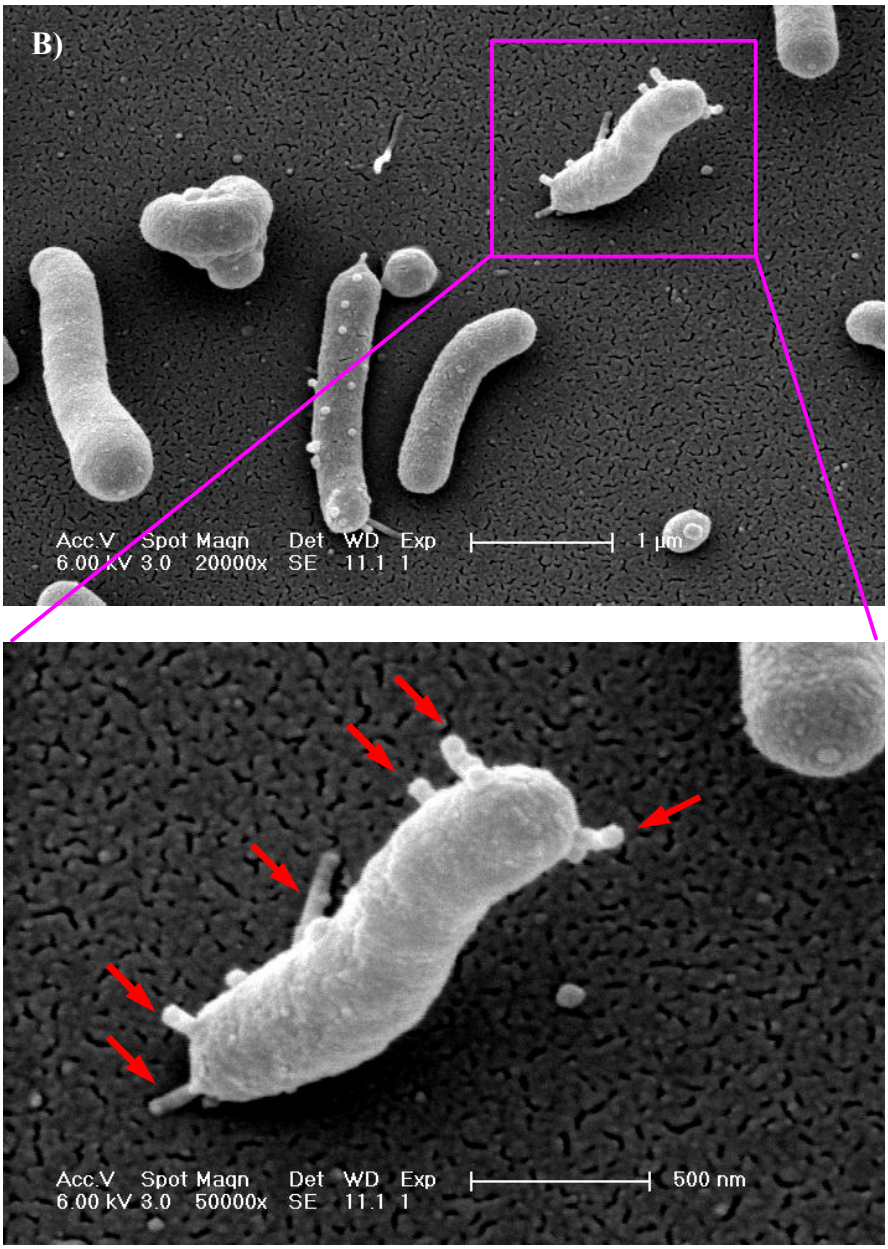

Figure 4.14. T4SS formation does not require host contact. B) wild type *H. pylori* 26695 without the presence of AGS cell. Red arrow indicates location of T4SS of bacteria.

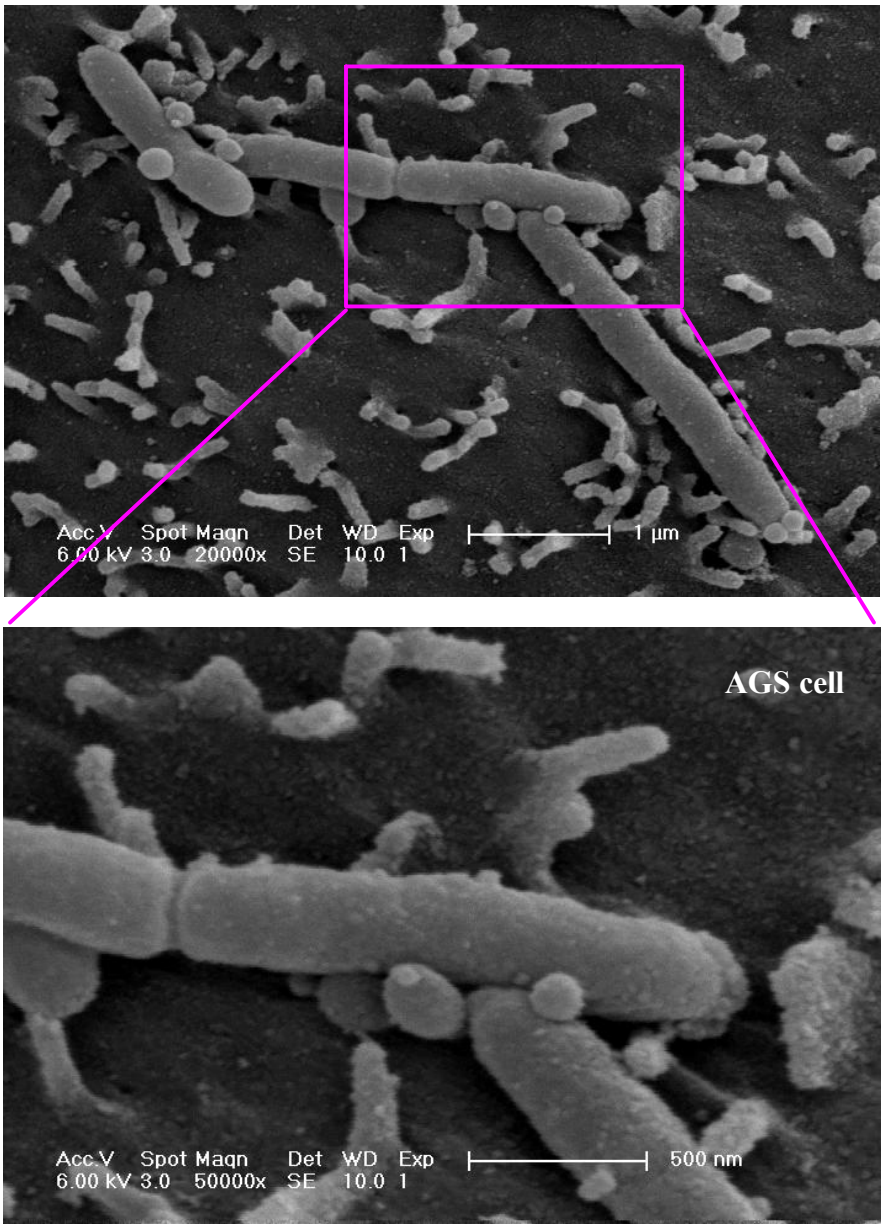

Figure 4.14. T4SS formation does not require host contact. C) *cag* PAI deletion mutant in the presence of AGS cells.

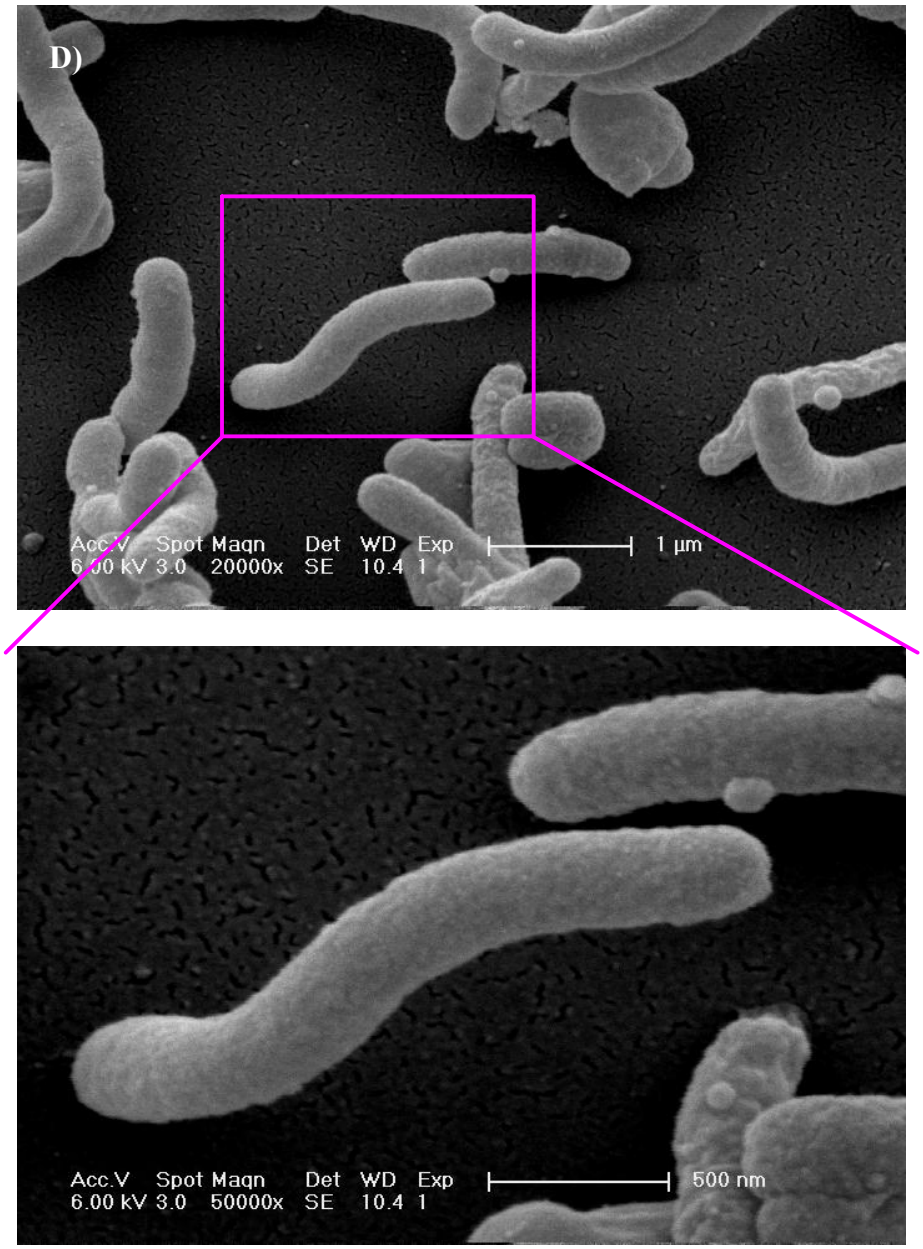

Figure 4.14. T4SS formation does not require host contact. D) *cag* PAI deletion mutant.

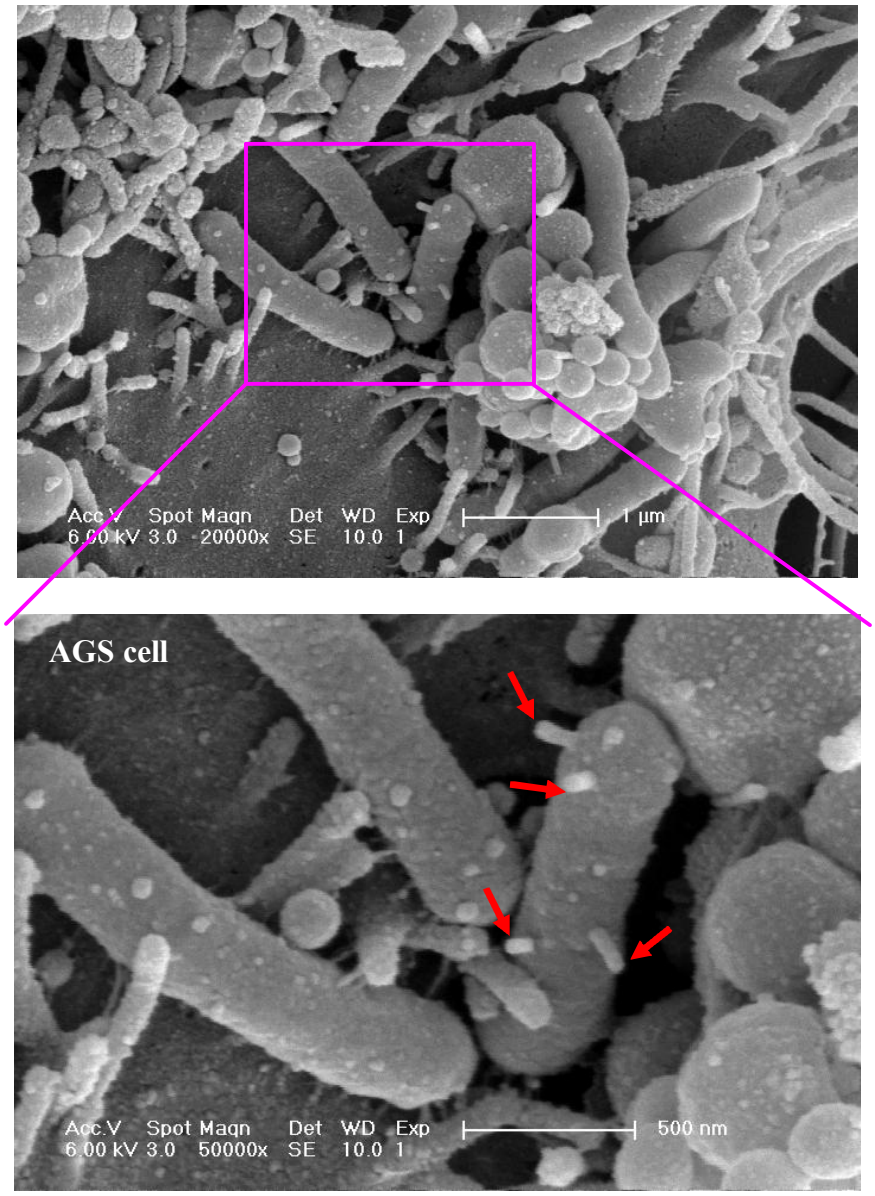

Figure 4.15. HSP20 and CagA do not play a role in T4SS formation. A) *hsp20* deletion mutant in the presence of AGS cells. Red arrows indicate location of T4SS of bacteria.

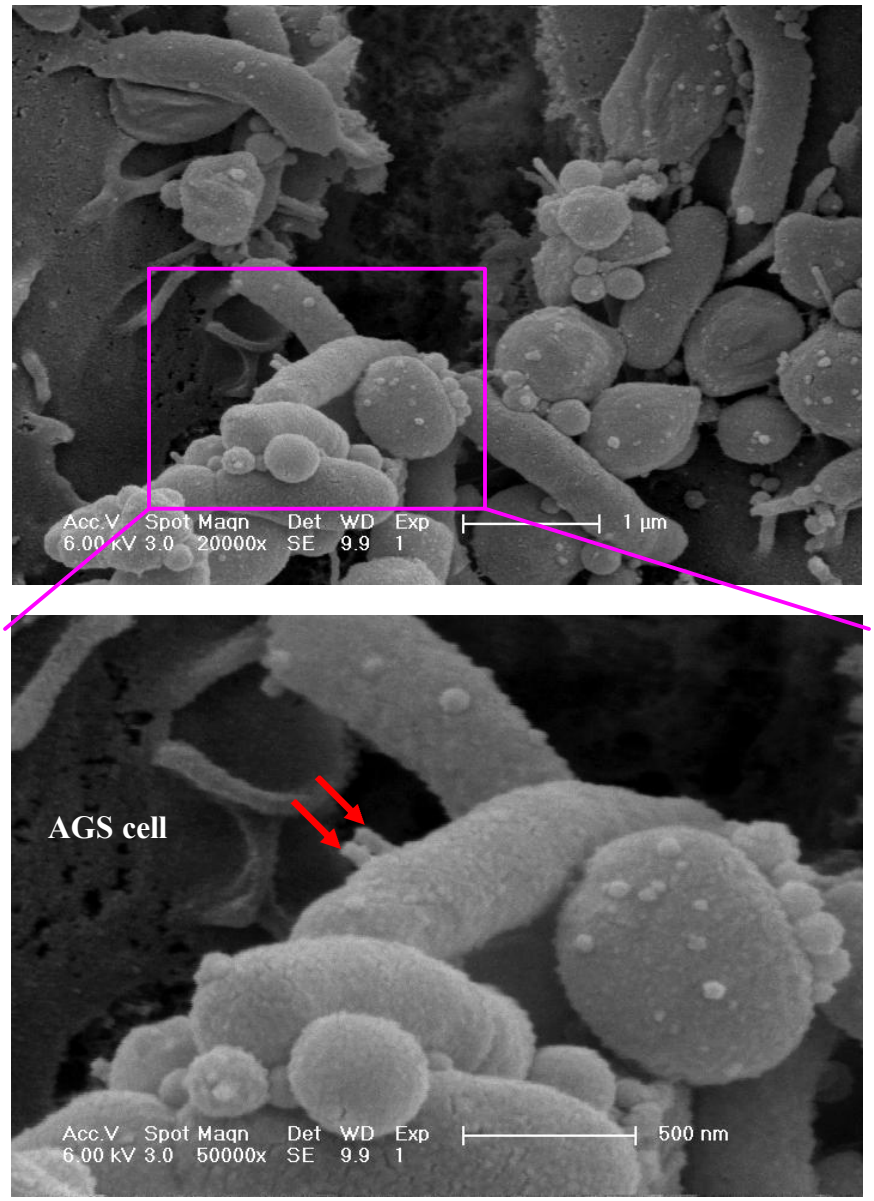

Figure 4.15. HSP20 and CagA do not play a role in T4SS formation. B) *cagA* deletion mutant in the presence of AGS cells. Red arrows indicate location of T4SS of bacteria.

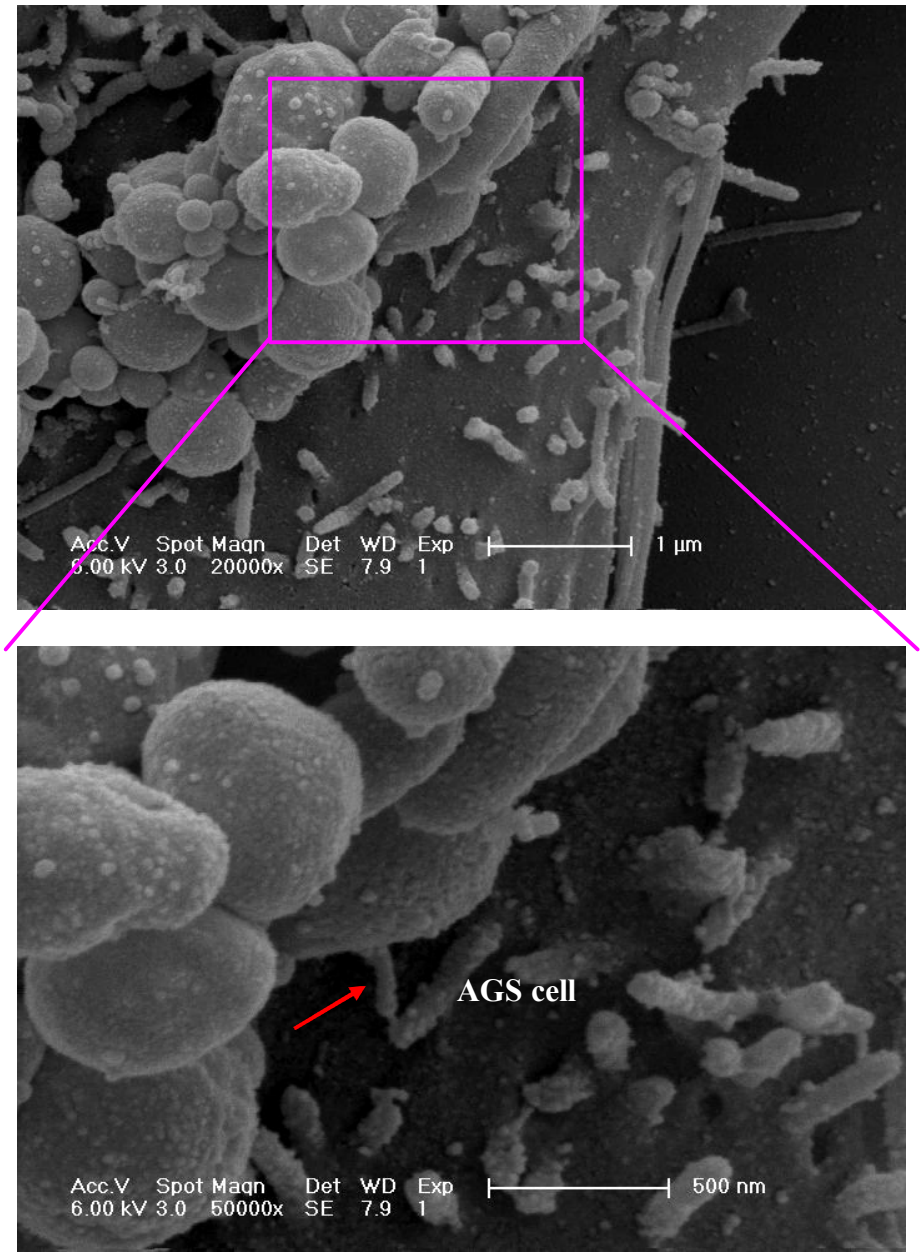

Figure 4.15. HSP20 and CagA do not play a role in T4SS formation. C) *hsp20/cagA* deletion mutant in the presence of AGS cells. Red arrows indicate location of T4SS of bacteria.

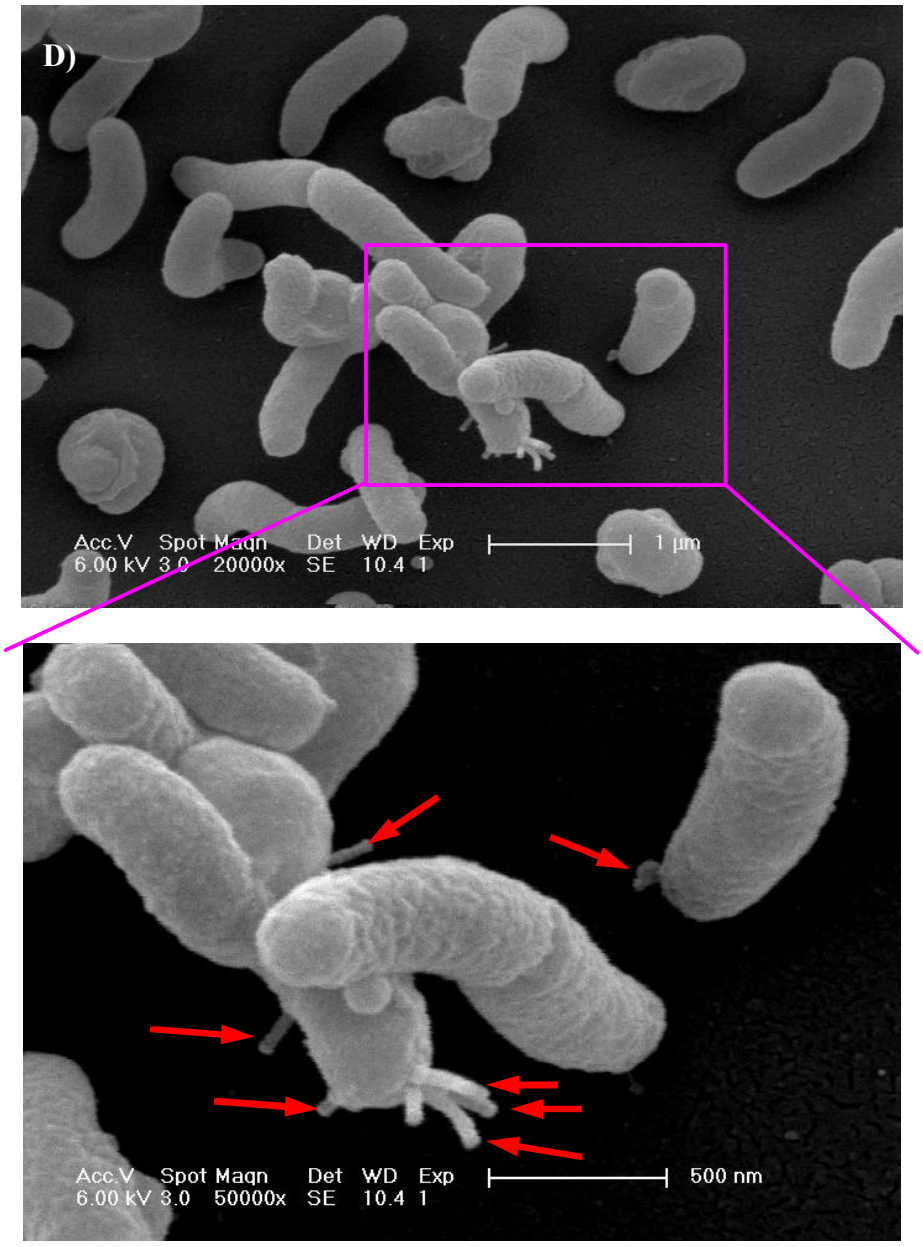

Figure 4.15. HSP20 and CagA do not play a role in T4SS formation. D) *hsp20* deletion mutant. Red arrows indicate location of T4SS of bacteria.

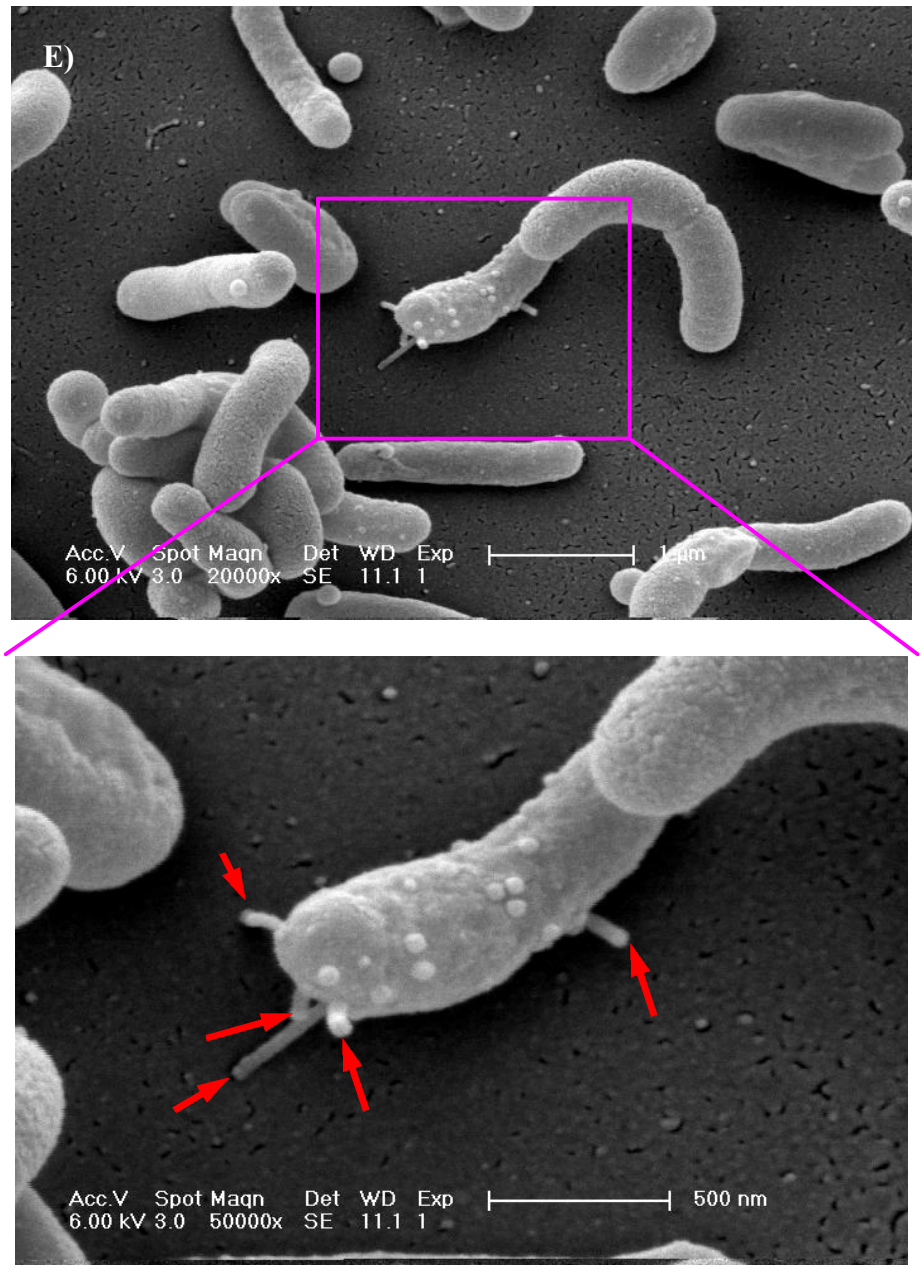

Figure 4.15. HSP20 and CagA do not play a role in T4SS formation. E) *cagA* deletion mutant. Red arrows indicate location of T4SS of bacteria.

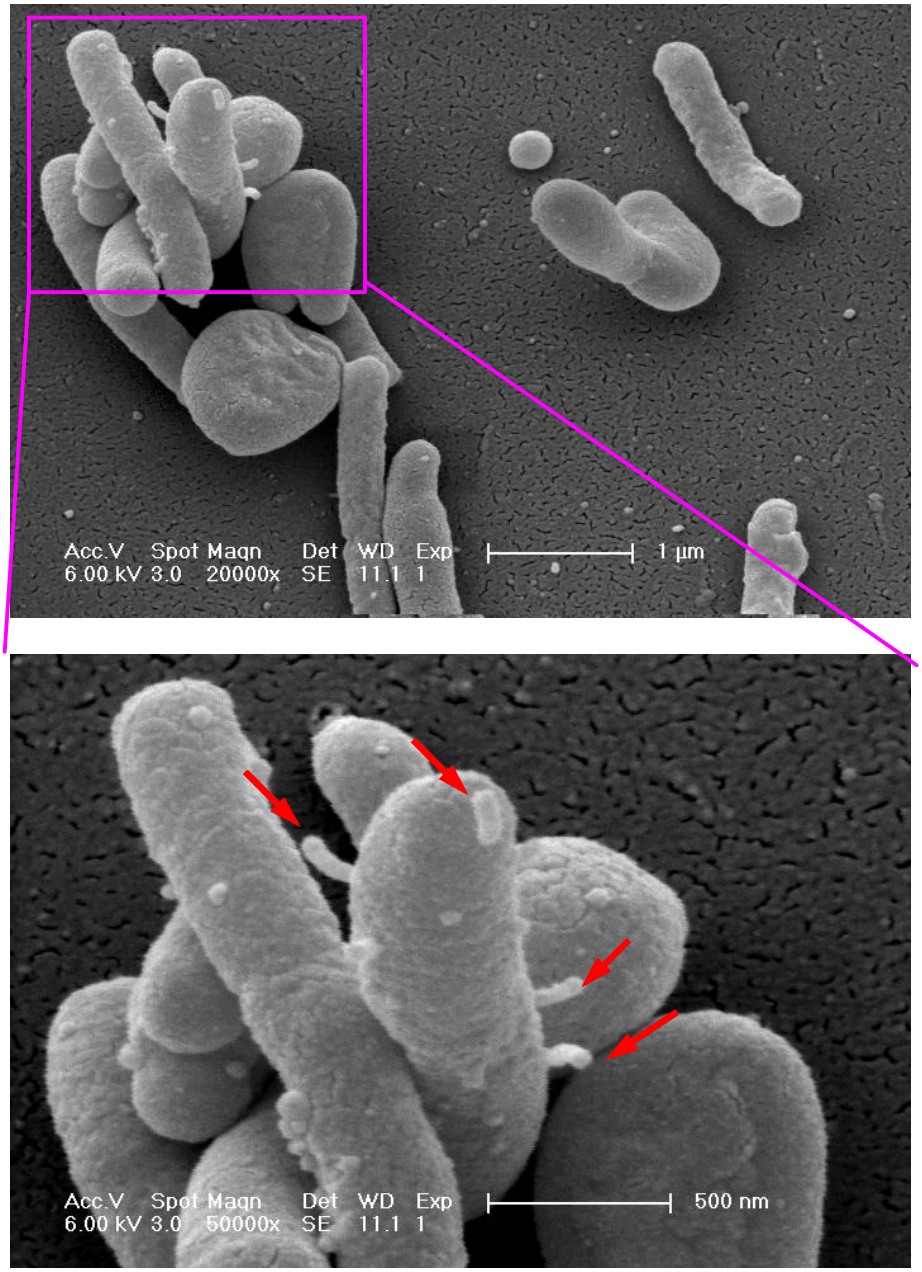

Figure 4.15. HSP20 and CagA do not play a role in T4SS formation. F) *hsp20/cagA* deletion mutant. Red arrows indicate location of T4SS of bacteria.

4.5 CagA translocation across T4SS

Proteins were extracted from infected AGS cells to determine if HSP20 plays a role in T4SS function as analysed by western blotting. In a time course reaction, CagA was found to be translocated into the wild type *H. pylori* 26695 infected host cells within15 minutes of infection (Figure 4.16A). CagA translocation was also found to peak at 4 hours upon infection and gradually started to decrease at 6 hours after bacteria-cell contact. A low basal level of CagA translocation was observed 8 hours into the infection.

Similar to wild type *H. pylori* 26695 infected AGS cells, CagA translocation was also observed in *hsp20* deletion mutant infected AGS cells, confirming results obtained in TEM studies (Figure 4.14 and 4.15). CagA was found to be translocated into the *hsp20* deletion mutant infected AGS cells 15 minutes into the infection (Figure 4.16B). However CagA translocation was found to peak at 6 hours instead of the 4 hours as shown by wild type *H. pylori* 26695 infected AGS cells. The translocatioion of CagA began to decrease gradually to a low basal level 8 hours post infection. The low basal level of CagA translocation was only observed 16 hours into the infection.

Figure 4.16C-D show the absence of CagA translocation. This confirms that *cagA* deletion mutant and *hsp20/cagA* deletion mutant truly do not have the *cagA* gene.

In order to compare differences between CagA translocation in wild type *H. pylori* 26695 infected AGS cells and *hsp20* deletion mutant infected AGS cells, protein extracts from the infected cells at each time points (0 hour, 15 minutes, 30 minutes, 2 hours, 4 hours, 6 hours, 8 hours, 16 hours) were examined by SDS-PAGE (Figure 4.17).

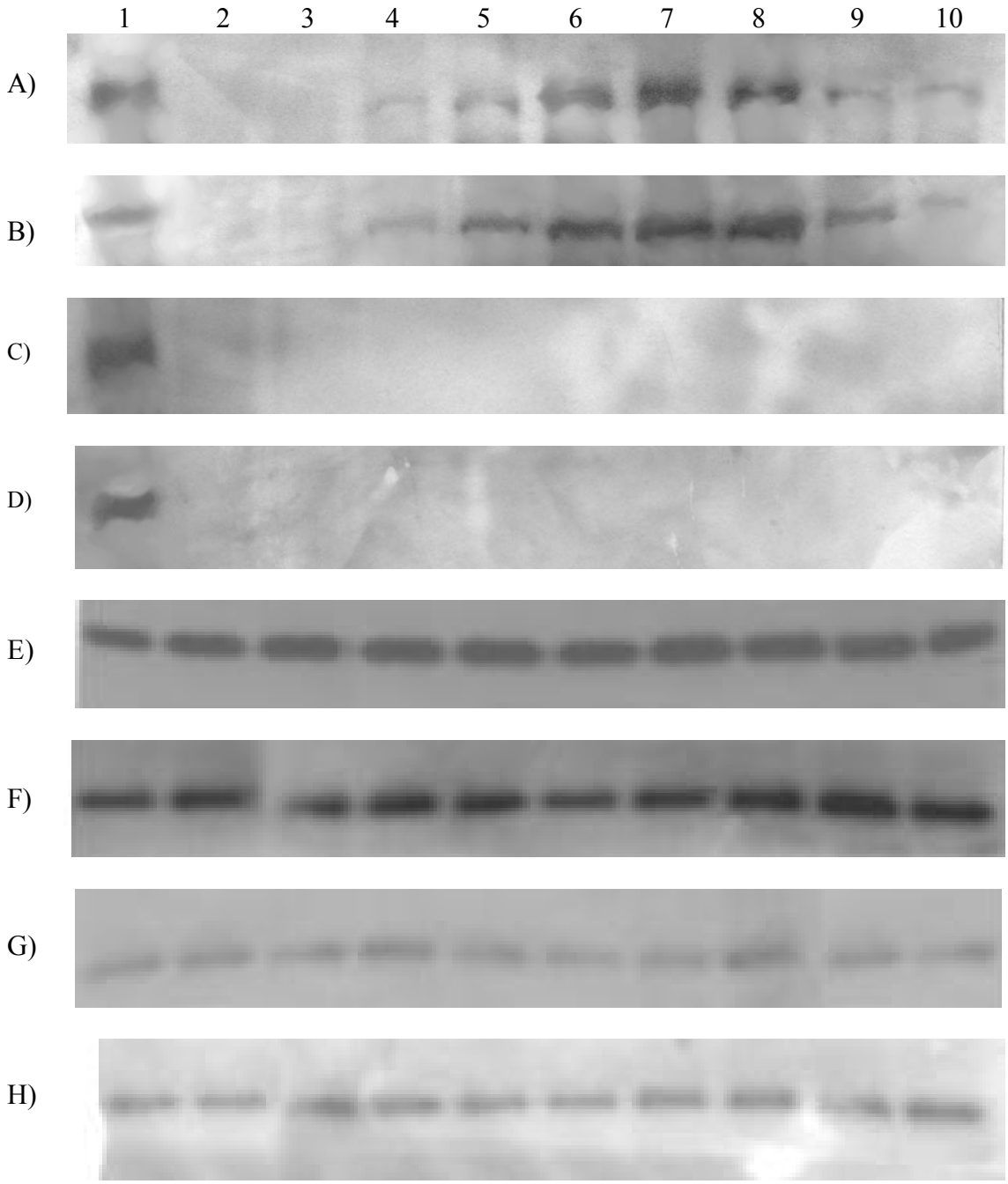

Figure 4.16. Time-dependent CagA translocation. Lane 1: *H. pylori* 26695 protein extract served as positive control; Lane 2: Uninfected AGS protein extract served as negative control; Lane 3-10: *H. pylori* infected AGS protein extracts for varying length of time: 0 minutes (Lane 3), 15 minutes (Lane 4), 30 minutes (Lane 5), 2 hours (Lane 6), 4 hours (Lane 7), 6 hours (Lane 8), 8 hours (Lane 9), 16 hours (Lane 10). A) and E): Wild type *H. pylori* 26695 infected AGS cells; B) and F): *hsp20* deletion mutant infected AGS cells; C) and G): *cagA* deletion mutant infected AGS cells; D) and H): *hsp20/cagA* deletion mutant infected AGS cells. (E)-(H): β-actin serves as a loading control. Proteins extracts of *H. pylori* infected cells were probed with antibody against CagA (A-D).

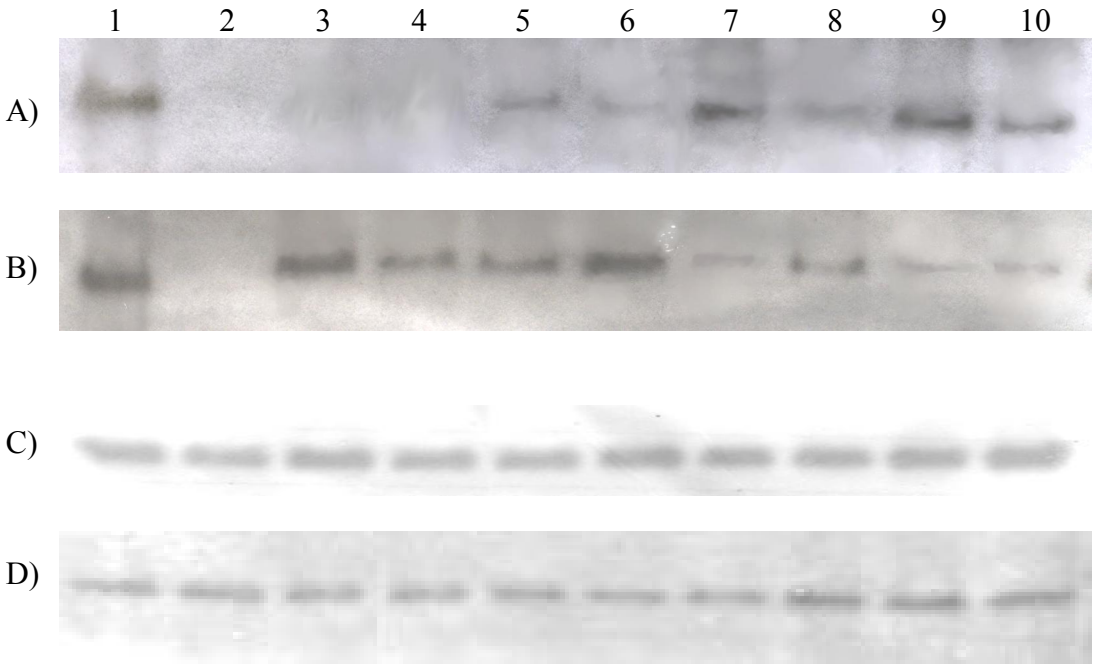

Figure 4.17. Differences between CagA translocation in AGS cells infected with wild type *H. pylori* 26695 and *hsp20* deletion mutant. Lane 1: wild type *H. pylori* 26695 protein extract served as positive control; Lane 2: Uninfected AGS protein extract served as negative control; Lanes 3, 5, 7 and 9: protein extracts from wild type *H. pylori* 26695; Lanes 4, 6, 8 and 10: protein extracts from *hsp20* deletion mutant infected AGS cells. A) and C): a comparison at various time points - 0 hour (Lane 3-4), 15 minutes (Lane 5-6), 30 minutes (Lane7-8), 2 hours (Lane 9-10). B) and D): a comparison at different time points - 4 hours (Lane 3-4), 6 hours (Lane 5-6), 8 hours (Lane7-8), 16 hours (Lane 9-10). C) and D): β-actin serves as loading control. Proteins extracts of *H. pylori* infected cells were probed with antibody against CagA (A-D).

Comparing Lanes 5 and 6 in Figure 4.17A, it was noted that the band in Lane 5 is significantly stronger than that in Lane 6, indicating a higher concentration of CagA was translocated into AGS cells infected with wild type *H. pylori* 26695 than by *hsp20* deletion mutant within 15 minutes post infection. Similar patterns appear for 30 minutes and 2 hours post infection as shown in the comparative gel analysis in Lanes 7 and 8 for 30 minutes and Lanes 9 and 10 for 2 hours post infection (Figure 4.17A) and persisted 4 hour post infection as shown in Lane 3 and 4 of Figure 4.17B. Interestingly, at 6 hours

post infection the intensity of protein band in Lane 5 is lower than that in Lane 6 in Figure 4.17B. This indicates a lower concentration of CagA was being translocated into AGS cells infected by the wild type *H. pylori* 26695 than by *hsp20* deletion mutant. Similarly, the band in Lane 7 is evidently weaker than that in Lane 8 (Figure 4.17B), indicating that a much weaker CagA translocation occurred in wild type *H. pylori* 26695 infected AGS cells than in *hsp20* deletion mutant infected AGS cells 8 hours post infection. However, the bands in Lanes 9 and 10 (Figure 4.17B) are of comparable intensity indicating that CagA translocation in both wild type *H. pylori* 26695 and *hsp20* deletion mutant infected AGS cells has reached a comparable low basal level 16 hours post infection.

Figure 4.18A shows that CagA translocation was only observed in AGS cells infected with wild type *H. pylori* 26695 (Lane 3) or *hsp20* deletion mutant (Lane 4) and not in AGS cells infected with *cagA* deletion mutant and *hsp20/cagA* deletion mutant (as seen in Figure 4.17). It should be noted that, similar to Lane 5 (wild type *H. pylori* 26695 infecting condition) and 6 (*hsp20* deletion mutant) in Figure 4.18B, the CagA bands observed in the wild type *H. pylori* 26695 (Lane 3 in Figure 4.18A) is weaker in intensity as compared to that observed in *hsp20* deletion mutant (Lane 4 in Figure 4.18A) infecting condition. In addition, Figure 4.18A (Lane 7) shows the absence of CagA translocation in *cag* PAI deletion mutant. This confirms the absence of the *cagA* gene in the genomic DNA of the *cag* PAI deletion mutant. This also confirms that, without the establishment of T4SS as seen in Figure 4.14C-D, translocation of CagA may not be possible. The results also indicate that CagA is translocated irrespective of the presence of HSP20.

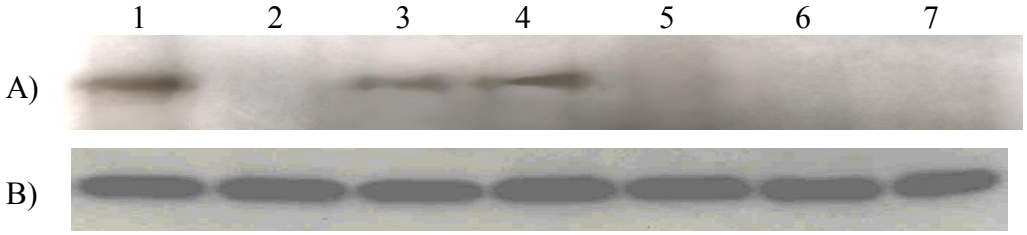

Figure 4.18. Absence of CagA translocation in AGS cells infected with *cag* PAI deletion mutant. Lane 1: *H. pylori* 26695 protein extract served as positive control; Lane 2: Uninfected AGS protein extract served as negative control; Lane 3-7: Proteins were extracted from AGS cells infected for 6 hours with: wild type *H. pylori* 26695 (Lane 3); *hsp20* deletion mutant (Lane 4); *cagA* deletion mutant (Lane 5); *hsp20/cagA* deletion mutant (Lane 6); *cag* PAI deletion mutant (Lane 7). A) probed with antibody against CagA; B) β-actin serves as loading control.

4.6 HSP20 translocation across T4SS

To explore the possibility of HSP20 being translocated across the T4SS, proteins were extracted from infected AGS cells and analyzed by western blotting. Figure 4.19 shows the absence of HSP20 in the infected AGS cellular protein lysates, regardless of the length of infection time (up to 16 hours) and the infecting strains of *H. pylori*. This is in line with our TEM studies (Section 4.4) during which no HSP20 translocation was observed irregardless of the infecting strains of *H. pylori* (Figure 4.11 and 4.12).

Figure 4.19B-D show the absence of HSP20 translocation. This confirms that *hsp20* deletion mutant and *hsp20/cagA* deletion mutant truly do not possess the *hsp20* gene. The absence of HSP20 translocation in AGS cells infected with wild type *H. pylori* 26695 was further exemplified in Figure 4.20A (Lane 3). Similarly, no HSP20 translocation was observed for AGS cells infected with *hsp20* deletion mutant (Lane 4), *cagA* deletion mutant (Lane 5), *hsp20/cagA* deletion mutant (Lane 6) and *cag* PAI deletion mutant (Lane 7).

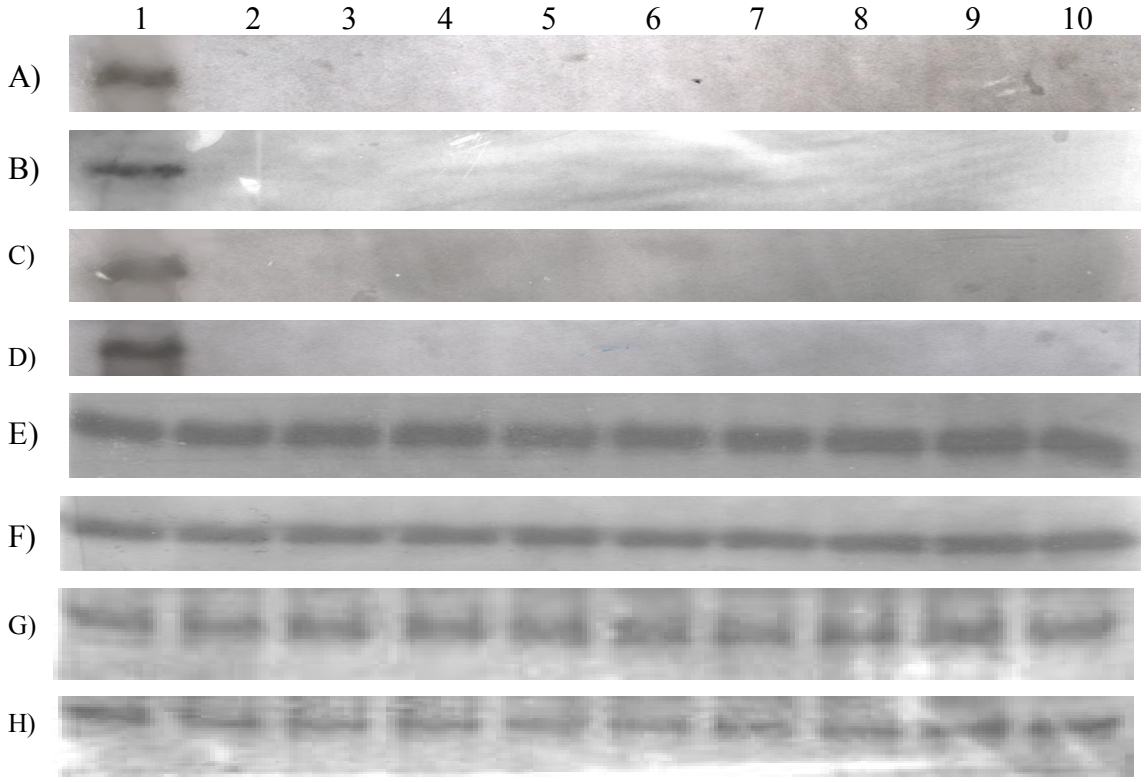

Figure 4.19. Absence of HSP20 translocation. Lane 1: wild type *H. pylori* 26695 protein extract served as positive control; Lane 2: Uninfected AGS protein extract served as negative control; Lane 3-10, wild type *H. pylori* 26695 infected AGS protein extracts for: 0 minutes (Lane 3), 15 minutes (Lane 4), 30 minutes (Lane 5), 2 hours (Lane 6), 4 hours (Lane 7), 6 hours (Lane 8), 8 hours (Lane 9), 16 hours (Lane 10). (A) and (E): Wild type *H. pylori* 26695 infected; (B) and (F): *hsp20* deletion mutant infected; (C) and (G): *cagA* deletion mutant infected; (D) and (H): *hsp20/cagA* deletion mutant infected. (E)-(H): β-actin serves as a loading control. Proteins extracts of *H. pylori* infected cells were probed with antibody against rHSP20 (A-D)

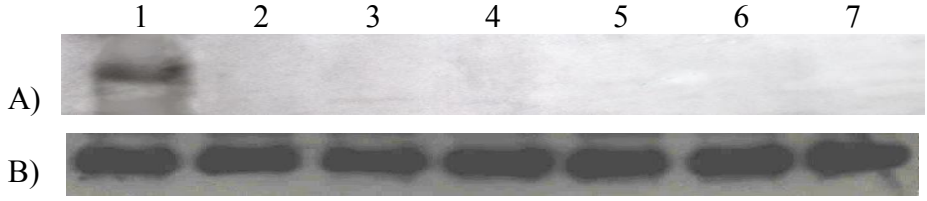

Figure 4.20. Absence of HSP20 translocation in AGS cells infected with *cag* PAI deletion mutant. Lane 1: wild type *H. pylori* 26695 protein extract served as positive control; Lane 2: Uninfected AGS protein extract served as negative control; Lane 3-7: Proteins were extracted from AGS cells infected for 6 hours. Lane 3: AGS cells infected with wild type *H. pylori* 26695; Lane 4: AGS cells infected with *hsp20* deletion mutant; Lane 5: *cagA* deletion mutant; Lane 6: AGS cells infected with *hsp20/cagA* deletion mutant; Lane7: AGS cells infected with *cag* PAI deletion mutant. A) probed with antibody against rHSP20; B) β-actin serves as loading control.

4.7 Hummingbird phenotype

Western blotting studies on CagA translocation have demonstrated that the absence of HSP20 has delayed the translocation of CagA into the host cells. Moese *et al* (2004) reported that infected AGS cells exhibit a dramatic elongation, where by thin, needle-like protrusions of 20 to 70 μm in length giving rise to hummingbird phenotype that is mainly dependent on the presence of CagA translocation. The study thus proceeded to examine if the absence of HSP20 also alters CagA's function in relation to the hummingbird phenotype formation.

Results showed that the hummingbird phenotype as defined by Moese *et al* (2004) was observed 2 hours post infection. The appearance of hummingbird phenotype became more dramatic and prominent with increase in time of infection. These observations were appearing in both wild type *H. pylori* 26695 infected AGS cells (Figure 4.21) and *hsp*20 deletion mutant infected AGS cells (Figure 4.22). In contrast, the hummingbird phenotype was absent in *cagA* deletion mutant infected AGS cells (Figure 4.23) and *hsp20/cagA* deletion mutant infected AGS cells (Figure 4.24) throughout the time course infection of 16 hours.

It was also observed that the hummingbird phenotype was well established at 4 hours post infection with wild type *H. pylori* 26695. Thus AGS cells infected with the various different strains of *H. pylori* for 4 hours were compared (Figure 4.25). Quantification of the hummingbird phenotype was performed by calculating the percentage of AGS cells exhibiting the hummingbird phenotype. Protrusions of 20 to 70 μm in length were included while smaller protrusions (< 20 μm in length) were excluded in the count.

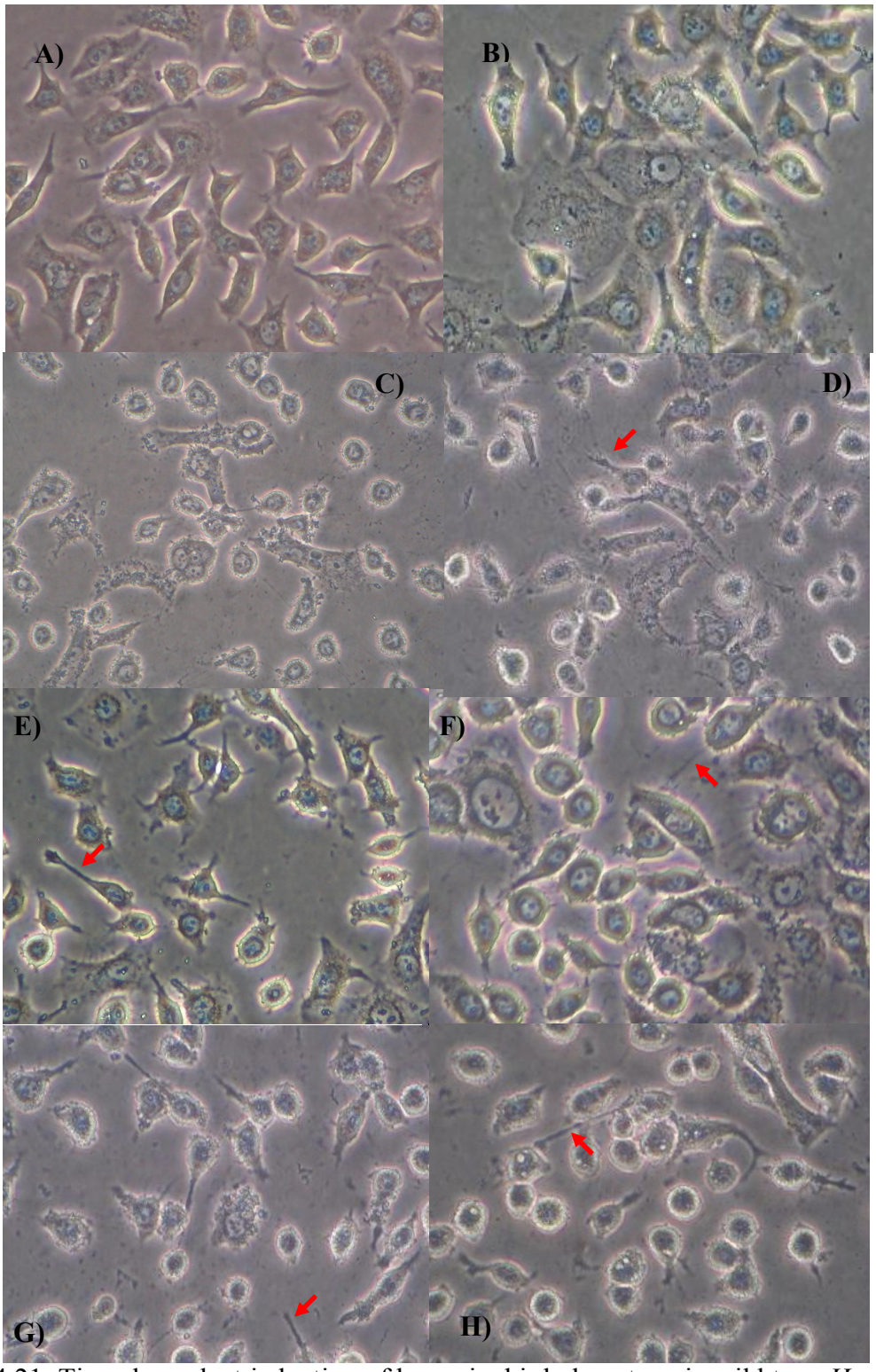

Figure 4.21. Time dependent induction of hummingbird phenotype in wild type *H. pylori* 26695 infected AGS cells. Uninfected AGS cells (A) showed negligible hummingbird phenotype. With increasing time of infection the hummingbird phenotype (as indicated by the red arrows) became more prominent. AGS cells infected for: 15 minutes (B); 30 minutes(C); 2 hours (D): 4 hours (E); 6 hours (F); 8 hours (G) and 16 hours.(H).

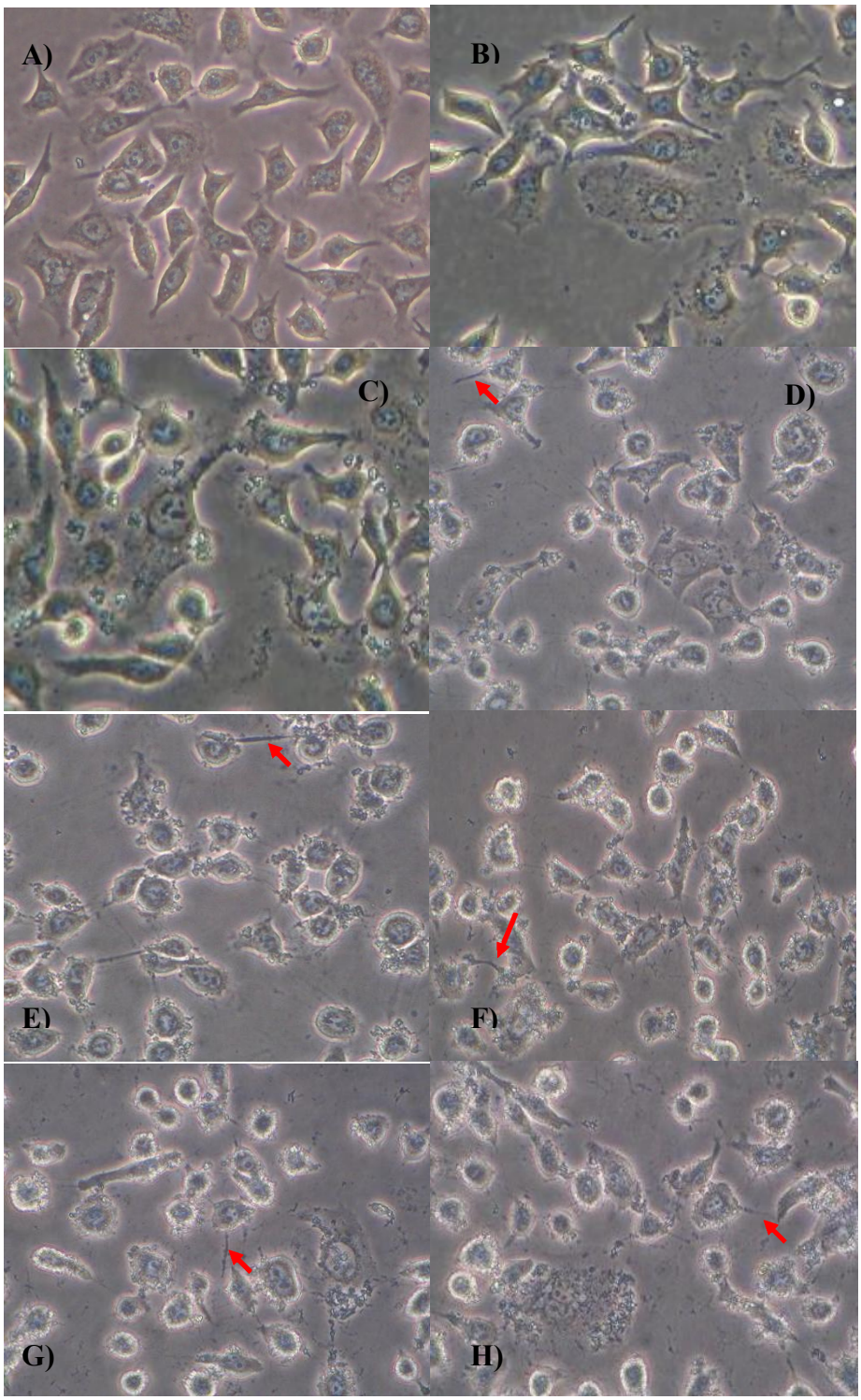

Figure 4.22. Time dependent induction of hummingbird phenotype in *hsp20* deletion mutant infected AGS cells. With increasing time of infection from 0 minute (A); 15 minutes (B); 30 minutes (C); 2 hours (D); 4 hours (E); 6 hours (F); 8 hours (G); 16 hours (H), the hummingbird phenotype (as indicated by the red arrows) became more prominent.

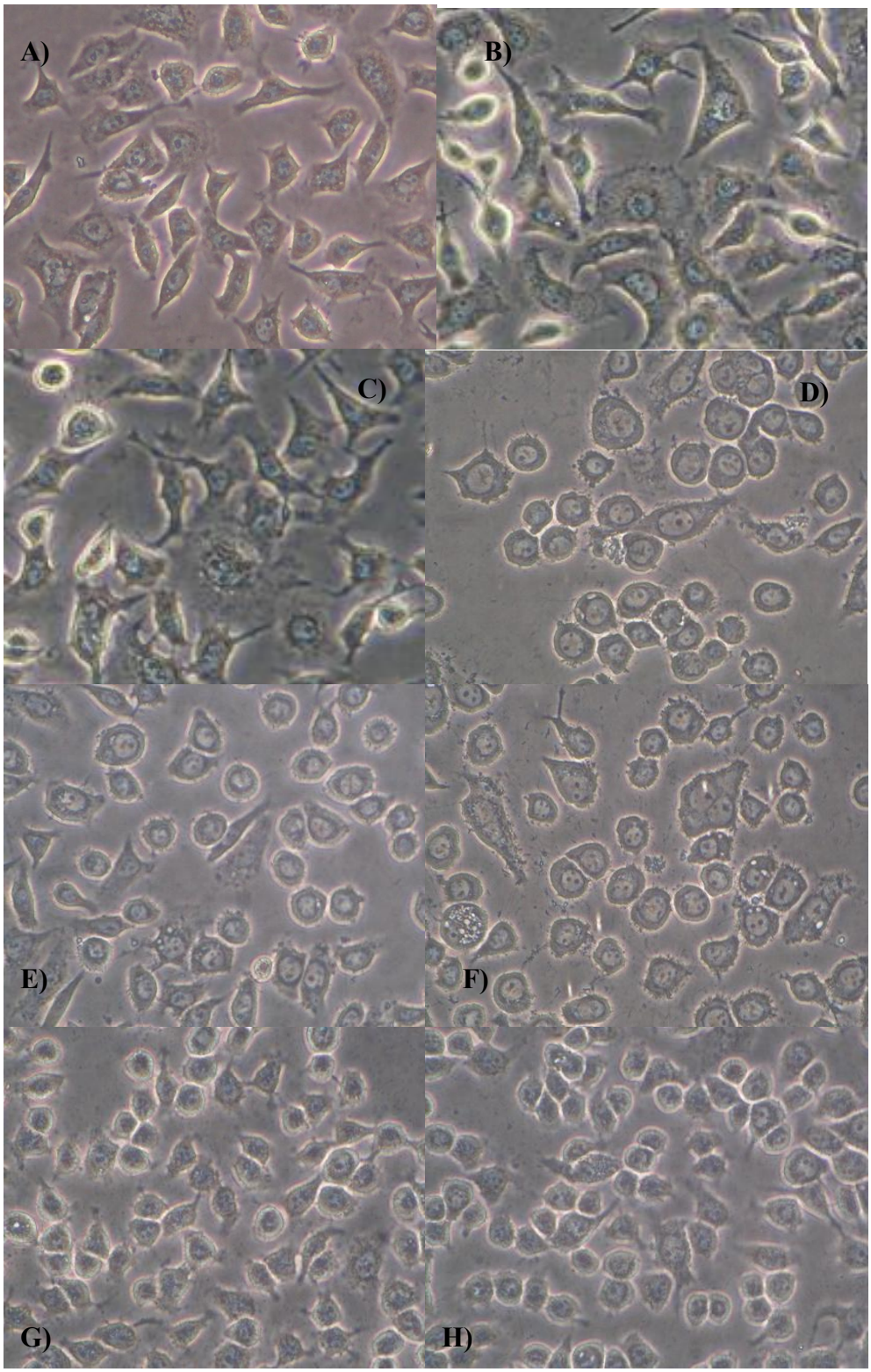

Figure 4.23. Absence of hummingbird phenotype induction in *cagA* deletion mutant infected AGS cells. No hummingbird phenotype was observed, regardless of length of infection time: 0 minutes (A); 15 minutes (B) to 30 minutes (C) to 2 hours (D) to 4 hours (E) to 6 hours (F) to 8 hours (G) to 16 hours (H).

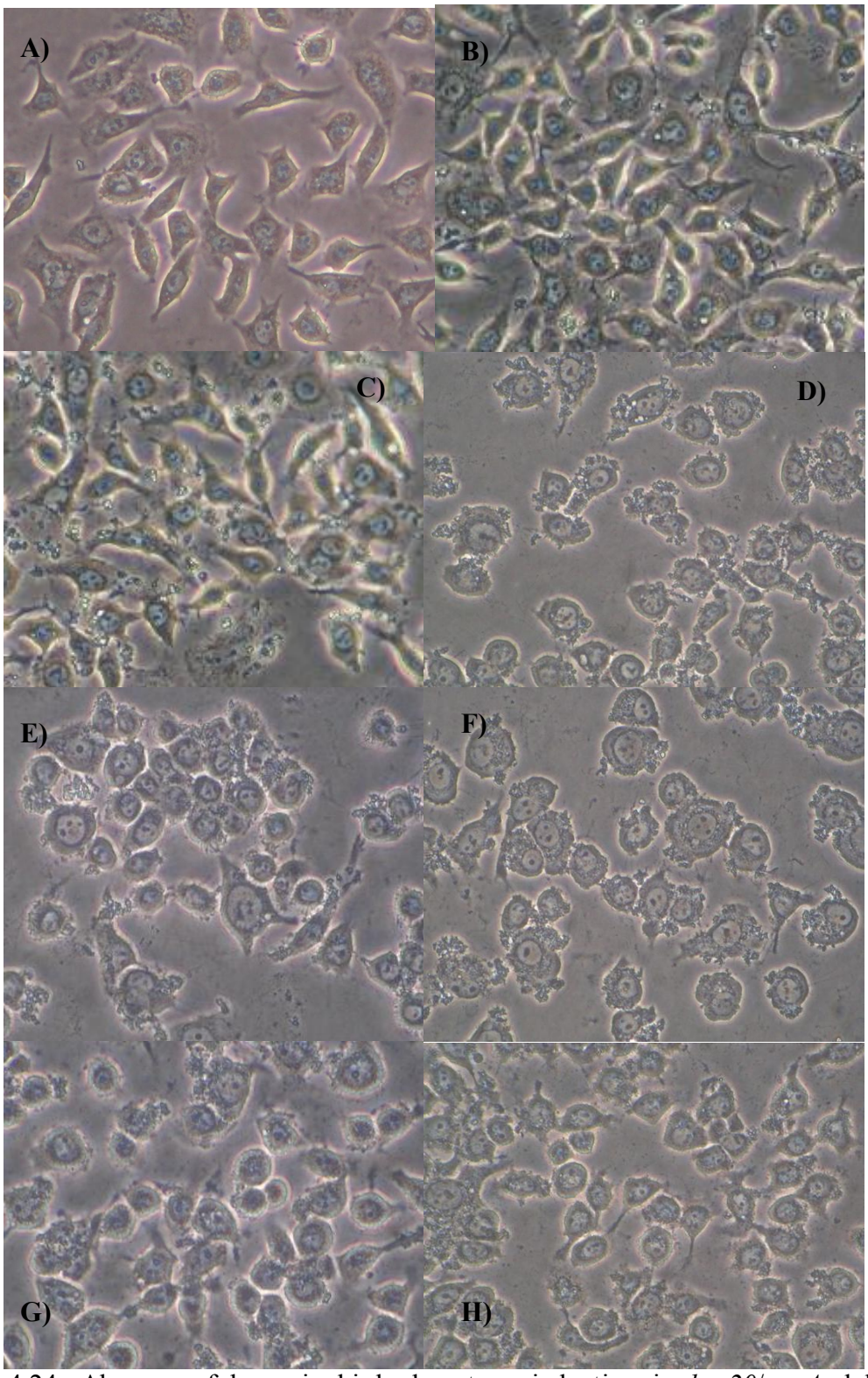

Figure 4.24. Absence of hummingbird phenotype induction in *hsp20*/*cagA* deletion mutant infected AGS cells. No hummingbird phenotype was observed, regardless of length of infection time: 0 minute; 15 minutes (B) to 30 minutes (C) to 2 hours (D) to 4 hours (E) to 6 hours (F) to 8 hours (G) to 16 hours (H).

The percentages of AGS cells exhibiting hummingbird phenotype in wild type *H. pylori* 26695 infected AGS cells and *hsp20* deletion mutant infected AGS cells were 34% and 32%, respectively. The induction by the two strains was comparable to one another. On the other hand, the percentages of AGS cells exhibiting hummingbird phenotype in *cagA* deletion mutant infected AGS cells (Figure 4.25C) and *hsp20/cagA* deletion mutant infected AGS cells (Figure 4.25D) were 5% and 6%, respectively. The percentage of hummingbird phenotype by these two strains of *H. pylori* 26695 was comparable to the basal percentage of 8% in uninfected AGS cells. Thus, it shows that the hummingbird phenotype observed for AGS cells infected with these 2 strains of *H. pylori* was negligible.

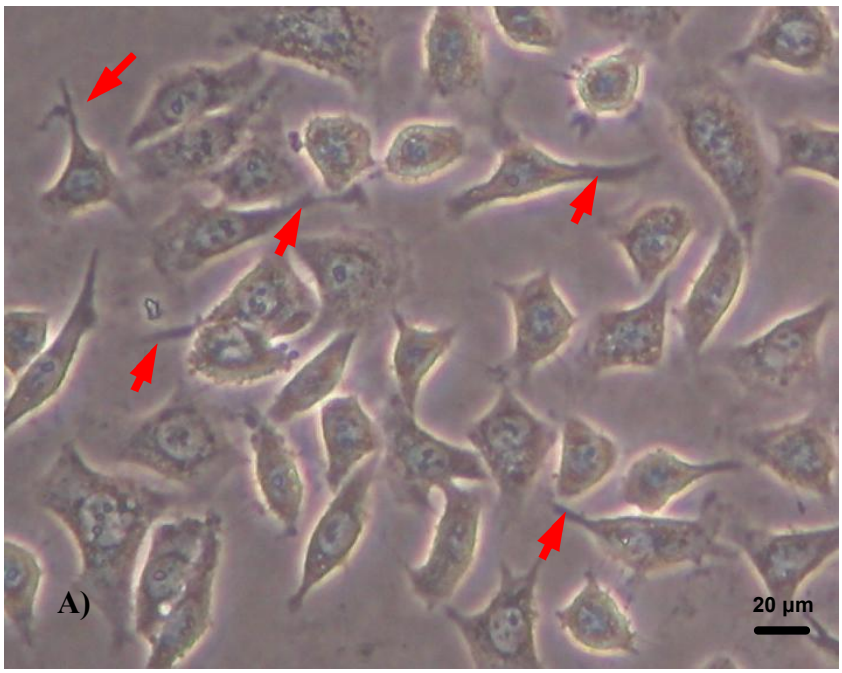

Figure 4.25. Quantification of the hummingbird phenotype in AGS cells. Negligible hummingbird phenotype was observed with the uninfected AGS cells (A). Red arrows indicated protrusions of 20 to 70 µm in length.

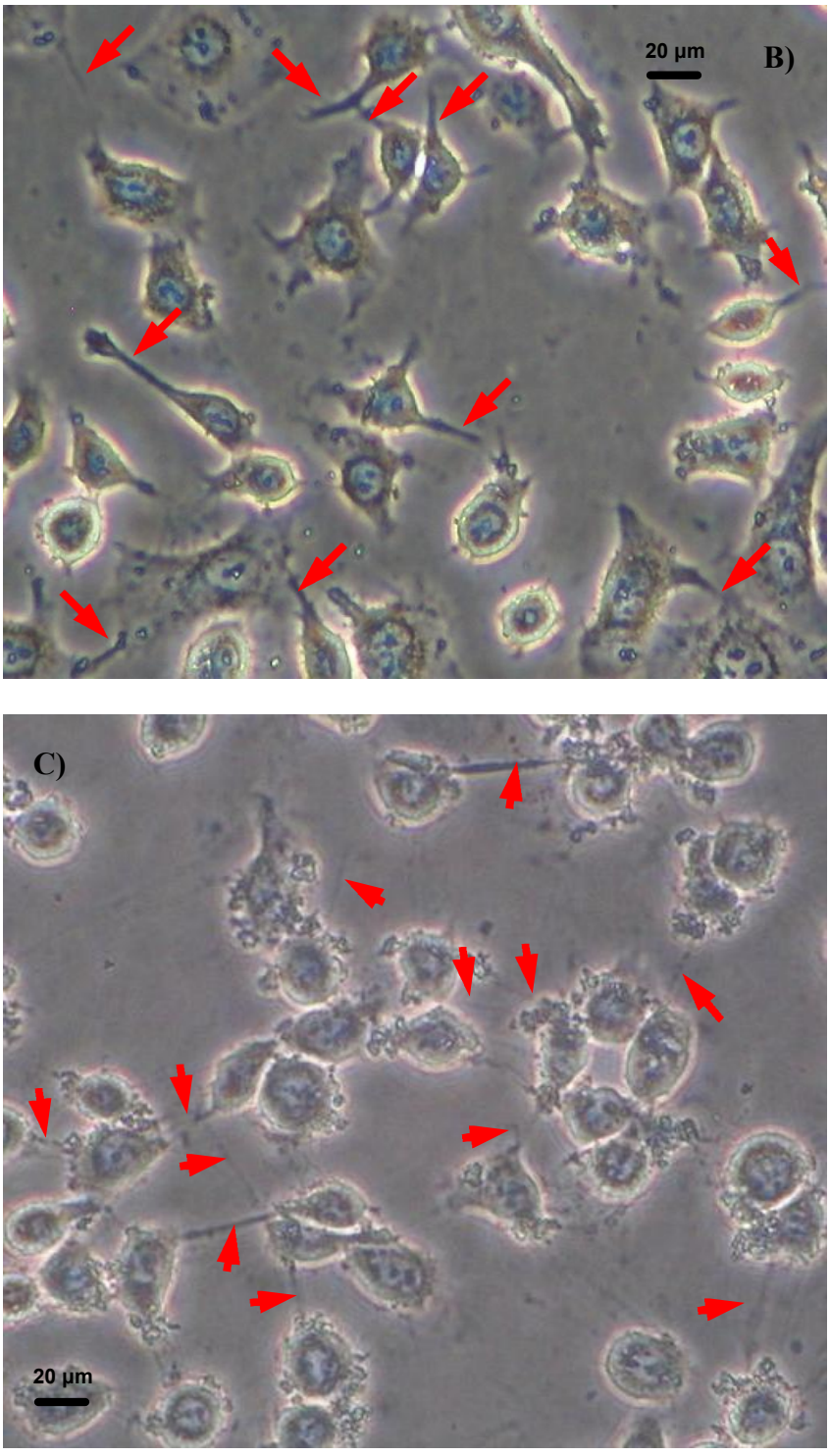

Figure 4.25. Quantification of the hummingbird phenotype in AGS cells. Significant induction of hummingbird phenotype was observed with AGS cells infected with wild type *H. pylori* 26695 (B) and AGS cells infected with *hsp20* deletion mutant (C). AGS cells were infected for 4 hours with the respective strains of *H. pylori*. Red arrows indicated protrusions of 20 to 70 µm in length.

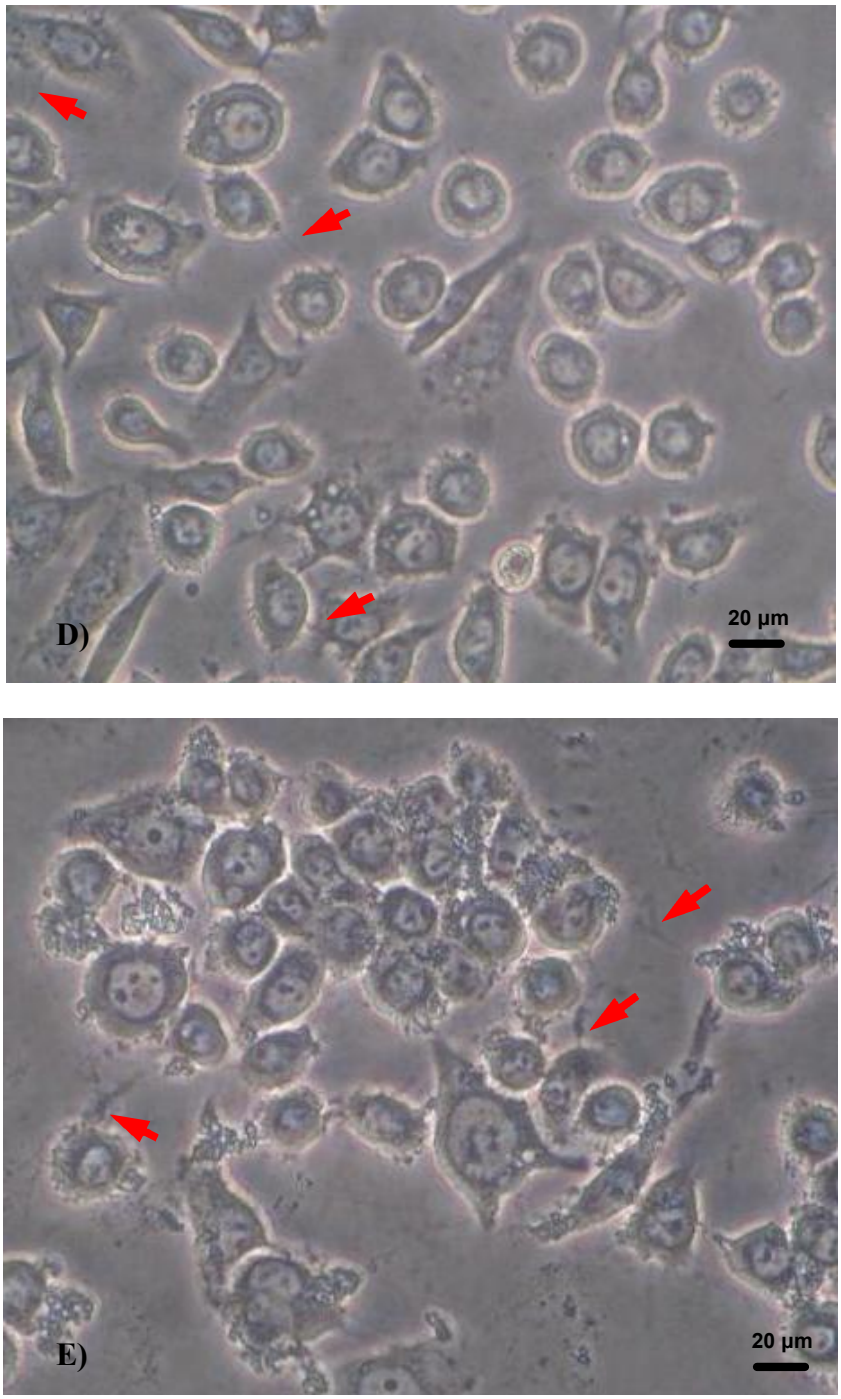

Figure 4.25. Quantification of the hummingbird phenotype in AGS cells. Insignificant induction of hummingbird phenotype was observed with AGS cells infected with *cagA* deletion mutant (D) and AGS cells infected with *hsp20/cagA* deletion mutant (E). AGS cells were infected for 4 hours with the respective strains of *H. pylori*. Red arrows indicated protrusions of 20 to 70 µm in length.

4.8 IL8 production

It has been reported that *H. pylori* induces generation of IL-8 (Munzenmaier *et al*, 1997; Yamaoka *et al*, 1997; Covacci *et al*, 1998; Odenbreit *et al*, 2001; Fischer *et al*, 2001; Selbach *et al*, 2002; Backert *et al*, 2004; Brandt *et al*, 2005). The study proceeded to analyse if HSP20 alters the ability of CagA to induce immunological responses such as IL8 production using the BD OptEIA™ Human IL8 ELISA kit (BD Biosciences).

Figure 4.26 shows that there was minimal IL8 production up to 2 hour post infection while a gradual increase in IL8 production was observed from 2 hour to 16 hours post infection. This trend was observed for all infected AGS cells in this study, regardless of the strains of *H. pylori* tested.

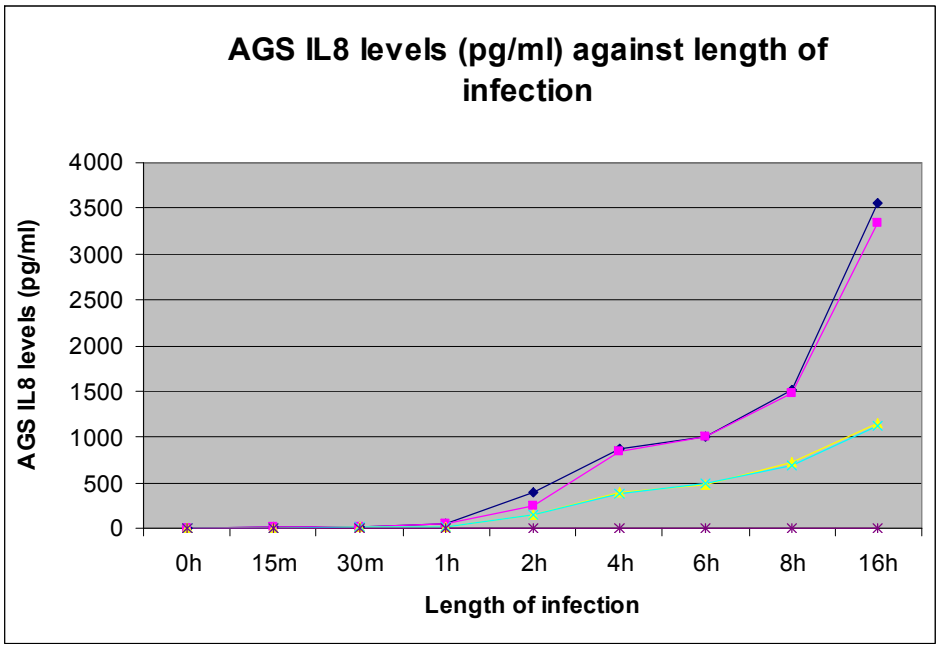

Figure 4.26. Time-dependent IL8 induction. Uninfected AGS cells (*) showed negligible IL8 production. AGS cells infected with wild type *H. pylori* 26695 (blue line) and AGS cells infected with *hsp20* deletion mutant (purple line) had a much elevated IL8 production as compared to that by AGS cells infected with *cagA* deletion mutant (yellow line) and AGS cells infected with *hsp20/cagA* deletion mutant (cyan line).

It was observed that IL8 production by *hsp20* deletion mutant infected AGS cells throughout the 16 hours time course of infection was highly comparable to that by wild type *H. pylori* 26695 infected AGS cells (Figure 4.26). Similarly, the IL8 production by *cagA* deletion mutant infected AGS cells and *hsp20/cagA* deletion mutant infected AGS cells throughout the 16 hours time course of infection was highly comparable. It is interesting to note that although IL8 production by *cagA* deletion mutant and *hsp20/cagA* deletion mutant infected AGS cells was observed to be 2-3 folds lower than that produced by wild type *H. pylori* 26695 infected AGS cells and *hsp20* deletion mutant infected AGS cells. However, the IL8 production generated by AGS cells infected by *cagA* and *hsp20/cagA* deletion mutants were still substantial, as compared to that produced by uninfected AGS cells.

4.9 ZO-1 redistribution

Amieva *et al* (2003) has found that CagA mediates assembly of ZO-1 at the extra-junctional sites of bacterial attachment and disrupts tight junction function. The ability of HSP20 to affect CagA to induce physiological changes such as tight junction disruption was analysed using confocal immunofluorescence.

Figure 4.27 shows that in wild type *H. pylori* 26695 infected T84 cells ZO-1 recruitment to extra-junctonal bacterial attachment sites was observed as early as 30 minutes post infection. An overlap of *H. pylori* (showed by the green fluorescence signal) and ZO-1 (showed by the red fluorescence signal) indicates the presence of ZO-1 co-localization with extra-junctional bacterial attachment sites. Although ZO-1 recruitment to bacterial attachment sites was observed 30 minutes post infection, disruption of tight junctions was only observed 8 hours post infection.

hsp20 deletion mutant infected T84 cells also showed ZO-1 recruitment to extra-junctional bacterial attachment sites as early as 30 minutes post infection (Figure 4.28). However, disruption of tight junctions was only observed 12 hours into the infection time course. Tight junction disruption was less substantial at each of the time points as compared to wild type *H. pylori* 26695 infected T84 cells.

Figures 4.29-4.30 show that no ZO-1 recruitment to extra-junctional bacterial attachment sites was observed in T84 cells infected with *cagA* deletion mutant or with *hsp20/cagA* deletion mutant. T84 cells infected with either of these deletion mutants retained intact tight junctions at the cell periphery even after 12 hours of infection.

We then investigated the possibility of rHSP20 supplementation to the *hsp20* deletion mutant infecting medium to restore a ZO-1 recruitment to extra-junctional bacterial attachment sites and tight junctional disruption. Figure 4.31 shows that ZO-1 recruitment to extra-junctional bacterial attachment sites was observed as early as 30 minutes post infection in *hsp20* deletion mutant infected T84 cells supplemented with rHSP20. However, disruption of tight junctions was only observed 12 hours post infection. With the supplementation of rHSP20 at each of the time points tested the tight junction disruption observed was more significant, as compared to *hsp20* deletion mutant infected T84 cells. However, when rCagA was supplemented to the *cagA* deletion mutant in the infecting medium ZO-1 recruitment to extra-junctional bacterial attachment sites was not observed. Intact tight junctions were retained at the cell periphery (Figure 4.32).

The sufficiency of rHSP20 alone to effect ZO-1 recruitment to extra-junctional sites and tight junctional disruption was examined. Figure 4.33 shows that these two phenotypic changes were absent even after 12 hours of incubation. Similarly, there is an

absence of ZO-1 recruitment to extra-junctional bacterial attachment sites in T84 cells incubated with rCagA (Figure 4.34). Intact tight junctions were also retained at the cell periphery. Both phenotypes were observed despite the 12 hours of incubation time. In addition to this, it was shown in Figure 4.35 that the incubation with supplementation of CagA did not result in the translocation of rCagA from the media inoculum into the host cells as probed using anti-CagA, despite a prolonged incubation of 12 hours.

In the infected T84 cells, there is a total absence of nicely formed tight junctions as seen in non-infected control (Figure 4.36A). ZO-1 was absent at the tight junctional sites located at the cell periphery. Figure 4.36B shows that wild type *H. pylori* 26695 recruited ZO-1 to bacterial attachment sites from the tight junctional sites at the cell periphery. In comparison, ZO-1 recruitment to bacterial attachment sites in T84 cells infected with *hsp20* deletion mutant was evidently reduced (Figure 4.36C). Also, the extra-junctional co-localization of ZO-1 and *H. pylori* was evident. However, there was still the presence of tight junctions, though it was significantly reduced. It is interesting to note that the addition of rHSP20 into *hsp20* deletion mutant infecting inoculum showed a ZO-1 recruitment to bacterial attachment sites (Figure 4.36F), which was comparable to that seen with the wild type *H. pylori* 26695 infecting inoculum. In contrast, no ZO-1 recruitment to the bacterial attachment sites and no tight junction disruption were observed in T84 cells infected with *H. pylori* 26695 *cagA* deletion mutant (Figure 4.36D) or T84 cells infected with *H. pylori* 26695 *hsp20/cagA* deletion mutant (Figure 4.36E), even after 12 hours of infection. Figure 4.36J also shows an absence of ZO-1 recruitment to extra-junctional bacterial attachment sites and tight junction disruption in T84 cells infected with *H. pylori* 26695 *cag* PAI deletion mutant.

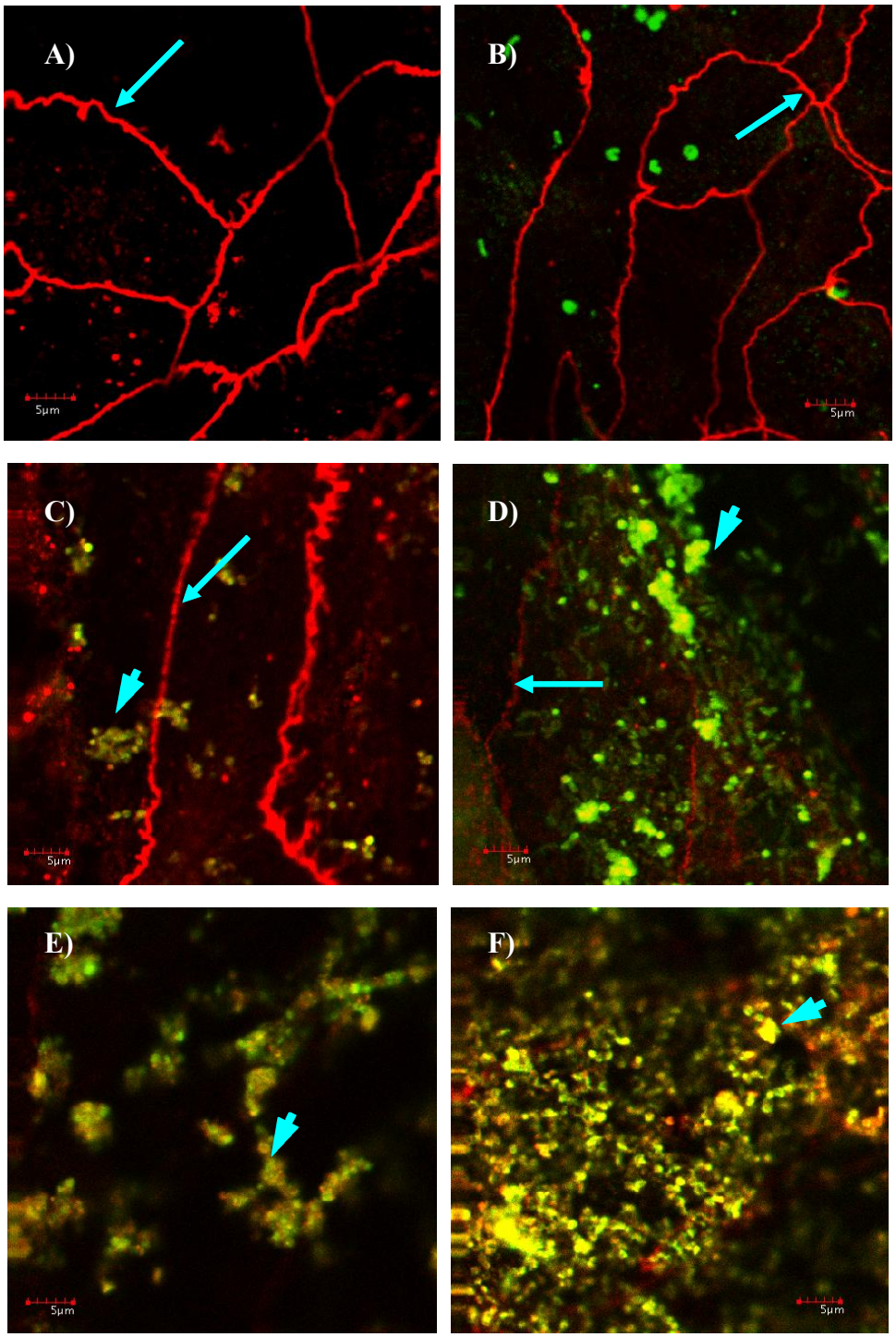

Figure 4.27. Presence of ZO-1 recruitment to extra-junctional bacterial attachment sites in wild type *H. pylori* 26695 infected T84 cells. (A): negative control (uninfected T84 cells); (B) - (F): T84 cells infected with increasing length of infection time: 30 minutes (B); 2 hours (C); 4 hours (D); 8 hours (E); 12 hours (F). A merged image shows co-localization of ZO-1 (red) with *H. pylori* (green) at extra-junctional bacterial attachment sites which is indicated by the big blue arrowhead. Small blue arrowhead indicates presence of ZO-1 at tight junctional sites.

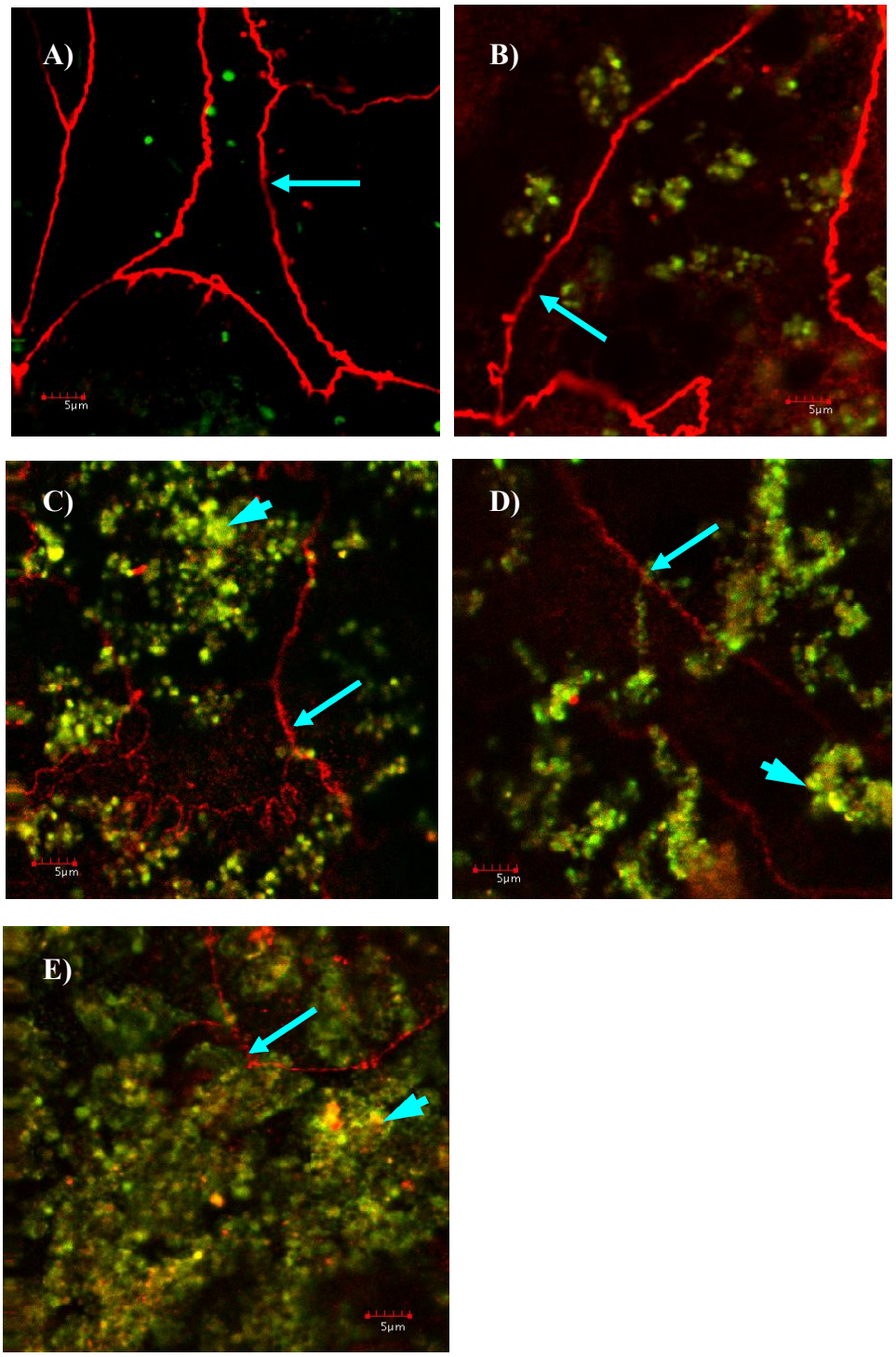

Figure 4.28. Presence of ZO-1 recruitment to extra-junctional bacterial attachment sites in *hsp20* deletion mutant infected T84 cells. (A) - (E): T84 cells infected with increasing length of infection time: 30 minutes (A); 2 hours (B); 4 hours (C); 8 hours (D); 12 hours (E). A merged image shows co-localization of ZO-1 (red) with *H. pylori* (green) at the extra-junctional bacterial attachment sites, which is indicated by the big blue arrowhead. Small blue arrowhead indicates presence of ZO-1 at tight junctional sites.

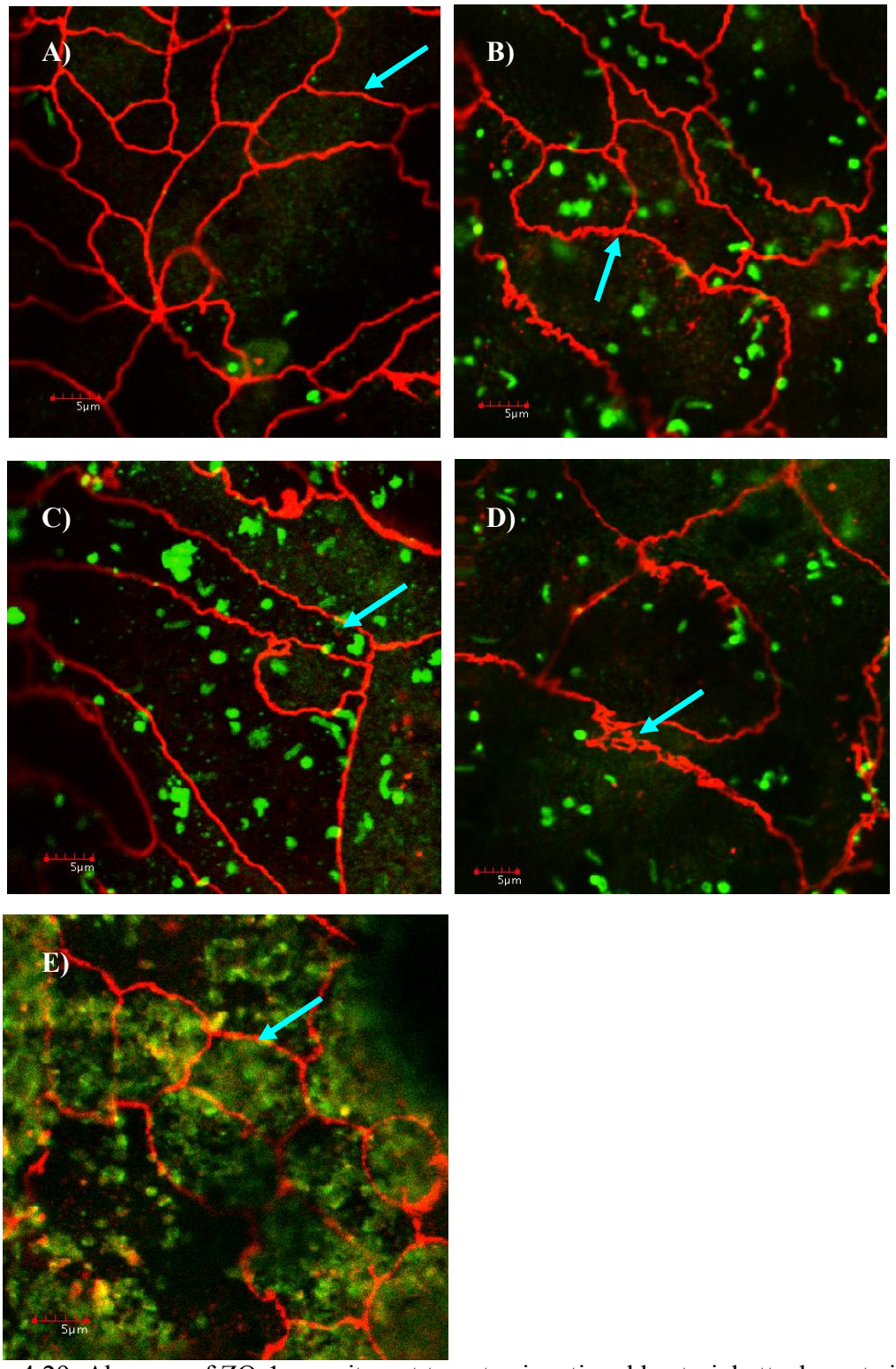

Figure 4.29. Absence of ZO-1 recruitment to extra-junctional bacterial attachment sites in *cagA* deletion mutant infected T84 cells. (A) - (E): T84 cells infected with increasing length of infection time: 30 minutes (A); 2 hours (B); 4 hours (C); 8 hours (D); 12 hours (E). Small blue arrowhead indicates presence of ZO-1 at tight junctional sites.

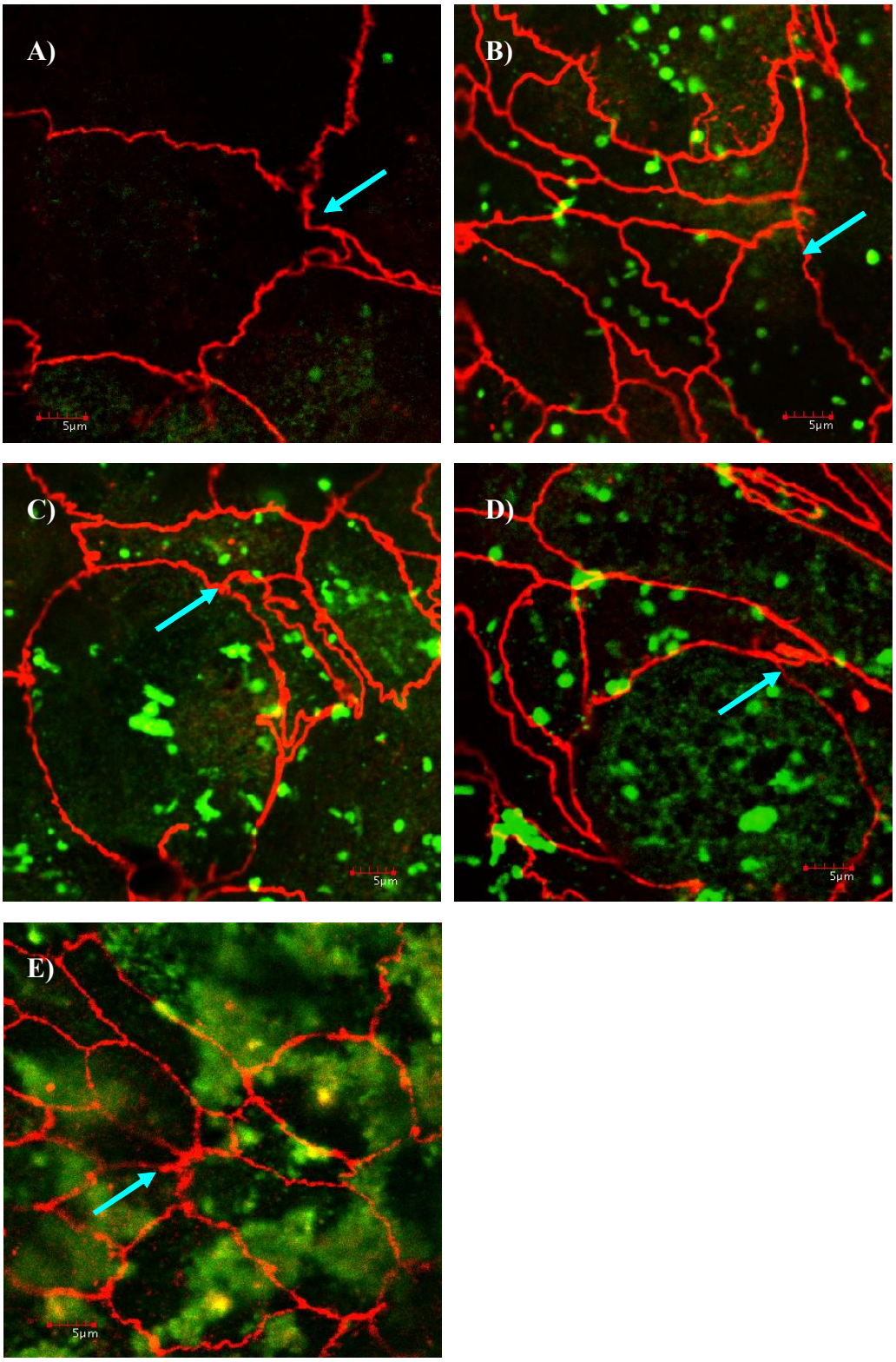

Figure 4.30. Absence of ZO-1 recruitment to extra-junctional bacterial attachment sites in *hsp20/cagA* deletion mutant infected T84 cells. (A) - (E): T84 cells infected with increasing length of infection time: 30 minutes (A); 2 hours (B); 4 hours (C); 8 hours (D); 12 hours (E). Small blue arrowhead indicates presence of ZO-1 at tight junctional sites.

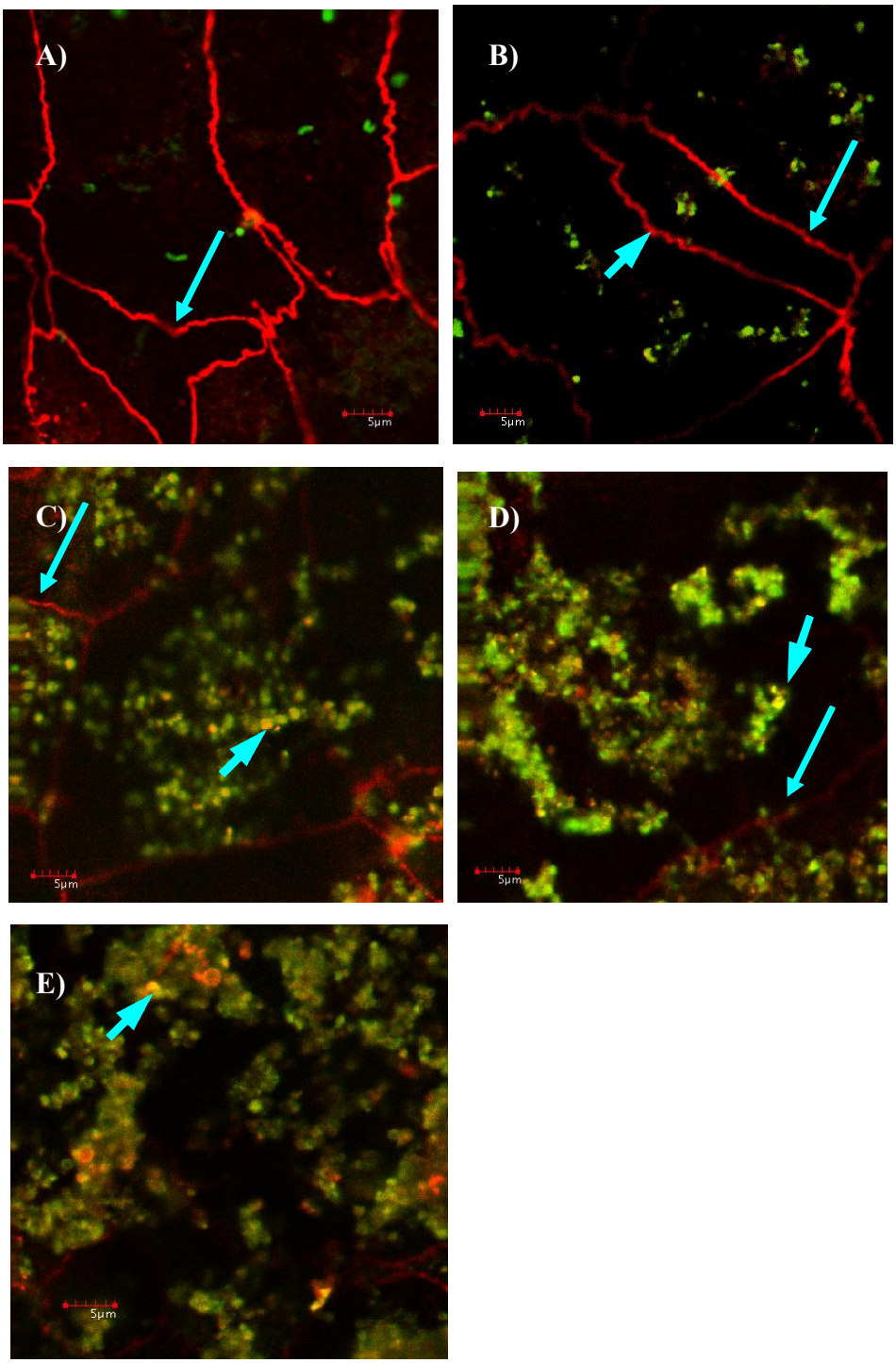

Figure 4.31. Presence of ZO-1 recruitment to extra-junctional bacterial attachment sites in *hsp20* deletion mutant infected T84 cells supplemented with rHSP20. (A) - (E): T84 cells infected with increasing length of infection time: 30 minutes (A); 2 hours (B); 4 hours (C); 8 hours (D); 12 hours (E). A merged image shows co-localization of ZO-1 (red) with *H. pylori* (green) at extra-junctional bacterial attachment sites, which is indicated by the big blue arrowhead. Small blue arrowhead indicates presence of ZO-1 at tight junctional sites.

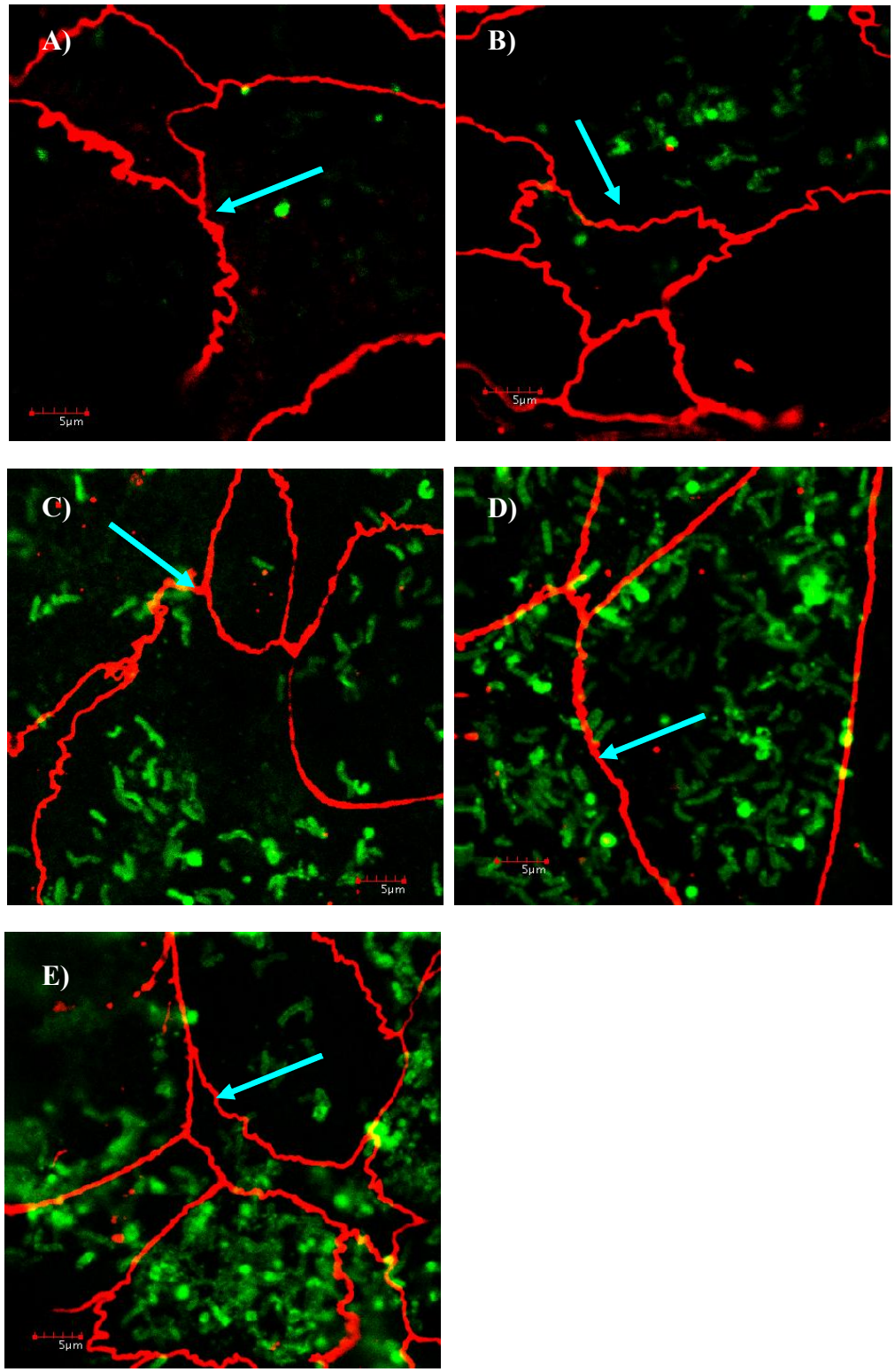

Figure 4.32. Absence of ZO-1 recruitment to extra-junctional bacterial attachment sites in *cagA* deletion mutant infected T84 cells supplemented with rCagA. (A) - (E): T84 cells infected with increasing length of infection time: 30 minutes (A); 2 hours (B); 4 hours (C); 8 hours (D); 12 hours (E). Small blue arrowhead indicates presence of ZO-1 at tight junctional sites.

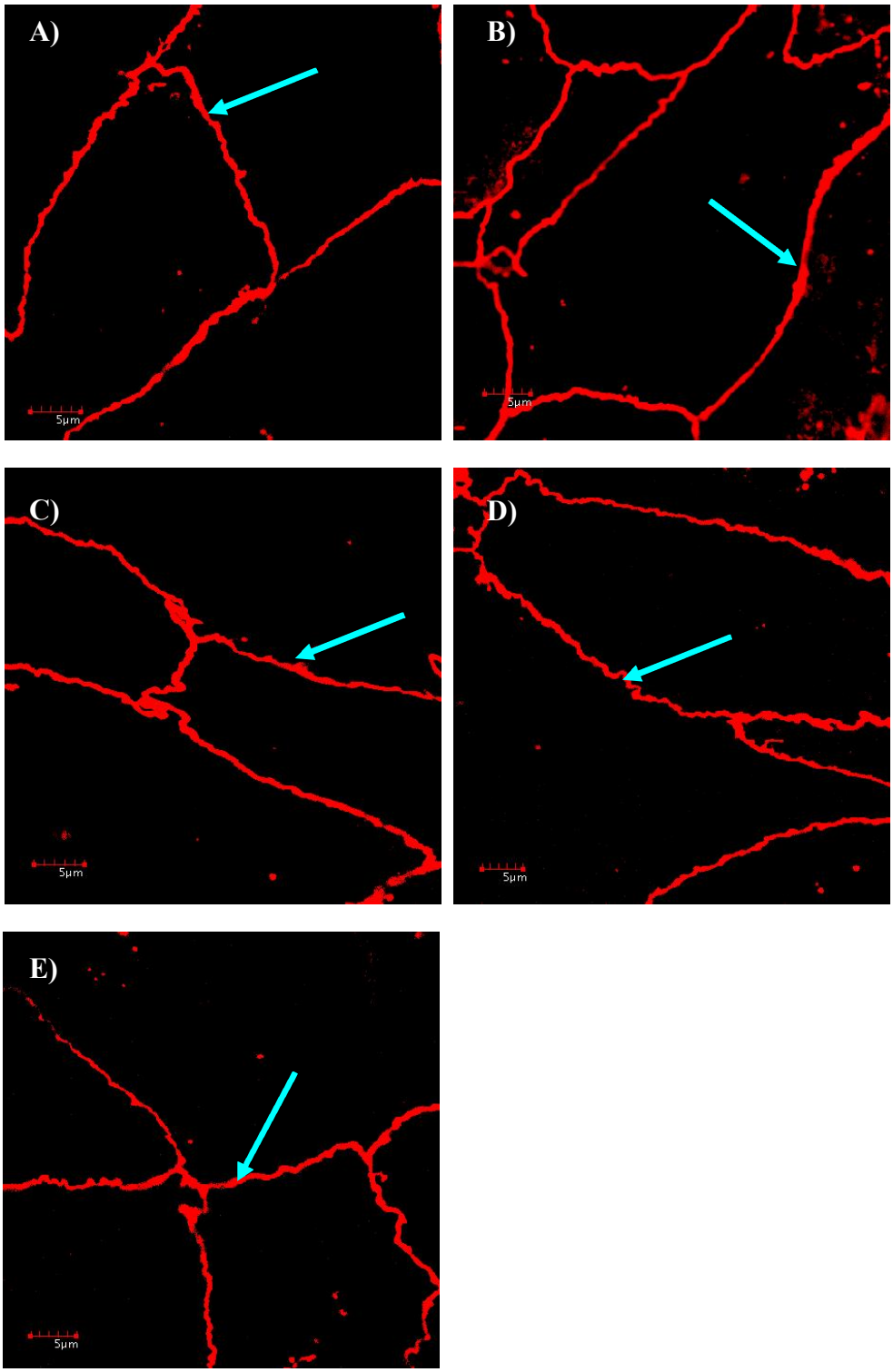

Figure 4.33. ZO-1 at tight junctional sites in T84 cells supplemented with rHSP20. (A) - (E): T84 cells infected with increasing length of infection time: 30 minutes (A); 2 hours (B); 4 hours (C); 8 hours (D); 12 hours (E). Small blue arrowhead indicates presence of ZO-1 at tight junctional sites.

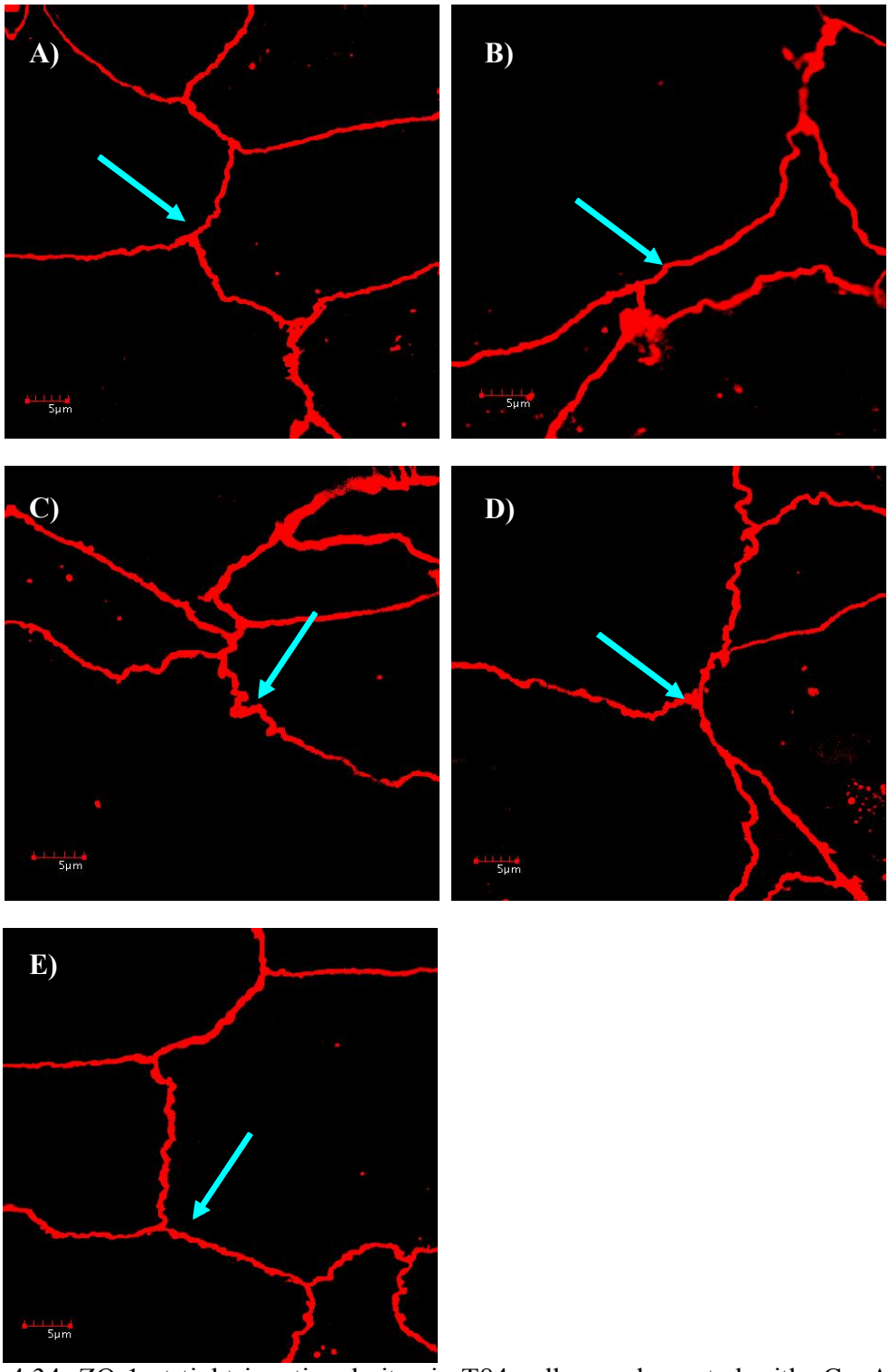

Figure 4.34. ZO-1 at tight junctional sites in T84 cells supplemented with rCagA. (A) - (E): T84 cells infected with increasing length of infection time: 30 minutes (A); 2 hours (B); 4 hours (C); 8 hours (D); 12 hours (E). Small blue arrowhead indicates presence of ZO-1 at tight junctional sites.

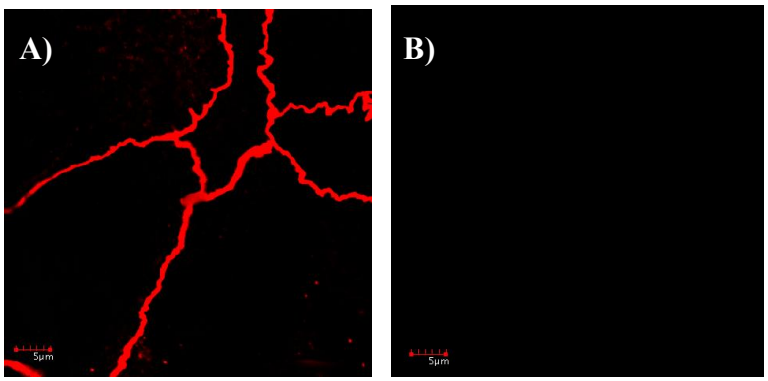

Figure 4.35. Absence of translocation of rCagA in T84 cells supplemented with rCagA for a period of 12 hours. (A): Cells were probed with anti-ZO-1; (B): Cells were probed with anti-CagA.

Figure 4.36B shows that wild type *H. pylori* 26695 recruited ZO-1 to bacterial attachment sites from the tight junctional sites at the cell periphery. In these infected cells, there is a total absence of nicely formed tight junctions as seen in non-infected control (Figure 4.36A). ZO-1 was absent at the tight junctional sites located at the cell periphery. In comparison, ZO-1 recruitment to bacterial attachment sites in T84 cells infected with *hsp20* deletion mutant was evidently reduced (Figure 4.36C). Also, the extra-junctional co-localization of ZO-1 and *H. pylori* was evident. However, there was still the presence of tight junctions, though it was very significantly reduced. It is interesting to note that the addition of rHSP20 into *hsp20* deletion mutant infecting inoculum showed a ZO-1 recruitment to bacterial attachment sites (Figure 4.36F), which was comparable to that seen with the wild type *H. pylori* 26695 infecting inoculum. In contrast, no ZO-1 recruitment to the bacterial attachment sites and no tight junction disruption were observed in T84 cells infected with *H. pylori* 26695 *cagA* deletion mutant (Figure 4.36D) or T84 cells infected with *H. pylori* 26695 *hsp20/cagA* deletion mutant (Figure 4.36E), even after 12 hours of infection. Figure 4.36J also shows an absence of ZO-1 recruitment to extra-junctional bacterial attachment sites and tight junction disruption in T84 cells infected with *H. pylori* 26695 *cag* PAI deletion mutant.

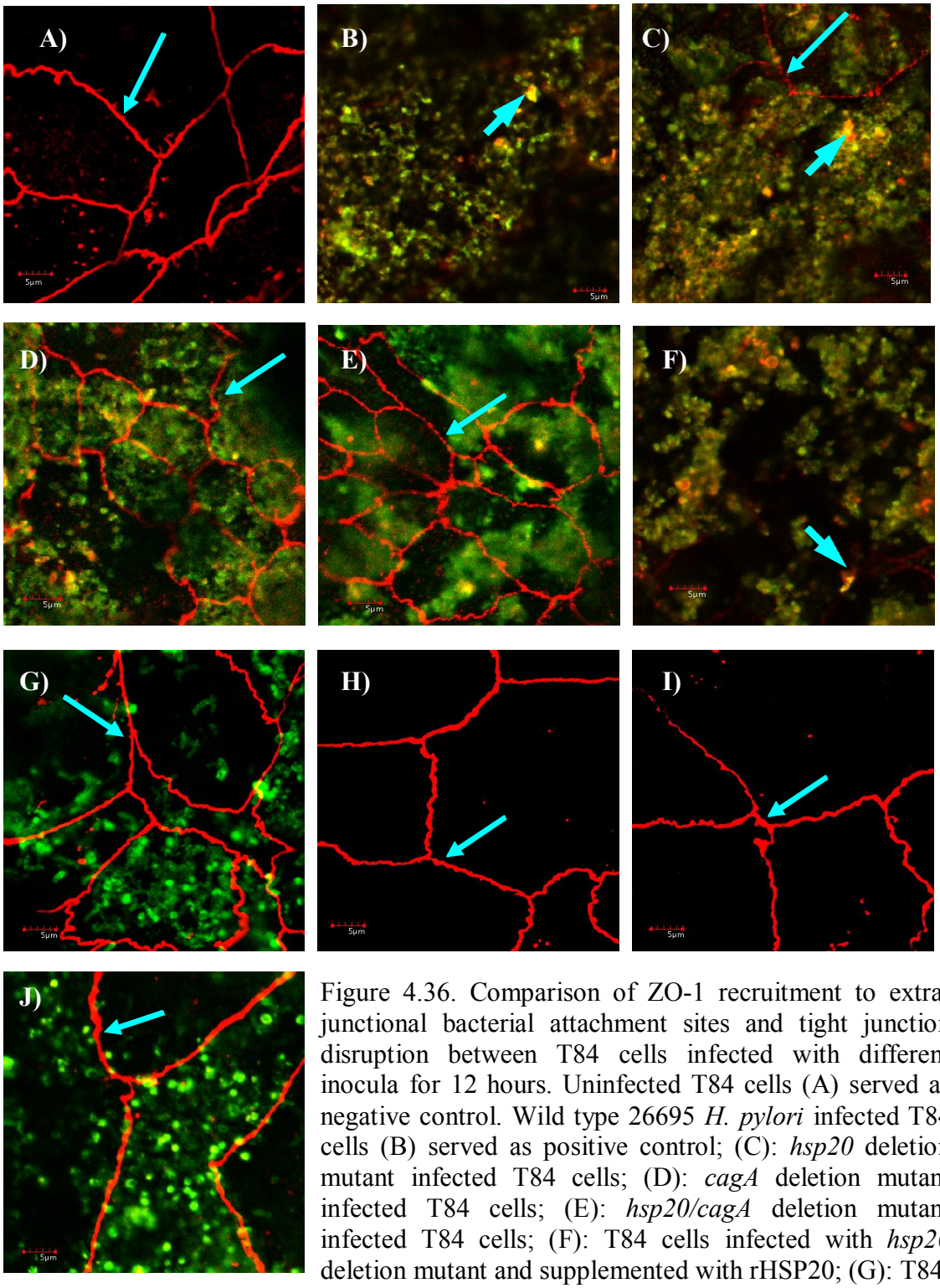

Figure 4.36. Comparison of ZO-1 recruitment to extra-junctional bacterial attachment sites and tight junction disruption between T84 cells infected with different inocula for 12 hours. Uninfected T84 cells (A) served as negative control. Wild type 26695 *H. pylori* infected T84 cells (B) served as positive control; (C): *hsp20* deletion mutant infected T84 cells; (D): *cagA* deletion mutant infected T84 cells; (E): *hsp20/cagA* deletion mutant infected T84 cells; (F): T84 cells infected with *hsp20* deletion mutant and supplemented with rHSP20; (G): T84 cells infected with deletion mutant supplemented with rCagA; (H): T84 cells infected with rHSP20: (I): T84 cells infected with rCagA; (J): T84 cells infected with *cag* PAI deletion mutant. Presence of ZO-1 co-localization with extra-junctional bacterial attachment sites is indicated by the big blue arrowhead. Small blue arrowhead indicates presence of ZO-1 at tight junctional sites.

4.10 Tight junction function disruption

4.10.1 Optimum infection period

From the confocal immunofluorescence studies, a complete disruption of the tight junction of T84 cells infected with *H. pylori* 26695, exemplified by total abolishment of intact tight junctions nicely formed around the cell periphery, was only observed 8 hours post infection (Figure 4.27). Therefore, 8 hours was chosen as the infecting time for the functional test.

Solute leakage may possibly be accorded to cells dying and the disintegration of the cell monolayer instead of disruption of the tight junction complex. To reduce the possibility of leakage of biotinylated albumin due to spontaneous cell death, the percentage of viability of the tissue culture cells was determined using MTT assay. Figure 4.37 shows that there was a gradual decrease of cell viability with increasing length of infection time. An 8 hours of infecting time showed that there was a good percentage of 90% of infected T84 cells that were still viable 8 hours post infection and complete disruption of tight junction of T84 cells infected with *H. pylori* 26695 was only observed 8 hours post infection (Figure 4.27). In addition, albumin is a relatively large compound and the disruption of the tight junction complex might not be sufficient enough to allow the biotinylated albumin to diffuse across. The longer period of 12 hours and beyond were not chosen as the infecting time because the cell viability falls below 90% and any solute leakage may possibly be accorded to cells dying and the disintegration of the cell monolayer instead of disruption of the tight junction complex.

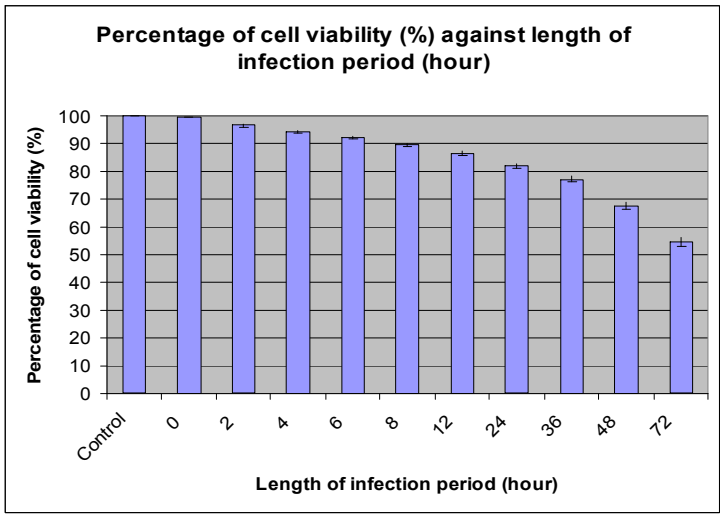

Figure 4.37. Cell viability reflecting optimum infection time for functional test. T84 cells were infected with wild type *H. pylori* 26695.

4.10.2 Detection of disruption of tight junction function

Biotinylated albumin assay was used to detect tight junction function disruption. The principle of the assay is that when tight junction barrier function is disrupted, biotinylated albumin leaks across the infected monolayer. Figure 4.38 shows the presence of solute leakage across the T84 monolayer as indicated by the presence of the biotinylated albumin. Sample in Lane 1 was extracted from the basolateral chamber, serving as a positive control. Sample in Lane 2 was extracted from the apical chamber in an uninfected T84 condition, serving as a standard. The presence of a weak band shows that there was a basal leakage of biotinylated albumin. This could be because of spontaneous decrease in cell viability (Figure 4.37).

Leakage of biotinylated albumin was observed for all the eight infecting inocula. Lanes 3, 4, and 7 (Figure 4.38) shows comparable band width and intensity, indicating rather similar biotinylated albumin leakage level among the three infecting inocula (wild type *H. pylori* 26695, *hsp20* deletion mutant, and *hsp20* deletion mutant supplemented with rHSP20 respectively). However, leakage was highest for Lanes 3 (wild type *H.*

pylori 26695) and Lane 7 (*hsp20* deletion mutant supplemented with rHSP20). The sizes and intensities of both Lanes 3 and 7 are somewhat similar to each other. Lane 4, which was sample infected with *hsp20* deletion mutant, shows a smaller band as compared to Lanes 3 and 7 indicating lower albumin leakage. Lane 5 (*cagA* deletion mutant) and 8 (*cagA* deletion mutant supplemented with rCagA) show band intensity and size comparable to each other. However bands in both lanes are considerably weaker than those in Lanes 3, 4 and 7, indicating a much lower leakage. It is interesting to note that both bands were noticeably of a greater intensity and size as compared to that observed in Lane 2 (uninfected T84 cells), indicating a leakage that is greater than the basal biotinylated albumin. Lane 6 (*hsp20/cagA* double deletion mutant) exhibits a slightly weaker biotinylated albumin leakage as compared to both Lanes 5 and 8, as indicated by a slightly weaker band. Lane 9 (rHSP20 alone) and Lane 10 (rCagA alone) exhibit the weakest bands, indicating the lowest biotinylated albumin leakage. The intensity of these bands is comparably similar to that seen with uninfected T84 cells (Lane 2), indicating a leakage that is similar to the basal leakage seen with the uninfected T84 cells.

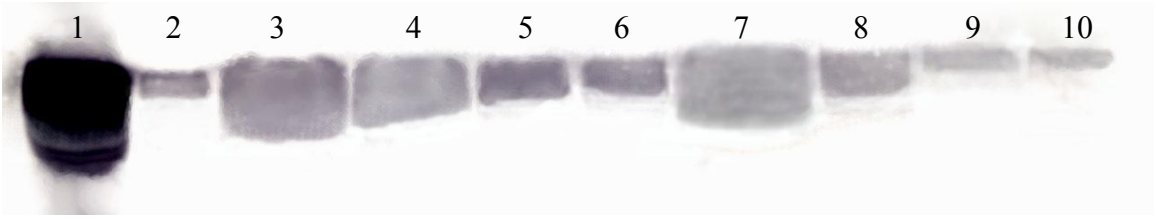

Figure 4.38. Leakage of biotinylated albumin across the T84 cell monolayer. Lane 1 indicated the presence of the biotinylated albumin in basolateral chamber, serving as positive control. Lane 2, uninfected T84 cells serve as negative control. Lane 3-10 showed samples extracted from the apical chamber where T84 cells were infected with: Lane 3, wild type *H. pylori* 26695; Lane 4, *hsp20* deletion mutant; Lane 5, *cagA* deletion mutant; Lane 6, *hsp20/cagA* deletion mutant; Lane 7, *hsp20* deletion mutant supplemented with rHSP20; Lane 8, *cagA* deletion mutant supplemented with rCagA; Lane 9, rHSP20 alone; Lane 10, rCagA alone. Presence of biotinylated albumin was detected using a streptavidin probe.

The inability of *cag* PAI deletion mutant of *H. pylori* 26695 to translocate CagA across T4SS into AGS cells, due to the absence of the *cagA* gene in the genome and the inability to establish T4SS, was demonstrated in Figure 4.14C-D. Similarly, CagA-mediated ZO-1 recruitment to extra-junctional bacterial attachment sites and tight junction disruption was not observed in T84 infected with *cag* PAI deletion mutant (Figure 4.29). Correspondingly, Figure 4.39 shows that *cag* PAI deletion mutant, which does not possess the T4SS due to absence of the genes responsible for the synthesis of T4SS, induced a biotinylated albumin leakage (Lane 9) that is comparable to that seen with *cagA* deletion mutant (Lane 5). Interestingly bands in Lane 9 (*cag* PAI deletion mutant) was markedly of a greater intensity and size as compared to that observed in Lane 2 (uninfected), indicating a leakage that is greater than the basal biotinylated albumin.

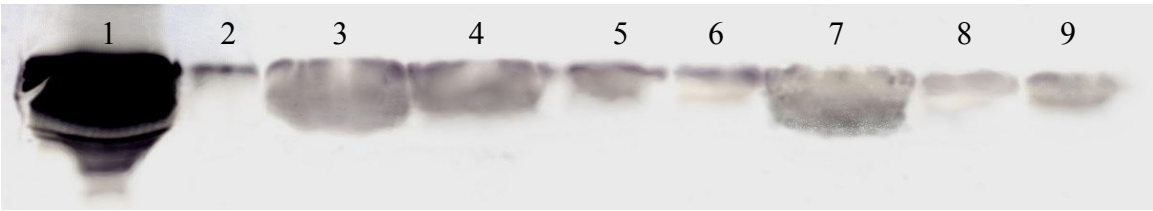

Figure 4.39. Leakage of biotinylated albumin across the T84 cell monolayer infected with *cag* PAI deletion mutant. Lane 1 indicated the presence of the biotinylated albumin in basolateral chamber, serving as positive control. Lane 2-9 showed samples extracted from the apical chamber infected with: Lane 2, uninfected T4 cells; Lane 3, wild type *H. pylori* 26695; Lane 4, *hsp20* deletion mutant; Lane 5, *cagA* deletion mutant; Lane 6, *hsp20/cagA* deletion mutant; Lane 7, *hsp20* deletion mutant supplemented with rHSP20; Lane 8, *cagA* deletion mutant supplemented with rCagA; lane 9, *cag* PAI deletion mutant. Presence of biotinylated albumin was detected using a streptavidin probe.

Since tight junction barrier function was deeply impaired, it was decided to examine if this tight junction disruption would not only allow passive diffusion of compounds such as biotinylated albumin but also the bacteria *H. pylori* 26695 itself. For

positive control, serial dilutions of sample from the apical chamber, prior and post infection, were plated onto chocolate agar plates to determine the viability of *H. pylori* in terms of colony-forming unit (CFU) per ml of sample. Table 4.1 shows that *H. pylori* that were exposed to host contact for 8 hours are still very much viable, with similar colony-forming unit (CFU) as that observed with *H. pylori* 26695 control. To investigate if either of the different strains of *H. pylori* was able to cross the disrupted T84 monolayer, serial dilutions of samples taken from the baso-lateral chamber were plated out. No *H. pylori*, regardless of the strain, was observed to be able to cross the T84 monolayer from the apical chamber to the baso-lateral chamber (Table 4.1). This was indicated by the absence of growth of strain of *H. pylori*.

Table 4.1. Absence of either strain of *H. pylori* in the baso-lateral chamber in each of the infecting conditions

Infecting conditions	Chamber samples take from	CFU/ml
H. pylori 26695 (preinfection)	Apical	35×10^6
H. pylori 26695 (8 hours post infection)	Apical	33×10^6
Uninfected T84	Baso-lateral	0
H. pylori 26695	Baso-lateral	0
H. pylori 26695 *hsp20* deletion mutant	Baso-lateral	0
H. pylori 26695 *cagA* deletion mutant	Baso-lateral	0
H. pylori 26695 *hsp20/cagA* deletion mutant	Baso-lateral	0
H. pylori 26695 *hsp20* deletion mutant supplemented with rhsp20	Baso-lateral	0
H. pylori 26695 *cagA* deletion mutant supplemented with rcagA	Baso-lateral	0
rhsp20	Baso-lateral	0
rcagA	Baso-lateral	0

DISCUSSION

Up to 50% of the world's human population is infected with *H. pylori* with the developing countries bearing the highest rates (Bumann *et al*., 2001). Disease outcome is determined by multiple factors such as genetic makeup of the host, environmental components, and the genetic composition of infecting strains of *H. pylori* (Blaser and Atherton, 2004).

It is interesting to note that, in diseases such as carcinoma, disruption of tight junction is common (Bilder *et al.*, 2000). The disruption of the integrity of tight junction might negatively affect the barrier function thereby causing leakage of ions and proteins across the epithelial layer. The disruption of tight junction might therefore provide the bacterium with nutrients but also allows the bacterium to invade the gastric epithelial layer.

Research interest on *H. pylori* centered mainly on type I strains harbouring *cag* PAI as patients infected with *cag* PAI was found to have a much greater risk of developing peptic ulcer disease, severe gastritis and gastric cancer than type II strains not harbouring *cag* PAI with the odds ratio of 5:13 (Nilsson *et al*., 2003). The *cag* PAI consists many genes that code for the Type IV secretion system (T4SS) which is essential for CagA translocation into host cells.

Upon translocation into host cells, CagA is phosphorylated, triggering many host signaling pathways and subsequently influencing many host cellular functions such as proliferation, apoptosis, cytokine release, and cell motility (Crabtree *et al*, 1991; Kuipers *et al*, 1995; Covacci *et al*, 1999; Hocker and Hohenberger, 2003). It was reported that CagA is first surface exposed before translocation into the host cells (Covacci *et al.*, 1993). However there were no subsequent findings that showed how a cytoplasmic

localized CagA was triggered and "brought" to the surface of *H. pylori* for translocation. On the other hand, HSP20 is a surface localized protein (Du and Ho, 2003). A preliminary finding that HSP20 co-immunoprecipitated with CagA indicated a possible interaction between CagA and HSP20 (Du and Ho, 2004). These earlier findings indicate that it might have a role to play as a chaperone, like the other heat shock proteins (such as HSP60), in adhesion and colonization (Yamaguchi *et al.*, 1998). This may also imply a potential role of HSP20 as a chaperone in assisting the entry of CagA into host cells via translocation through T4SS. Furthermore, the possibility of HSP20 in assisting CagA to function in the induction of hummingbird phenotype, IL8 generation and tight junction disruption cannot be undermined. It is the aim of this project to study the association between HSP20 and CagA in relation to pathogenesis of *H. pylori* infections. Therefore, this project attempts to examine some of these questions.

5.1 Localization of HSP20 and CagA in *H. pylori*

In examining the localization of HSP20 and CagA within the bacterial cell, it was found that in the absence of host contact, HSP20 was shown to be localized mainly at the cell membrane of *H. pylori* 26695 while CagA was found to be localized mainly in the cell cytoplasm of *H. pylori* 26695 (Figure 4.11A). The absence of HSP20 in the *hsp20* deletion mutant did not affect localization of CagA in the cytoplasm of the bacterial cells (Figure 4.11B). Similarly, the absence of CagA in *cagA* deletion mutant did not affect localization of HSP20 at the cell membrane of the bacterial cells (Figure 4.11C). From these findings, it can be inferred that the 2 proteins do not associate with each other in the absence of host contact.

Interestingly, it was observed that the localization of HSP20 and CagA within the *H. pylori* 26695 changed when the bacteria were in contact with host cells. Upon host contact, there was the presence of HSP20 co-localizing with CagA in the cytoplasm (Figure 4.12A). This suggests that HSP20 maybe acting as a chaperone in intracellular transport of CagA from the cytoplasm to the cell membrane. The result also implies that host contact serves as the trigger to HSP20 to migrate into the cell cytoplasm to associate and recruit CagA. Upon association, CagA was then transported into the vicinity of cell membrane (Figure 4.11A and 4.12A).

It was noted that upon host contact, the absence of HSP20 in *hsp20* deletion mutant did not prevent CagA being presented to the cell membrane (Figure 4.12B). It is therefore presumed that transportation of CagA from the cell cytoplasm to the cell membrane is not solely dependent on HSP20. It indicates that apart from HSP20, there might be involvement of other proteins. Recent studies by Fischer *et al* (2001) using systemic mutagenesis indicate that each of the seven genes in *cag* PAI (that are homologous to genes encoding the *A. tumefaciens* T4SS) is essential for CagA translocation into host cells. The products of HP0524, HP0526 and HP0540 were reported to be absolutely essential for CagA translocation. It is possible that these products might be involved in the intracellular transport of CagA too.

In *cagA* deletion mutant, HSP20 was found to remain localized at the cell membrane despite host contact (Figure 4.12C) instead of the cell cytoplasm (Figure 15A). This event suggests that the intracellular transport of HSP20 to the cell cytoplasm to recruit CagA is dependent on the presence of CagA. As *hsp20/cagA* deletion mutant is

devoid of both the *hsp20* and *cagA* genes, none of these proteins was found in the ultrathin sections (Figure 4.12D).

The TEM studies reveal that HSP20 was not present in AGS cells infected with either wild type *H. pylori* 26695 or *hsp20* deletion mutant (Figure 4.13B-E). The finding indicates that HSP20 is not translocated into host cells. However, CagA was found to be translocated into AGS cells infected with either wild type *H. pylori* 26695 (Figure 4.13B) or hsp20 deletion mutant of *H. pylori* 26695 (Figure 4.13C). The amount of translocated CagA was higher in AGS cells infected with wild type *H. pylori* 26695 than AGS cells infected with *hsp20* deletion mutant. This further affirms that CagA translocation can still occur in the absence of HSP20. However, the efficiency of CagA translocation is shown to be significantly decreased in the absence of HSP20.

5.2 Host contact and T4SS formation

Formation of T4SS is closely related to CagA translocation (Amieva *et al*, 2003). T4SS apparatus has been reported to be of 20-70 nm in diameter (Rohde *et al*, 2003). From our scanning electron microscopy studies, the formation of T4SS was observed in *H. pylori* 26695 exposed to host cells (Figure 4.14A) as well as in the absence of host cells (Figure 4.14B). Thus, it is implied that host contact is not necessary for T4SS formation. While T4SS was often observed with *H. pylori* strains with intact *cag* PAI, no T4SS was observed with the *cag* PAI deletion mutant, with or without host contact (Figure 4.14C-D). It is therefore inferred that the presence of the surface appendages that extend from the *H. pylori* observed was strictly dependent on the presence of *cag* PAI. It

is thus assumed that these surface appendages of ~60nm are the T4SS of *H. pylori* which are formed in the presence and absence of host contact.

5.3 Effect of HSP20 and CagA on T4SS formation

Since the trigger signal for T4SS formation was found not to rely on host contact, the study proceeded to investigate if HSP20 or CagA would play a role in effecting T4SS formation. SEM was carried out on *H. pylori* 26695 *hsp20* deletion mutant, *cagA* deletion mutant and *hsp20/cagA* deletion mutant with the wild type *H. pylori* 26695 serving as positive control. Figure 4.15 shows that T4SS formation was still observed for each of the 3 deletion mutants both in the presence or absence of host contact. The finding shows that HSP20 and CagA are not essential in T4SS formation and do not affect T4SS formation. Instead, *cag* PAI is the determinant factor supporting anearlier report by Backert *et al.*, 2002.

5.4 Effect of HSP20 on CagA translocation across T4SS

Although HSP20 does not play a role in T4SS formation, it is still possible that the protein has a role to play in CagA translocation. In order to examine this process, proteins were extracted from AGS cells infected with different deletion mutants over a time period and analysed by western blotting.

The results show that CagA translocation began 15 minutes and returned to basal level at 16 hours post infection in both wild type *H. pylori* 26695 (Figure 4.16A) and *hsp20* deletion mutant infected AGS cells (Figure 4.16B). However, CagA translocation into the wild type *H. pylori* 26695 infected AGS cells peaked 2 hours earlier than the

hsp20 deletion mutant infected AGS cells post infection. Interestingly, translocation decreased 2 hours later post infection in the latter as compared to the former. The reverse pattern of the 2 hours difference in the presence of peak in CagA translocation and delay in descend to basal level in AGS cells infected between wild type and *hsp20* deletion mutant is further confirmed (Figure 4.17) and the use of cag PAI deletion mutant where both HSP20 and CagA were absent (Figure 4.18). The results demonstrate that HSP20 plays an assisting role in CagA translocation and that without HSP20, the efficiency of CagA translocation was evidently lowered and delayed.

5.5 HSP20 translocation across T4SS

To explore the possibility of HSP20 being a translocated protein of *H. pylori* across the T4SS, proteins were extracted from infected AGS cells. Both TEM studies (Figure 4.12) and the western blotting analysis (Figure 4.19) show the absence of HSP20 in the infected AGS cellular protein lysates, regardless of the length of infection time and the strains of *H. pylori* (wild type and deletion mutants) used. These results indicate strongly that HSP20 is not translocated across the T4SS.

5.6 HSP20 and the functions of CagA

5.6.1 Hummingbird Phenotype

In this study, hummingbird phenotype caused by translocated CagA reported by Moese *et al* (2004) was observed as early as 2 hours post infection. The phenotype was well established 4 hours post infection. The dramatic and prominent effect of hummingbird phenotype was time dependent. Our findings agree with those of Moese *et*

al (2004). These were seen with both wild type *H. pylori* 26695 (Figure 4.21) and *hsp20* deletion mutant *H. pylori* 26695 infected AGS cells (Figure 4.22), but not with both *cagA* deletion mutant *H. pylori* 26695 (Figure 4.23) and *hsp20/cagA* deletion mutant *H. pylori* 26695 infected AGS cells (Figure 4.24).

Using 4 hours post infection as standard for presentation of hummingbird phenotype, the percentages of infected AGS cells exhibiting hummingbird phenotype were comparable at 34% and 32% between wild type *H. pylori* 26695 and *hsp20* deletion mutant infected AGS cells (Figure 4.25). These percentages were evidently much higher than the 8% observed with uninfected AGS cells. However, since the percentages of infected AGS cells exhibiting hummingbird phenotype were comparable to each other, it is inferred that the absence of *hsp20* did not affect the ability of CagA to induce hummingbird phenotype.

On the other hand, the percentages of infected AGS cells exhibiting hummingbird phenotype in *cagA* deletion mutant (Figure 4.25C) and *hsp20/cagA* deletion mutant infected AGS cells (Figure 4.25D) were 5% and 6%, respectively. This is close to the basal percentage of 8% in uninfected AGS cells indicating that the hummingbird phenotype observed for AGS cells infected with these 2 strains of *H. pylori* was negligible. In comparing the low percentages (5-6%) of hummingbird phenotype present in these 2 deletion mutants that are devoid of the *cag*A gene to the high percentages in wild type (34%) and hsp20 deletion mutant (32%) which possess *cag*A gene, clearly implies that CagA is the crucial factor in effecting hummingbird phenotype, in line with various earlier studies (Segal *et al,* 1999; Backert *et al*, 2000, 2001, 2005; Higashi *et al*,

2002; Mimuro *et al*, 2002; Stein *et al*, 2002; Selbach *et al*, 2002, 2003; Moese *et al*, 2004).

5.6.2 IL8 secretion

In examining the ability of HSP20 ability to affect CagA in IL8 production, a similar trend of minimal IL8 production up to 1 hour post infection and a gradual increase in IL8 production from 1 hour to 16 hours post infection (Figure 4.26) was observed for all infected AGS cells in this study, regardless of the strains of *H. pylori*. It was shown that IL8 production by *hsp20* deletion mutant infected AGS cells throughout the 16 hours time course of infection was highly comparable to A merged image shows co-localization of ZO-1 (red) with *H. pylori* (green) at IL8 generated by wild type *H. pylori* 26695 infected AGS cells. This suggests that HSP20 does not affect the ability of CagA to induce IL8 production.

IL8 production by *cagA* deletion and *hsp20/cagA* deletion mutant infected AGS cells throughout the 16 hours time course of infection was also highly comparable. It is interesting to note that IL8 production by *cagA* deletion mutant infected AGS cells and *hsp20/cagA* deletion mutant infected AGS cells was still substantially high as compared to that produced by uninfected AGS cells. This shows that, although CagA is a major factor in inducing IL8 production, CagA may not be the only factor in inducing IL8 production. The results hint that there are other factors that are involved in IL8 production in the host.

5.6.3 ZO-1 redistribution

Although the studies have shown that HSP20 does not alter the ability of CagA to induce morphological changes and immunological responses, the confocal immunofluorescence studies show that HSP20 does alter the ability of CagA to induce physiological changes such as tight junction disruption as indicated by the differential redistribution of tight junctional protein, ZO-1 (Figure 4.27-4.36).

T84 cells when infected with wild type *H. pylori* and *hsp20* deletion mutant shows that ZO-1 recruitment to extra-junctional bacterial attachment sites occurred at 30 minutes post infection. However, tight junction disruption occurred at 8 hours and 12 hours post infection by wild type *H. pylori* and *hsp20* deletion mutant, respectively. It is therefore proposed that the inability to produce functional HSP20 by *hsp20* deletion mutant might have delayed or decreased its ability to recruit ZO-1 to the extra-junctional bacterial attachment sites and to efficiently disrupt the tight junctions.

Even with the rHSP20 supplementation to the *hsp20* deletion mutant (Figure 4.31), the recruitment of ZO-1 to the extra-junctional bacterial attachment sites and tight junctional disruption were not completely restored. However, this feature was comparable to that of wild type *H. pylori* 26695 infected T84 cells. It has been reported that CagA is responsible for recruitment of ZO-1 from the extrajunctional site to the tight junction leading to disruption of tight junction (Amieva *et al*, 2003?). This clearly shows that HSP20 enhances ZO-1 recruitment to the bacterial attachment sites and tight junctional disruption, reinforcing the potential role of HSP20 in assisting the CagA-mediated ZO-1 recruitment to the extra-junctional bacterial attachment sites.

Figure 4.33 shows that rHSP20 alone is not sufficient to effect ZO-1 recruitment to extra-junctional sites and tight junctional disruption even after 12 hours of incubation. This shows that though HSP20 plays a role in effecting ZO-1 recruitment to extra-junctional bacterial attachment sites and tight junctional disruption, the presence of CagA is a pre-requisite. Without CagA, HSP20 cannot, by itself effect the phenotypic changes.

Figure 4.29 and 4.30 showed that no ZO-1 recruitment to extra-junctional bacterial attachment sites were observed in T84 cells infected with *cagA* deletion mutant and *hsp20/cagA* deletion mutant *H. pylori* 26695. T84 cells infected with either infecting inocula retained intact tight junctions at the cell periphery even after 12 hours of infection. This further confirms that CagA is a very crucial factor in ZO-1 recruitment to the extra-junctional bacterial attachment sites to effect tight junction disruption.

Figure 4.32 and Figure 4.34 show that rCagA supplementation to the *cagA* deletion mutant was not able to re-establish ZO-1 recruitment to extra-junctional bacterial attachment sites and tight junctional disruption. Despite a prolonged incubation of 12 hours, rCagA was not translocated from the media inoculum into the host cells (Figure 4.35). This highlights the necessity of CagA to be translocated into host cells to effect ZO-1 recruitment to extra-junctional bacterial attachment sites and tight junctional disruption through T4SS.

As expected, T84 cells infected with *cag* PAI deletion mutant did not exhibit ZO-1 recruitment to extra-junctional bacterial attachment sites with tight junction disruption even after a prolonged period of 12 hours infecting time (Figure 4.36J). Figures 4.18 and 4.20 show that CagA and HSP20 are both not translocated into AGS cells in *cag* PAI deletion mutant infected cells, respectively. Thus, the inability to effect ZO-1 recruitment

to extra-junctional bacterial attachment sites can be accorded to the absence of the effector CagA protein and the inability to form T4SS for the translocation of the CagA effector protein into host cells. This finding indicates that CagA is the main effector protein for the resultant ZO-1 recruitment to extra-junctional bacterial attachment sites and tight junction disruption. It also points out that none of the other Cag proteins on the PAI is required for the resultant ZO-1 recruitment to extra-junctional bacterial attachment sites and tight junction disruption. However, a study using deletion mutants of each of these Cag proteins might be needed to elucidate this emphatically.

5.6.4 Functional leakage test

5.6.4.1 Determination of infection period

It is essential to determine an optimum infection period for the functional leakage test. This is because the disruption of the tight junction complex might not be sufficient enough to allow the relatively large biotinylated albumin to diffuse across. Thus, even if the tight junction function was indeed interfered, it might not be detected. An infection period which is too long might effect in cell death. This is detrimental. It is understood that if leakage of biotinylated albumin was indeed detected, it might possibly be accorded to cells dying and the disintegration of the cell monolayer instead of disruption of the tight junction complex. The confocal immunofluorescence study shows a complete disruption of the tight junction of T84 cells infected with *H. pylori* 26695, exemplified by total abolishment of intact tight junctions that were formed around the cell periphery, was observed 8 hours post infection (Figure 4.27). To reduce the possibility of leakage of biotinylated albumin due to spontaneous cell death, 8 hours of infecting time was chosen

as it produced a percentage of 90% of infected T84 cells that were still viable (Figure 4.37).

.

5.6.5 Tight junction function disruption

Disruption of the function of the tight junction complex as examined by detection of the presence of biotinylated albumin leakage across the T84 monolayer shows that there was minimum basal leakage of biotinylated albumin seen with uninfected in T84 monolayer (indicated by the very weak band in Figure 4.38, Lane 2). This could be due to the presence of spontaneous cell death leading to the disintegration of the cell monolayer.

Biotinylated albumin leakage was shown to be highest in T84 cells infected with wild type *H. pylori* 26695 and *hsp20* deletion mutant supplemented with rHSP20. These 2 infecting conditions exhibited a solute leakage that was comparable to each other. On the other hand, leakage caused by infection with the *hsp20* deletion mutant was considerably lower. The results show that the presence of HSP20 enhances the effect of CagA on tight junction function disruption.

Both *cagA* deletion mutant and *cagA* deletion mutant supplemented with rCagA induced very low biotinylated albumin leakage. However, the leakage was still evidently higher than the basal leakage as seen in uninfected T84 monolayer. This highlights that CagA may not be the only protein involved in tight junction disruption, and that other proteins might be involved. It also shows that CagA has to be translocated into host cells to effect tight junction barrier function disruption.

hsp20/cagA double deletion mutant induced a weaker biotinylated albumin leakage than that induced by both *cagA* deletion mutant and *cagA* deletion mutant

supplemented with rCagA. This further reinforces that HSP20 assists CagA-mediated tight junction barrier function disruption.

rHSP20 incubation and rCagA incubation exhibited the weakest biotinylated albumin leakage, almost similar to the basal leakage as seen with uninfected T84 cells. This clearly shows that neither of the proteins is sufficient to effect tight junction barrier junction disruption by itself.

cag PAI deletion mutant induced a biotinylated albumin leakage that is considerably similar to that seen with *cagA* deletion mutant (Figure 4.39). Interestingly, *cag* PAI deletion mutant induced a leakage that is greater than the basal biotinylated albumin. This further confirms that CagA, though probably the main protein, may not be the only protein involved in tight junction disruption, and that other proteins might be involved. This is in agreement with the hypothesis of Amieva *et al* (2003). In the study, it was shown that CagA might play a role in disrupting tight junction function. Since both *cag* PAI deletion mutant and *cagA* deletion mutant induced sinilar biotinylated albumin leakage, it further strengthens the presence of other protein(s) that might be involved but not found on the *cag* PAI.

Although tight junction barrier function of the infected T84 monolayer was so deeply impaired that the relatively large biotinylated albumin was able to diffuse across the monolayer, the results show that this tight junction disruption was not enough to allow passage of bacteria to gain entry across the monolayer. This is shown by the absence of either strain of *H. pylori* in the baso-lateral chamber as demonstrated by the absence of growth of either strains of *H. pylori* when samples extracted from baso-lateral chamber were plated out on chocolate blood agar. Table 4.1 shows that *H. pylori* that

were exposed to host contact for 8 hours were viable and were similar to the bacterial population of uninfected *H. pylori* 26695 inoculum. This evidently shows that the absence of growth using samples extracted from the baso-lateral chamber was solely due to the inability of either strain of *H. pylori* to cross the T84 monolayer from the apical chamber to the baso-lateral chamber and not the absence of viable *H. pylori*.

It is worth noting that the biotinylated albumin leakage test results corroborate with the confocal immunofluorescence results. This is in line with what Miyoshi and Takai (2005) had discussed that displacement of ZO-1 tight junctions is associated with tight junction disassembly which is, in turn, associated with increased paracellular permeability. The reduction in efficiency in ZO-1 recruitment to extra-junctional bacterial attachment sites in T84 cells infected with *hsp20* deletion mutant reflects a reduction in ability to disrupt the paracellular tight junction function which equates to the decreased leakage of biotinylated albumin across the T84 monolayer infected with *hsp20* deletion mutant. This collaboration of ectopic assembly of ZO-1 at bacterial attachment sites with disruption of tight junction barrier function suggests that the HSP20-assisted ZO-1 recruitment to the extra-junctional sites of bacterial attachment has a negative functional implication.

5.7 Conclusion

Our studies illustrate a possible interaction between HSP20 and CagA, which might be triggered in the presence of host contact. It was shown that upon host contact, HSP20 acted as a "chaperone" in intracellular transport of CagA, prior to translocation into host cells. HSP20 did not affect T4SS establishment for CagA translocation.

However, the western blotting studies have shown HSP20 to be a "chaperonic" protein of *H. pylori* that facilitates CagA translocation into host cells. In addition, HSP20 was also found to assist CagA in an ectopic assembly of the tight junction protein, ZO-1, to bacterial attachment sites from the tight junctional sites (i.e. the cell periphery). This recruitment had been shown to have a causal relationship with the disruption of paracellular barrier function of the tight junction complexes. This suggests a functional impact of HSP20-assisted ZO-1 recruitment to the extra-junctional bacterial attachment sites that is mediated by CagA. Although our studies did not illustrate the ability of the bacterium to cross the disrupted monolayer, this might still be of significance in *in vivo* conditions in which the prolonged infection may perturb the epithelial layer which might aid the bacterium in invasion, or in acquiring of nutrients and facilitating *H. pylori* infections.

This study highlights the significant role of HSP20 in CagA intracellular transport prior to translocation into host cells, CagA translocation into host cells, CagA-mediated ZO-1 recruitment to sites of bacterial attachment and CagA-mediated tight junction disruption. Furthermore, its role as a "chaperone" in facilitating *H. pylori* infection cannot be undermined.

FUTURE WORK

6. Future Work

The association of HSP20 with CagA is the beginning of function and translocation of CagA into host cell. Covacci *et al* (1993) has reported the surface presentation of CagA upon cell contact without elaborating how this cytoplasmic protein was tranlocated from the cell cytoplasm to the cell surface of *H. pylori*.

In this project, the TEM and western blotting studies showed that HSP20 assisted in CagA translocation. However, it will be worthwhile to investigate how HSP20 aids CagA in its translocation. Some interesting questions to be answered will be: "Is HSP20 the first line of intercellular contact (with the host cell)? Is/Are there any other signals or molecules that help the translocation process in recruiting CagA from the cell cytoplasm? Or is it simply by facilitating CagA in associating with components of T4SS for more efficient transport into host?"

Haas *et al* (1993) has used shuttle mutagenesis to study the function of major flagellin (FlaA). Similarly, shuttle vectors can be used to complement the gene knockouts. Shutter vectors with the *hsp20* gene can be transfected into *hsp20* deletion mutant 26695 *H. pylori*. If the complementation of *hsp20* in *hsp20* deletion mutant can restore the phenotypes observed in the wild type *H. pylori* such as intracellular transport of CagA within *H. pylori*, CagA translocation into host and tight junction disruption of host cells, it will further support our results that HSP20 plays a role in CagA translocation and tight junction disruption. Gene complementation studies can be carried out to confirm our findings of HSP20 as a chaperone in assisting CagA in executing its functions.

Our study shows that HSP20 did not affect the ability of CagA to induce hummingbird phenotype in the infected host cells nor to induce IL8 production by the

infected host cells. However, HSP20 was shown to facilitate CagA in inducing ZO-1 recruitment from the tight junctional sites to extra-junctional bacterial sites resulting in a more drastic tight junction barrier function disruption. It is possible that the association of HSP20 with CagA might have changed the structure of CagA allowing CagA to interact more efficiently with downstream signaling molecules resulting in greater amplification for CagA to disrupt tight junction. In addition, the interaction between translocated CagA and ZO-1 has not been established. It would be interesting to investigate the events that occur between the translocation of CagA and the eventual tight junction disruption.

DNA microarray can be performed to study if the expression profiles of genes in the infected host cells were characteristically different when the host cells were infected with *hsp20* or *cag*A or *hsp*20/*cag*A deletion mutants in comparison with the wild type *H. pylori* 26695. What is the gene(s) that is/are responsible for the differentiating phenotypic changes? This will yield a large amount of information that might aid us in identifying how HSP20 facilitate CagA in translocation and tight junction disruption. The signaling events within the bacteria upon contacting the host cells and the events leading to the triggering of various molecules that resulted in CagA translocation and the various cellular events are important in the role of *H. pylori* as a gastric bacterial pathogen.

REFERENCES

Alberts B, Johnson A, Julian L, *et al*. 2002. Molecular biology of the cell. 4th Edition. Garland Science. New York: pg 1066-1070.

Amieva MR, Vogelmann R, Covacci A, *et al*. 2003. Disruption of the epithelial apical-junctional complex by *Helicobacter pylori* CagA. *Science*. **300**:1430-1434.

Anderson JM and Van Itallie CM. 1999. Tight junctions: closing in on the seal. *Curr Biol.* **9**: R922–924.

Andruitis KA, Fox JG, Schauer DB, *et al*. 1997. Inability of an isogenic urease negative strain of *Helicobacter mustelae* to colonize ferret stomach. *Infect Immun*. **63**: 3722-3725.

Backert S, Ziska E, Brinkmann V, *et al*. 2000. Translocation of the *Helicobacter pylori* CagA protein in gastric epithelial cells by a type IV secretion apparatus. *Cell Microbiol*. **2**: 155-164.

Backert S, Moese S, Selbach M, *et al*. 2001. Phosphorylation of tyrosine 972 of the *Helicobacter pylori* CagA protein is essential for induction of a scattering phenotype in gastric epithelial cells. *Mol. Microbiol.* **42**: 631-644.

Backert S, Schwarz T, Miehlke S, *et al*. 2004. Functional analysis of the *cag* pathogenicity island in *Helicobacter pylori* isolates from patients with gastritis, peptic ulcer, and gastric cancer. *Infect. Immun*. **72**: 1043-1056.

Backert S, Gressmann H., Kwok T, *et al*. 2005. Gene expression and protein profiling of AGS gastric epithelial cells upon infection with *Helicobacter pylori*. *Proteomics*. **5**: 3902-3918.

Balda MS and Matter K. 1998. Tight junctions. *J Cell Sci.* **111**:541–547.

Berkelman T and Stenstedt T. 1998. 2-D electrophoresis (using immoblized pH gradients) *Principles and Methods.* Amersham Pharmacia Biotech.

Bilder D, Li M and Perrimon N. 2000. Cooperative regulation of cell polarity and growth by Drosophila tumour suppressors. *Science*. **289**:113-116.

Bizzozero G. 1893. Ueber die schlauchfoermigen druseen des magendarmkanais and die beziehungen ihres epithels zudem oberfachenepithelder schleimihant. *Arch. Mikr Anat*. **42**:82-152.

Blaser MJ, Perez-Perez GI, Kleanthous H, *et al.* 1995. Infection with *Helicobacter pylori* strains possessing cagA is associated with an increased risk of developing adenocarcinoma of the stomach. *Cancer Res*. **55**: 2111-2115.

Blaser MJ and Atherton JC. 2004. *Helicobacter pylori* persistence: biology and disease. *J Clin Invest*. **113**: 321-333.

Brandt S, Kwok T, Hartig R, *et al*. 2005. NF-$_k$B activation and potentiation of proinflammatory responses by the *Helicobacter pylori* CagA protein. *Proc. Natl Acad. Sci. USA*. **102**: 9300-9305.

Bumann D, Meyer TF and Jungblut PR. 2001. Proteome analysis of the common human pathogen *Helicobacter pylori*. *Proteomics*. **1**: 473-479.

Bourzac KM and Gullemin K. 2005. *Helicobacter pylori*-host cell interactions mediated by type IV secretion. *Cell Microbiol.* **7**: 911-919.

Censini S, Lange C, Xiang ZY, *et al*. 1996. *cag*, a pathogenicity island of *Helicobacter pylori,* encodes type I-specific and disease-associated virulence factors. *Proc. Natl Acad. Sci. USA*. **93**: 14648-14653.

Chalker AF, Minehart HW, Hughes NJ, *et al.* 2001. Systematic identification of selective essential genes in *Helicobacter pylori* by genome prioritization and allelic replacement mutagenesis. *J Bacteriol*. **183**: 1259-1268

Chen ML, Pothoulakis C, LaMont JT, *et al*. 2002. Protein kinase C signaling regulates ZO-1 translocation and increased paracellular flux of T84 colonocytes exposed to *Clostridium difficile* toxin A. *J Biol Chem*. **277**: 4247-4254.

Christie PJ and Vogel JP. 2000. Bacterial type IV secretion: conjugation systems adapted to deliver effector molecules to host cells. *Trends Microbiol*. **8**: 354-360.

Crabtree JE, Taylor JD, Heatley RV, *et al*. 1991. Mucosal IgA recognition of *Helicobacter pylori* 120 kDa protein, peptic ulceration, and gastric pathology. *Lancet*. **338**: 332-335.

Couturier MR, Tasca E, Montecucco C, *et al*. 2006. Interaction with CagF is required for translocation of CagA into the host via the *Helicobacter pylori* type IV secretion system. *Infect. Immun.* **74**: 273-281.

Covacci A, Censini S, Bugnoli M, *et al*. 1993. Molecular characterization of the 128-kDa immunodominant antigen of Helicobacter pylori associated with cytotoxicity and duodenal ulcer. *Proc Natl Acad Sci USA*. **90:** 5791-5795.

Covacci A and Rappuoli R. 1998. *Helicobacter pylori*: molecular evolution of a bacterial quasi-species. *Curr Opin Microbiol*. **1**: 96-102.

Covacci A, Telford JL, Guidice DG, *et al*. (1999). *Helicobacter pylori* virulence and genetic geography. *Science*. **284**: 1328-1333.

Cywes C and Wessels MR. 2001. Group A *Streptococcus* tissue invasion by CD44-mediated cell signaling. *Nature*. **414**: 648-652.

Debbie A, Krzysztof L, Dorota S, *et al*. 1991. Biological role and regulation of universally conserved heat shock proteins. *J Biol Chem.* **266**: 24233-6.

Dhawan P, Singh AB, Deane NG, *et al*. 2005. Claudin-1 regulates cellular transformation and metastatic behavior in colon cancer. *J Clin Invest*. **115**: 1765-1776.

Doenges JL. 1939. Spirochetes in the gastric glands of Macacus rhesus of Man without related disease. *Arch. Pathol*. **27**:469-477.

Du RJ and Ho B. 2003. Surface localized heat shock protein 20 (HsIV) of *Helicobacter pylori*. *Helicobacter*. **8**:257-267.

Du RJ and Ho B. 2004. Cloning, expression and characterization of a novel helicobacter pylori differentiating antigen – Heat chock protein 20. PhD Thesis. National University of Singapore.

Dunn BE, Roop II RM, Sung CC, *et al*. 1992. Identification and purification of a cpn60 heat shock protein homolog from *Helicobacter pylori*. *Infect. Immun*. **60**: 1946-1951.

Epidemiological news Bulletin. 1996. Seroprevalence of *Helicobacter pylori* infection in Singapore. Jun **22** (6): 31-32.

Ferrero RL, Cussac V, Courcoux P, *et al*. 1992. Construction of isogenic urease-negative mutants of *H. pylori* by allelic exchange. *J Bacteriol*. **174**: 4212-4217.

Fischer W, Puls J, Buhrdorf R, *et al*. 2001. Systematic mutagenesis of the *Helicobacter pylori cag* pathogenicity island: essential genes for CagA translocation into host cells and induction of interleukin-8. *Mol Microbiol*. **42**: 1337-1348.

George LL, Borody TJ, Andrews P *et al*. 1990. Cure of duodenal ulcer after eradication of Helicobacter pylori. *Med J Aust*. **153**: 145-149.

Goodwin CS, McCulloch RK, Armstrong JA, *et al*. 1985. Unusual cellular fatty acids and distinction ultrastructure in a new spiral bacterium *Camphylobacter pyloridis* from the human gastric mucosa. *J Med Microbiol*. **19**:257-261.

Gumbiner B, Lowenkopf T and Apatira D. 1991. Identification of a 160-kDa polypeptide that binds to the tight junction protein ZO-1. *Proc. Natl. Acad. Sci. USA*. **88:** 3460–3464.

Haas R, Meyer TF and van Putten TP. 1997. Aflagellated mutants of *Helicobacter pylori* generated by genetic transformation of naturally competent strains using transposon shuttle mutagenesis. *Mol Microbiol*. **8**:753-60.

Hansen SJ and Holm J. 1989. Quantification of biotin in serum by competition with solid-phase biotin for binding to peroxidase-avidin conjugate. *Clin Chem*. **35**: 1721-1722.

Harhaj NS, Barber AJ and Antonetti DA. 2002. Platelet-derived growth factor mediates tight junction redistribution and increases permeability in MDCK cells. *J Cell Physiol.* **193**: 349-364.

Haskins J, Gu L, Wittchen ES, *et al*. 1998. ZO-3, a novel member of the MAGUK protein family found at the tight junction, interacts with ZO-1 and occludin. *J. Cell Biol*. **141**: 199–208.

Heczko U, Smith VC, Meloche MR, *et al*. 2000. Characteristics of Helicobacter pylori attachment to human primary antral epithelial cells. *Microbes Infect.* **2**:1669-76.

Higashi H, Tsutsumi R, Muto S, *et al*. 2002. SHP-2 tyrosine phosphatase as an intracellular target of *Helicobacter pylori* CagA protein. *Science*. **295**: 683-686.

Hocker M and Hohenberger P. 2003 *Helicobacter pylori* virulence factors – one part of a big picture. *Lancet*. **362**: 1231-33.

Hoffman PS and Garduno RA. 1999. Surface-associated heat shock proteins of Legionella pneumophila and Helicobacter pylori: roles in pathogenesis and immunity. *Infect Dis Obstet Gynecol*. **7**:58-63.

Hsu PI, Hwang IR, Cittelly D, *et al*. 2002. Clinical Presentation in relation to diversity within the *Helicobacter pylori cag* pathogenicity island. *Am J Gastroenterol*. **97**: 2231-2238.

Kaji T, Ishihara S, Ashizawa N, *et al*. 2002. Adherence of Helicobacter pylori to gastric epithelial cells and mucosal inflammation. *J Lab Clin Med*. **139**:244-50.

Kuipers EJ, Perez-Perez GI, Kleanthous H, *et al*. 1995. *Helicobacter pylori* and atrophic gastritis: importance of CagA status. *J. Natl. Cancer Inst*. **87**: 1777-1780.

Kusters KG, van Vliet AH and Kuipers EJ. 2006. Pathogenesis of *Helicobacter pylori* infections. *Clin Microbiol Rev*. **19**: 449-490.

Lage AP, Godfroid E, Fauconnier A, *et al*. 1995. Diagnosis of Helicobacter pylori infection by PCR: comparison with other invasive techniques and detection of CagA found in gastric biopsy specimen. *J Clin Microbiol*. **33**: 2752-2756.

Laksanalamai P and Rodd FT. 2004. Small heat shock proteins from extremophiles: a review. *Extremophiles*. **8**: 1-11.

Laquinto G, Todisco A, Giardullo N, *et al*. 2000. Antibody response to *Helicobacter pylori* CagA and heat-shock proteins in determining the risk of gastric cancer development. *Digest Liver Dis*. **32**: 378-83.

Lee SK, Moon J, Park SW, *et al*. 2005. Loss of the tight junction protein Claudin 4 correlates with histological growth-pattern and differentiation in advanced gastric adenocarcinoma. *Oncel Rep*. **13**: 193-199

Lowry OH, Rosenbrough NJ, Farr AL, *et al*. 1951. Protein measurement with Folin Phenol reagent. *J Biol Chem*. **193**: 265-275.

Malaty HM and Nyren O. 2003. Epidemiology of *Helicobacter pylori* infection. *Helicobacter*. **8** Suppl 1: 8-12.

Marshall BJ and Warren JR. 1984. Unidentified curved bacilli in the stomach of patients with gastritis and peptic ulceration. *Lancet*. **6**:1311-5.

Megraud F, Trimoulet P, Lamouliatte H, *et al*. 1991. Bactericidal effect of amoxilin on *Helicobacter pylori* in an in vitro model using epithelial cells. *Antimicrob Agents Chemother*. **35**:869-872.

Mimuro H, Suzuki T, Tanaka J, *et al*. 2002. Grb2 is a key mediator of *Helicobacter pylori* CagA protein activites. *Mol. Cell*. **10**: 745-755.

Mitic LL and Anderson JM. Molecular architecture of tight junctions. *Annu Rev Physiol*. **60**: 121–142.

Miyoshi J and Takai Y. 2005. Molecular perspective on tight-junction assembly and epithelial polarity. *Adv Drug Delivery Rev*. **57**: 815-855.

Mobley HLT, Island MD and Hausinger RP. 1995. Molecular biology of microbial ureases. *Microb Rev*. **59**: 451-480.

Moese S, Selbach M, Kwok T, *et al*. 2004. *Helicobacter pylori* induces AGS cell motility abd elongation via independent signaling pathways. *Infect Immun*. **72**: 3646-3649.

Mostov K and Zegers M. 2003. Just mix and patch. *Nature*. **422**: 267-268.

Mukhopadhyay AK, Kersulyte D, Jeong JY, *et al*. 2000. Distinctiveness of genotypes of *Helicobacter pylori* in Calcutta, India. *J Bacteriol*. **182**: 3219-3227.

Munzenmaier A, Lange C, Glocker E, *et al*. 1997. A secreted/shed product of Helicobacter pylori activates transcription factor nuclear factor-$_k$B. *J Immunol*. **159**: 6140-6147.

Muza-Moons MM, Schneeberger EE and Hecht GA. 2004. Enteropathogenic *Escherichia coli* infection leads to appearance of aberrant tight junctions strands in the lateral membrane of intestinal epithelial cells. *Cell Microbiol*. **6**: 783-793.

Nakamato H and Vigh L. 2006. The small heat shock proteins and their clients. *Cell Mol Life Sci*. [Epub ahead of print]

Nilius M, Buchler M and Malfertheiner P. 1994. Adhesion of *H. pylori* and *Escherichia coli* to human bovine surface mucus cells *in vitro*. *Eur J Clin Invest*. **24**: 454-459.

Nilsson C, Sillen A, Eriksson L, *et al*. 2003. Correlation between *cag* pathogenicity island composition and *Helicobacter pylori*-associated gastroduodenal disease. *Infect Immun*. **71**: 6573-81.

Nishihara K, Nozawa Y, Nomura S, *et al*. 1999. Analysis of Helicobacter pylori binding site on HEp-2 cells and three cell lines from human gastric carcinoma. *Fundam Clin Pharmacol*. **13:** 555-61.

Odenbreit S, Puls J, Sedmaier B, *et al*. 2000. Translocation of *Helicobacter pylori* CagA into gastric epithelial cells by type IV secretion. *Science*. **287**: 1497-1500.

Odenbreit S, Gebert B, Puls J, *et al*. 2001. Interaction of *Helicobacter pylori* with professional phagocytes: role of the *cag* pathogenicity island and translocation, phosphorylation and processing of CagA. *Cell Microbiol*. **3**: 21-31.

Ogura K, Maeda S, Nakao M *et al*. 2000. Virulence factors of *Helicobacter pylori* responsible for gastric diseases in Mongolian gerbil. *J Exp Med*. **192**: 1601-1610.

Parkin DM, Laara E and Muir LS. 1988. Estimates of the worldwide frequencies of 16 major cancers in 1980. *Int Cancer* **41**: 184-197.

Parsonnet J, Friedman GD, Vandersteen DP, *et al*. 1991. *Helicobacter pylori* infection and risk of gastric carcinoma. *N Engl J Med*. **325**: 1127-1131.

Peek RM and Blaser MJ. 2002. *Helicobacter pylori* and gastrointestinal tract and adenocarcinomas. *Nat Rev. Cancer*. **2**: 28-37.

Ramelah M, Aminuddin A, Alfizah H, *et al*. 2005. *cagA* gene variants in Malaysian *Helicobacter pylori* strains isolated from patients of different ethnic groups. *FEMS Immunol Med Microbiol*. **44**: 239-242.

Rieder G, Hatz RA, Morgan AP, *et al*. 1997. Role in adherence in interleukin-8 induction in *Helicobacter pylori*-associated gastritis. *Infect Immun*. **65**: 3622-3630.

Rohde M, Puls J, Buhrdorf R, *et al*. 2003. A novel sheathed surface organelle of the *Helicobacter pylori cag* type IV secretion system. *Mol Microbiol*. **49**: 219-234.

Rokbi B, Seguin D, Guy B, *et al*. 2001. Assessment of *Helicobacter pylori* gene expression within mouse and human gastric mucosae by real-time reverse transcriptase PCR. *Infect Immun*. **69**: 4759-66.

Rozen S and Skaletsky H. 2000. Primer3 on the WWW for general users and for biologist programmers. *Methods Mol Biol.* **132**: 365-86.

Segal ED, Cha J, Lo L, *et al*. 1999. Altered states: involvement of phosphorylated CagA in the induction of host cellular growth changes by *Helicobacter pylori*. *Proc. Natl. Acad. Sci. USA*. **96**: 14559-14564.

Selbach M, Moese S, Meyer TF, *et al*. 2002. Functional analysis of the *Helicobacter pylori cag* pathogenicity island reveals both VirD4-CagA dependent and VirD4-CagA independent mechanisms. *Infect Immun*. **70**: 665-671.

Selbach M, Moese S, Hurwitz R, *et al*. 2003. The *Helicobacter pylori* CagA protein induces cortactin dephosphorylation and actin rearrangement by c-Src inactivation. *EMBO J*. **22**: 515-528.

Seong IS, Oh JY, Yoo SJ, *et al*. 1999. ATP-dependent degradation of SulA, a cell division inhibitor, by the HslVU protease in *Escherichia coli. FEBS Letts*. **456**: 211-214.

Sharon N and Ofek L. 2000. Safe as mother's milk: carbohydrate as future anti-adhesion drugs for bacterial diseases. *Glycoconjugate*. **17**: 659-664.

Shevchenko A, Wilm M, Vorm O, *et al*. 1996. Mass spectrometric sequencing of proteins silver-stained polyacrylamide gels. *Anal Chem*. **68**: 850-858.

Song NL, Ayada K, Zhao Y, *et al*. 2005. *Helicobacter pylori* heat-shock protein 60 induces production of the pro-inflammatory cytokine IL8 in monocytic cells. *J Med Microbiol*. **54:** 225–233

Stein M, Bagnoli F, Halenbeck R, *et al*. 2002. C-src/Lyn kinase activates *Helicobacter pylori* CagA through tyrosine phosphorylation of the EPIYA motifs. *Mol. Microbiol*. **43**: 971-980.

Stevenson BR, Siliciano JD, Moosker MS, *et al*. 1986. Identification of ZO-1: a high molecular weight polypeptide associated with the tight junction (zonula occludens) in a variety of epithelia. *J Cell Biol*. **103:** 755– 766.

Stevenson BR. 1999. Understanding tight junction clinical physiology at the molecular level. *J Clin Iinvest.* **104**: 3-4.

Suerbaum S, Thiberge JM, Kansau I, *et al*. 1994. *Helicobacter pylori* hspA-hspB heat-shock gene cluster: nucleotide sequence, expression, putative function and immunogenicity. *Mol. Microbiol.* **14**: 959-974.

Sugiyama T and Asaka M. 2004. *Helicobacter pylori* and gastric cancer. *Med Electron Microsc*. **37**: 149-157.

Tan S and Berg DE. 2004. Motility of urease-deficient derivatives of *Helicobacter pylori*. *J Bacteriol*. **186**: 885-888

Tanaka J, Suzuki T, Mimuro H, *et al*. 2003. Structural definition on the surface of *Helicobacter pylori* type IV secretion apparatus. *Cell Microbiol*. **5**: 395-404.

Taylor DN and Blaser MJ. 1991. The epidemiology of *Helicobacter pyloris* infections. *Epidemiol. Rev.* **13**:42-59.

Terradot L, Bayliss R, Oomen C, *et al*. 2005. Structures of two core subunits of the bacterial type IV secretion system, VirB8 from *Brucella suis* and ComB10 from *Helicobacter pylori*. *Proc Natl Acad Sci*. **102**: 4596-4601.

Terres AM, Windle HJ, Ardini E, *et al*. 2003. Soluble extracts from Helicobacter pylori induce dome formation in polarized intestinal epithelial monolayers in a laminin-dependent manner. *Infect Immun*. **71**:4067-78.

Tsukita S, Furuse M and Itoh M. 2001. Multifunctional strands in tight junctions. *Nature Rev Mol Cell Biol.* 2: 285-293.

Vijayakumari S, Khin MM, Jiang B *et al.* 1994. Importance of coccoid forms in *Helicobacter pylori* pathogenesis? *Am J Gastroenterol*. **89:** 1397.

Vincent P. 1995. Transmission and acquisition of *Helicobacter pylori* infections. *Biomed and Pharmacother.* **49**:11-18.

Voland P, Weeks DL, Marcus EA, *et al*. 2003. Interaction among the seven *Helicobacter pylori* proteins encoded by the urease gene cluster. *Am J Physiol Gastrointest Liver Physiol*. **284**: G96-G106.

Watanabe T, Tada M, Nagai H, *et al*. 1998. Helicobacter pylori infection induces gastric cancer in Mongolian gerbils. *Gastroenterology*. **115**: 642-648.

Wu S, Lim KC, Huang RF, *et al*. 1998. *Bacteroides fragilis* enterotoxin cleaves the zonula adherens proteins, E-cadherin. *Proc Natl Acad Sci*. **95**: 14979-14984.

Yamaguchi H, Osaka T, Taguchi H, *et al*. 1998. Relationship between expression of HSP60, urease activity, production of vacuolating toxin, and adherence activity of *Helicobacter pylori*. *Gastroenterol*. **33**: 6-9.

Yamaguchi H, Osaki T, Kurihara N, *et al*. 1999. Induction secretion of interlukin-8 from human gastric epithelial cells by heat shock protein 60 homologue of *Helicobacter pylori*. *J Med Microbiol.* **48**:927-33

Yamamoto T, Harada N, Kano K, *et al*. 1997. The Ras target AF-6 interacts with ZO-1 and serves as a peripheral component of tight junctions in epithelial cells. *J Cell Biol*. **139**: 785-795.

Yamaoka Y, Kita M, Kodama T, *et al*. 1997. Induction of various cytokines and development of severe mucosal inflammation by *cagA* gene positive *Helicobacter pylori* strains. *Gut*. **41**: 442-451.

Yamaoka Y, Kita M, Kodama T, *et al*. 1998. Chemokines in gastric mucosa in *Helicobacter pylori* infection. *Gut*. **42**: 609-617.

Zhang ZW, Dorrell N, Wren BW, e*t al*. 2002. Helicobacter pylori adherence to gastric epithelial cells: a role for non-adhesin virulence genes. *J Med Microbiol.* **51**:495-502.

Zheng PY, Hua J, Yeoh KG, *et al*. 2000. Association of peptic ulcer with increased expression of Lewis antigens but not *cagA, iceA,* and *vacA* in *Helicobacter pylori* isolates in an Asian population. *Gut*. **47**: 18-22.

APPENDICES

Appendix 1

Chocolate blood agar

For 500 ml preparation:

Blood agar base No.2 (Oxoid)	: 20.0g
Distilled water	: 475ml
Horse Blood (5%) (Gibco)	: 25ml

1. The blood agar base No.2 and distilled water was mixed in a 500ml bottle.
2. The mixture was autoclaved at 121^{o}C for 20 minutes.
3. The agar was then cooled to 50^{o}C before the horse blood was added aseptically.
4. The blood was lysed by immersing the flask in an 80^{o}C water bath for 10 minutes.
5. The chocolate agar was subsequently cooled to 50^{o}C before pouring into sterile pertri dishes (Sterilin).
6. The plates were stored at 4^{o}C until use.

Appendix 2

Selective chocolate blood agar

For a 500 ml preparation:

Blood agar base No. 2 (Oxoid)	: 20.0g
Distilled water	: 474.5ml
Horse Blood (5%) (Gibco)	: 25ml
Kanamycin stock solution (Final concentration : 20 μg/ml)	: 0.5ml

1. The blood agar base No.2 and distilled water was mixed in a 500ml bottle.
2. The mixture was autoclaved at 121^{o}C for 20 minutes.
3. The agar was then cooled to 50^{o}C before the horse blood was added aseptically.
4. The blood was lysed by immersing the flask in an 80^{o}C water bath for 10 minutes.
5. After cooling to 50^{o}C, the antibiotics aliquoted into the agar and mixed thoroughly before pouring into sterile petri dishes (Sterilin).
6. The plates were stored at 4^{o}C until use.

Kanamycin Stock Solution

1. 8 mg of kanamycin (Sigma) was dissolved in 1 ml distilled water.
2. The solution was sterilised by filtration using a 0.22 μm filter.
3. It was then aliquoted into Eppendorf tubes and stored at –20 ^{o}C until use.

Appendix 3

Brain Heart Infusion Broth

For a 300ml preparation:

Brain Heart Infusion (Gibco BRL / Oxoid)	: 11.4g
Yeast Extract (10 %) (Oxoid)	: 1.2g
Distilled water	: 270ml
Horse serum (10%) (Gibco BRL)	: 30ml

Without glycerol

1. The brain heart infusion, yeast extract and distilled water were mixed
2. The mixture was autoclaved at 121 ^{o}C for 20 minutes.
3. It was then cooled and 10 % of horse serum was added
4. It was then kept at 4 ^{o}C until use.

With glycerol

1. The brain heart infusion, yeast extract, 60 ml of glycerol and 210 ml of distilled water were mixed.
2. The mixture was autoclaved at 121^{o}C for 20 minutes.
3. The medium was cooled and 10% horse serum was added.
4. It was then kept at 4^{o}C until use.

Appendix 4

Luria-Bertani broth

Tryptone (Oxoid)	: 10g
Sodium chloride	: 10g
Yeast extract	: 5g
Distilled water (qsp)	: 1L

1. The tryptone, sodium chloride, and yeast extract and distilled water were mixed
2. The mixture was autoclaved at 121 ^{o}C for 20 minutes.
3. It was then kept at room temperature until use.

Selective Luria-Bertani broth

Tryptone	: 10g
Sodium chloride	: 10g
Yeast extract	: 5g
Distilled water (qsp)	: 1L

1. The tryptone, sodium chloride, and yeast extract and distilled water were mixed
2. The mixture was autoclaved at 121 ^{o}C for 20 minutes.
3. The broth was subsequently cooled to 50^{o}C and the antibiotics were aliquoted into the broth and mixed thoroughly before use.

Appendix 5

Luria-Bertani agar

Non-selective Luria-Bertani broth	: 1L
Agar Solidifying Agent (DIFCO)	: 15g

1. The mixture was autoclaved at 121^{o}C for 20 minutes.
2. The agar was cooled to 50^{o}C before pouring into sterile pertri dishes (Sterilin).
3. The plates were stored at 4^{o}C until use.

Selective Luria-Bertani agar

Luria-Bertani broth	: 1L
Agar Solidifying Agent (DIFCO)	: 15g

1. The mixture was autoclaved at 121^{o}C for 20 minutes.
2. The agar was then cooled to 50^{o}C before the antibiotics were aliquoted.
3. It is then mixed thoroughly before pouring into sterile pertri dishes (Sterilin).
4. The plates were stored at 4^{o}C until use.

Appendix 6

Urease Reagent (pH 6.8)

For a 500ml preparation

Urea (Sigma)	: 10g
$NaH_2PO_4.H_2O$ (Merck)	: 0218g
Na_2HPO_4 (Merck)	: 0.51g
Distilled water (qsp)	: 500ml
Phenol Red (Sigma)	: 750µl

1. After mixing urea, $NaH_2PO_4.H_2O$, Na_2HPO_4 and water, the pH was adjusted to 6.8 and the solution was sterilized by filtration through a 0.22 µm filter.
2. Phenol red that was sterilized by autoclaving at 121 ^{o}C for 20 minutes and filtered with 0.22 µm filter was added to the filtrate.
3. The reagent was stored at 4 ^{o}C until use.

When using, 0.5 ml of the culture was added to 0.5 ml of urease test reagent. A colour change from yellow to magenta-red indicated a positive result.

Appendix 7

Catalase Test

3 % of H_2O_2 was diluted 10 folds from H_2O_2 (30%) (BDH)

The test was based on the conversion of the 3 % H_2O_2 to water and oxygen (gas production observed) by catalase produced by the bacteria.

Appendix 8

Phosphate Buffer Saline (PBS) (pH 7.4)

For a litre of 10 X PBS preparation:

Sodium chloride (Merck 6404)	: 80 g
Potassium dihydrogen phosphate (AnalaR-BDH)	: 2 g
Sodium hydrogen phosphate (Merck 6580)	: 29 g
Potassium chloride (Merck 4936)	: 2 g

1. pH of the solution was adjusted to 7.4.
2. Distilled water was added to dissolve the chemicals and made up to 1 litre.
3. The mixture was autoclaved at 121^{o}C for 20 minutes.
4. It was then stored at room temperature till use.

For a litre of 1X PBS preparation:

1. 100ml from 10 × stock was added to 900ml of distilled water.
2. The mixture was then autoclaved at 121^{o}C for 20 minutes again to ensure sterility.
3. It was then stored at room temperature till use.

Appendix 9

Growth medium for AGS cells

For 100 ml preparation:

RPMI-1640 (Sigma)	: 89 ml
L-glutamine (2%) (GIBCO-BRL)	: 2 ml
Fetal Bovine Serum (10 %) (Gibco)	: 10 ml

The 3 solutions were mixed well and stored at 4°C until further use.

Appendix 10

Growth medium for T84 cells

For 100 ml preparation:

Dulbecco's Modified Eagle medium (DMEM) (Sigma)	: 87 ml
L-glutamine (2%) (GIBCO-BRL)	: 2 ml
Fetal Bovine Serum (10 %) (Gibco)	: 10 ml

The 4 solutions were mixed well and stored at 4°C until further use.

Appendix 11

10% trypsin-EDTA

For a 100 ml preparation:

1 X PBS	:90 ml
Trypsin-EDTA (Sigma)	:10 ml

Appendix 12

For 10 ml preparation:

Growth medium	:9 ml
DMSO (10%) (Sigma)	:1 ml

Appendix 13

10 % Sodium dodecly sulphate (SDS)

SDS (Merck)	: 10 g
Distilled water (qsp)	: 100 ml

Appendix 14

Reaction mixture for PCR amplification

For 50 µl reaction mixture:

50 ng genomic DNA (working stock with 10 ng/ µl)	: 5µl
50 pmol primer (forward and reverse)	: 1µl
1 unit *Taq* DNA polymerase (DynaZyme)	: 0.5µl
200 µM each of dATP, dGTP, dTTP, dCTP	: 1µl
10 X incubation buffer	: 5µl
(10 mM Tris - HCl, 50 mM KCl, 2 mM $MgCl_2$, 0.01 % gelatin)	
Sterile distilled water	: 34.5µl

Appendix 15

Tris-Acetate-EDTA (TAE) Buffer

For a 1 litre of 50 X TAE buffer preparation:

Tris Base (Sigma) (40mM)	: 242.2g
Glacial Acetic acid (Merck) (0.114%) (v/v)	: 57.1ml
EDTA (Sigma) (2 mM)	: 37.2g
Distilled water (qsp)	: 1 L

For a litre of 1X TAE buffer preparation:

20 ml of the 50 X TAE prepared earlier was mixed with 980 ml of water.

Appendix 16

6 X loading buffer

0.2 % bromophenol blue	: 0.2g
0.2 % xylene cyanol FF	: 0.2g
60 % glycerol	: 60ml
50 mM EDTA	: 18.76g

Appendix 17

Ethidium Bromide

For preparation of a 10 mg /ml stock solution:

Ethidium Bromide	: 100mg
Distilled water	: 10ml

Appendix 18

Lysis buffer for AGS and T84 cells

For 10 ml preparation:

1M Tris-HCL (pH 7.4)	: 0.2 ml
5M NaCl	: 0.1 ml
1M NaF	: 0.1 ml
0.5 M EDTA	: 0.04 ml
1M Na Orthovanadate	: 0.01 ml
Triton X	: 0.1 ml
Distilled water	: 9.45 ml
Proteinase inhibitor (Roche)	: 1 tablet

For 10 ml of 1M Tris-HCL (pH7.4):

Tris-HCl	: 1.576 g
Distilled water (qsp)	: 10 ml

For 10 ml of 5M NaCl:

NaCl	: 2.922 g
Distilled water (qsp)	: 10 ml

For 10 ml of 1M NaF:

NaF	: 0.4199 g
Distilled water (qsp)	: 10 ml

For 10 ml of 0.5 M EDTA:

EDTA	: 1.8612 g
Distilled water	: 10 ml

For 10 ml of 1M Na Orthovanadate:

Na Orthovanadate	: 1.8576
Distilled water	: 10 ml

The buffer was mixed well and aliquoted into eppendoff tubes. It was then stored at 4°C until use.

Appendix 19

Copper solution for Lowry's assay

Solution A

Sodium carbonate	: 25 g
Sodium hydroxide	: 5 g
Potassium sodium tartrate	: 0.5 g
Distilled water (qsp)	: 200 ml

Solution B

Copper sulphate	: 0.125 g
Distilled water	: 2 ml

1. Dissolve solution B in A with stirring.
2. Top up the final solution to 250 ml with distilled water.

Appendix 20

SDS-PAGE gel

Solution A (Separating gel buffer) (pH 8.8)

Tris-HCl (Sigma)	: 90.75 g
Distilled water (qsp)	: 500 ml

Solution B (Stacking gel buffer) (pH 6.7)

Tris-HCl	: 30.17 g
Distilled water (qsp)	: 500 ml

10% Ammonium persulphate (APS)

Ammonium persulphate (Merck)	: 0.5 g
Distilled water	: 5.0 ml

Only freshly-prepared solution was used.

Resolving gel (12%)

For 1 gel (8.5 cm by 7.5 cm):

Solution A	: 1.5 ml
40% acrylamide (Sigma)	: 1.8 ml
10% SDS	: 60 µl
TEMED (Sigma)	: 6 µl
10% APS	: 30 µl
Distilled water	: 2.61 ml

Stacking gel (4%)

For 1 gel (8.5 cm by 7.5 cm):

Solution B	: 0.63 ml
40% acrylamide (Sigma)	: 0.25 ml
10% SDS	: 25 µl
TEMED (Sigma)	: 5 µl
10% APS	: 12.5 µl
Distilled water	: 1.59 ml

5 × Reducing loading buffer

For a 10 ml preparation:

10% SDS	: 0.75 g
1 M Tris HCl (pH 6.8)	: 1.563 ml
β-mercaptoethanol	: 1.25 ml
Glycerol	: 2.5 ml
Bromophenol blue	: 2.5 mg
Distilled water (qsp)	: 10 ml

For 2 × Reducing loading buffer:

5 × Reducing loading buffer	: 0.8 ml
Distilled water (qsp)	: 2ml

Appendix 21

SDS-PAGE running buffer

For a litre of 10 X SDS-PAGE running buffer:

Tris	: 30 g
Glycine (Merck)	: 144 g
SDS	: 0.375 g
Distilled water (qsp)	: 1 L

For a litre of 1 X SDS-PAGE running buffer:

10 × SDS-PAGE running buffer	: 100 ml
Distilled water	: 900 ml

Appendix 22

Transfer buffer (pH 9.2)

Tris	: 3 g
Glycine (Merck)	: 14.4 g
Methanol	: 200 ml
Distilled water (qsp)	: 1 L

Appendix 23

Wash buffer (PBS-Tween)

Tween 20	: 0.5 ml
1X PBS (qsp)	: 1L

Appendix 24

Blocking Buffer and Primary Antibody Diluent

2% Bovine serum albumin (BSA) (Amresco)	: 20 g
0.01% Soduim azide (Sigma)	: 0.1 g
0.2% Triton-X (BioRad)	: 2 ml
Distilled water (qsp)	: 1000 ml

The solutions were kept at 4°C until use.

Appendix 25

Secondary antibodies diluent

% Bovine serum albumin (BSA) (Amresco)	: 20 g
0.2% Triton-X (BioRad)	: 2 ml
Distilled water (qsp)	: 1000 ml

The solutions were kept at 4°C until use.

Appendix 26

4% paraformaldehyde

Paraformaldehyde (Merck)	: 4 g
1X PBS	: 100 ml

To dissolve, the mixture was incubated at 60°C for 20 minutes. The fixative was prepared freshly before use.

Appendix 27

0.2% Glutaraldehyde

25% glutaraldehyde	: 0.08 ml
1 X PBS	: 10 ml

Appendix 28

0.05 M glycine

Glycine	: 3.75 mg
1 X PBS	: 10 ml

Appendix 29

2% Glutaraldehyde

25% glutaraldehyde	: 0.8 ml
1 X PBS	: 10 ml

Appendix 30

Coating buffer (pH 9.5)

Sodium bicarbonate	: 0.84 g
Sodium carbonate	: 0.36 g
Distilled water (qsp)	: 100 ml

Appendix 31

Assay diluent

Fetal Bovine Serum (Gibco)	: 5 ml
1 X PBS (qsp)	: 50 ml

Appendix 32

Working detector

Detection antibody	: 20 µl
Avidin HRP	: 20 µl
Assay diluent	: 5 ml

The working detector was freshly prepared before use.

Appendix 33

Substrate solution (BD Pharmingen™ TMB Substrate Reagent Set)

Substrate solution A	: 5 ml
Substrate solution B	: 5 ml

The 2 substrate solution were mixed well and freshly prepared before use.

Appendix 34

Stop solution (1M sulfuric acid)

Sulfuric acid	: 9.81 g
Distilled water (qsp)	: 100 ml

Appendix 35

0.2% Triton-X

Triton-X (BioRad)	: 0.2 ml
1X PBS	: 100 ml

Appendix 36

MTT stock solution

MTT	: 25 mg
PBS buffer (pH 7.4)	: 5 ml

The solution was fitlter steriled and stored at 4°C.

Appendix 37

Lysis solution

SDS	: 10 g
DMSO (Merck)	: 99.4 ml
Glacial acetic acid	: 0.6 ml

Appendix 38

Biotinylated albumin preparation

Albumin solution (30 µmole/L)

BSA	: 0.0102 g
1X PBS (qsp)	: 5 ml

Biotin solution preparation (5 mmole/L)

N-hydroxysuccinimidobiotin (Roche)	: 0.0009 g
1X PBS (qsp)	: 0.5 ml

1. Mix the albumin solution with the biotin solution well.
2. Incubate for 4 hours at room temperature.
3. Dialyze in 1X PBS for 4 hours at 4°C.
4. Store at -20°C till use.